Characterization of the enzymes involved in the diolsynthase pathway in *Pseudomonas aeruginosa*

Shirin Shoja Chaghervand

FACULTAT DE FARMÀCIA I CIÈNCIES DE L'ALIMENTACIÓ

PROGRAMA DE DOCTORAT: BIOTECNOLOGIA

CHARACTERIZATION OF THE ENZYMES INVOLVED IN THE DIOLSYNTHASE PATHWAY IN *PSEUDOMONAS AERUGINOSA*

SHIRIN SHOJA CHAGHERVAND

2019

FACULTAT DE FARMÀCIA I CIÈNCIES DE L'ALIMENTACIÓ
DEPARTAMENT DE BIOLOGIA, SANITAT I MEDI AMBIENT
SECCIÓ MICROBIOLOGIA

PROGRAMA DE DOCTORAT: BIOTECNOLOGIA

CHARACTERIZATION OF THE ENZYMES INVOLVED IN THE DIOLSYNTHASE PATHWAY IN *PSEUDOMONAS AERUGINOSA*

Thesis presented by **Shirin Shoja Chaghervand** to compete to PhD degree by the University of Barcelona

Thesis supervisor's agreement:

Dr. Montserrat Busquets

Dr. Angeles Manresa

PhD student:

SHIRIN SHOJA CHAGHERVAND
2019

This PhD thesis was partially funded by the Ministerio de Economía y Competitividad (Nuevos bioproductos para nuevos retos: desarrollo de biomateriales mediante estrategias microbianas y enzimáticas, project CTQ2014-59632-R).

’’تنها راهی که به شکست می‌انجامد،
تلاش نکردن است‘‘.
(کورش بزرگ)

ACKNOWLEDGMENTS

ACKNOWLEDGMENTS

Foremost, I would like to express my sincere gratitude to my supervisors Prof. Angeles Manresa and Prof. Montse Busquets for the continuous support of my Ph.D. study and research, for their patience, motivation, enthusiasm, and immense knowledge. Their guidance helped me in all the time of research and writing of this thesis.

Besides my supervisors, I would like to thank my friend Dr. Monica Estupiñán, for her encouragement, insightful comments, and hard questions.

My sincere thanks also goes to Dr. Francesc Rabanal, Dr. Yolanda Cajal, Dr. M. J. Espuny and Dr. David Miñana.

Thanks to Dr. J. Badia coordinator of the doctoral program in Biotechnology for her support during my Ph.D.

I would like to thanks Alberto Adeva, technician of liquid chromatography-mass spectrometry service, Gemma Martinez and Yolanda Muela technician of Electron Microscopy in Parc Científic and Jordi Diaz for AFM from Scientific and Technological Centers of University of Barcelona.

I am also very grateful to all those at the Department of Microbiology, especially Lucia who was always so helpful.

I thank my friends Anderson, Mark, Montse, Nazanin, Nico, Guille, Yaima and Carla.

Lastly, I would like to thank my family for all their love and encouragement and I would also like to say a heartfelt thank you to my mother for always believing in me and encouraging me to follow my dreams. Thank you.

CONTENTS

1. INTRODUCTION

1.1. Bioeconomy and Biocatalysis

Recent scientific and technological advances within the bioeconomy are characterized by a holistic approach to biotechnology and have made notable contributions to sustainable development (Aguilar *et al.*, 2018). The aim of achieving sustainable production of both raw materials and final products is prevalent in different areas, including nutrition and health, fuels, polymers, and industrial products (Lokko *et al.*, 2018).

One of the major tools in the bioeconomy is enzyme technology, which has wide industrial application. It is used in the chemical industry to catalyze chemical reactions and promotes green chemistry by replacing chemical processes in a wide range of industries. It includes food enzymes (derived from gene technology), feeds enzymes (to increase the digestibility of nutrients in animal feeds), technical enzymes (textile, leather, pulp, and paper enzymes) and detergent enzymes (Drepper *et al.*, 2006; Lokko *et al.*, 2018).

1.2. The genus *Pseudomonas*

The genus *Pseudomonas* is one of the most complex Gram-negative bacteria, containing 144 species and 10 subspecies (Parte, 2014). Multilocus sequencing, analysis of housekeeping genes and whole-genome sequencing have provided taxonomic definition and species reorganization within the genus (Gomila *et al.*, 2015). *Pseudomonas* bacteria inhabit a wide range of environments (Fig. 1) and show remarkable metabolic and physiology versatility and the ability to adapt to different environmental conditions. Due to these features, these bacteria play important roles in plant and human disease and biotechnology (Silby *et al.*, 2011). Many pseudomonads interact with plants, contributing to plant health by antagonizing plant-pathogenic microorganisms (biocontrol) and directly influencing plant resistance to disease and promoting growth, both as plant endophytes (Ryan *et al.*, 2008) and as rhizosphere colonizers.

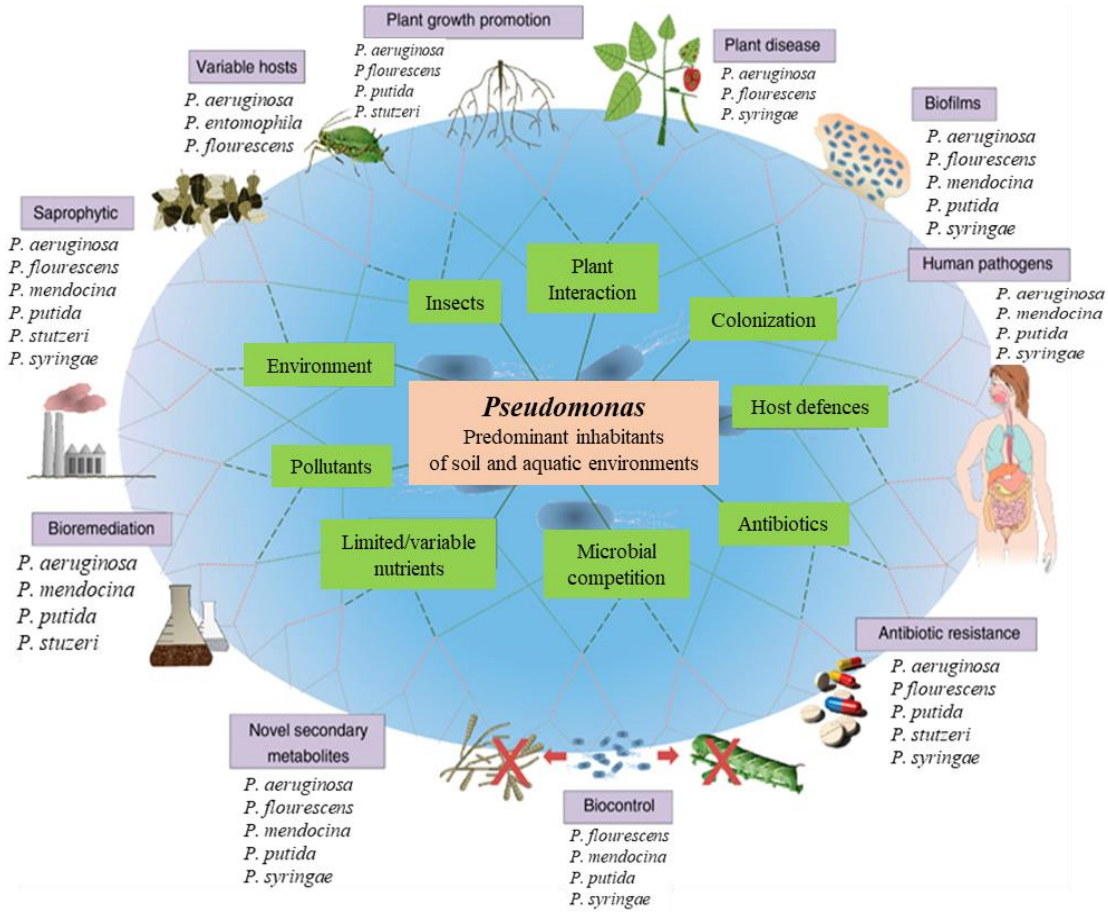

Figure 1. The functional and environmental range of *Pseudomonas* spp. The *Pseudomonas* common ancestor encountered a wide range of abiotic and biotic environments that have led to the evolution of a multitude of traits and lifestyles with significant overlap among species (from Silby *et al.*, 2011).

P. fluorescens can act as a biocontrol species that protects plants by producing antifungal agents (Haas and Défago, 2005). The study of genomes of *Pseudomonas* spp. has revealed the importance of life style, diversity, and adaptability of this genus especially in human and plant health. *P. aeruginosa*, an opportunistic pathogen in humans, has been studied extensively due to its metabolic versatility. *P. syringae* is described as a plant pathogen, and displays several complex networks of interactions between the plant defense mechanisms and pathogen-associated molecular patterns (Jones and Dangl, 2006; Bender *et al.*, 1999) It is an important tool for bioremediation because it produces a great variety of enzymes (Lyczak *et al.*, 2000).

Bioremediation is a process that uses microorganisms to reduce or detoxify waste products and environmental pollutants. The exceptional nutritional versatility of *Pseudomonas* spp., coupled with their capacity to produce biosurfactants, which can mobilize hydrocarbons and non-aqueous phase liquids into an aqueous phase (Desai and Banat, 1997), makes them excellent candidates for bioremediation. *P. aeruginosa,* which is frequently isolated from petroleum-contaminated soils and groundwater (Ridgway *et al.*, 1990 ; Zhang *et al.*, 2011), and *P. putida* have been extensively studied in environmental biotechnology because of their capacity to biotransform toxic organic wastes, including aromatic hydrocarbon compounds (Cao and Loh, 2008). *P. aeruginosa* is found in soil and water, can grow at 42 °C, and synthesizes siderophore pyoverdine, a fluorescent yellow-green pigment (Meyer *et al.*, 2002). This species is also a major producer of rhamnolipids (Abalos *et al.*, 2001a; Benincasa *et al.*, 2004) and accumulates different polyhydroxyalkanoates (PHA) (Vidal-Mas *et al.*, 2001; Bassas *et al.*, 2008b). *P. aeruginosa* 42A2 NCIMB 40045, isolated by our group from oil-contaminated water (Bosch *et al.*, 1988) has lost the capacity to produce pigments and rhamnolipids, whereas it accumulates unsaturated hydroxy fatty acids with surfactant activity (Mercade *et al.*, 1988). The genome of the type strain *P. aeruginosa* PAO1 encodes more than 500 regulatory genes, about 150 outer membrane components, and 300 cytoplasmic membrane proteins, which regulate the bacterium in different environments (Silby *et al.*, 2011).

1.3 Pseudomonas aeruginosa as a cell factory

Due to its great catabolic diversity, the genus *Pseudomonas* can act as a powerful natural tool to transform substrates into products of high added-value (Nikel *et al.*, 2014). Moreover, *Pseudomonas* spp. can produce or biotransform diverse compounds that are difficult or impossible to achieve by chemical synthesis due to the complexity of their structure and/ or stereochemistry requirements (de Boer and Schmidt-Dannert, 2003). Different strains of *P. aeruginosa* can use oily waste water as a carbon source to produce rhamnolipids, polyhydroxyalkanoates **(**PHAs) or

oxylipins, which are a class of oxygenated fatty acids (Bassas *et al.*, 2006; Martinez *et al.*, 2010; Bleé, 1995).

1.3.1 Rhamnolipids

Rhamnolipids are well studied glycolipids secreted by *P. aeruginosa* that have excellent surface activity. Already used in various application areas, including environmental, health, food, cosmetics, and oil industries, rhamnolipids are attractive candidates to replace chemically synthesized surfactants because they are derived from a natural source at high purities and have low toxicity levels (Fig. 2). Recent advances in recovery methods have resulted in 99.9% pure rhamnolipids (personal information). Rhamnolipids have several beneficial characteristics: they are easily degradable, nontoxic, nonmutagenic, and have the highest surface-tension-reduction (high effective agent) index of any surfactant currently in use.

The surface tension activity of rhamnolipids depends on the composition of the carbon source (Abalos *et al.*, 2001b; Haba *et al.*, 2003; Benincasa *et al.*, 2004). Since rhamnolipids have application in industry, much effort has been devoted to increasing their production, and yields of 70 g/l and 42 g/l have been achieved (Zhu *et al.*, 2012; Sodagari *et al.*, 2018).

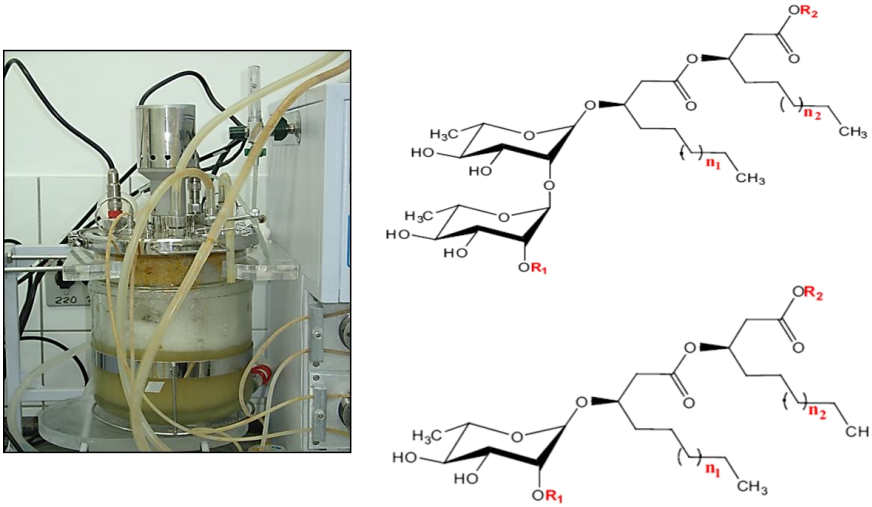

Figure 2. Mono- and di-rhamnolipid structures. When grown on oily substrates, the length of the lipidic moiety depends on the nature of the carbon source.

1.3.2 Polyhydroxyalkanoates (PHAs)

Polyhydroxyalkanoates (PHAs) comprise a family of biodegradable polyesters that are produced by a variety of microorganisms for intracellular carbon and energy storage purposes. PHA synthesis is promoted by unbalanced growth, and they accumulate inside the cell as lipidic droplets, as part of a survival mechanism of the microbes.

The general molecular structure of PHAs is presented in Figure 3. Depending on the carbon numbers in the monomeric constituents, PHAs can be classified as short-chain-length PHAs (C3–C5), which consist of 3–5 carbon monomers, and medium-chain-length PHAs (MCL-PHA, C6–C14), which consist of 6–14 carbon monomers in 3-hydroxyalkanoate units (Bassas *et al.*, 2006; Bassas *et al.*, 2008a). More than 125 bacterial and Archea species have been described as producers of different types of PHAs, with variable numbers of monomers (Rehm and Steinbüchel, 1999).

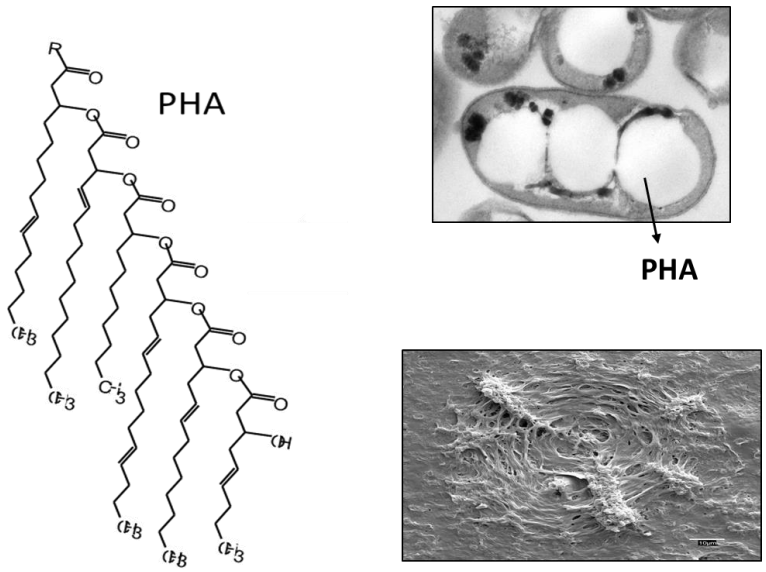

Figure 3. PHA polymeric structure and micrographies of the lipidic inclusion within the cell and the purified material (Rodriguez, 2006; Bassas-Galia, 2007).

1.3.3 Hydroxy fatty acids (HFAs)

Hydroxy fatty acids (HFAs) belong to the family of oxylipins. Over fifty years have passed since the first reported transformation of oleic acid by *Pseudomonas* spp. into hydroxylated fatty acids, 10-hydroxy-stearic acid (Wallen *et al.*, 1962; Schroepfer, 1966) or 10-ketostearic acid (Davis *et al.*, 1969; Wallen *et al.*, 1971), either in whole microorganisms or cell-free preparations (Niehaus *et al.*, 1970). In 1988, our group first reported the biotransformation of oleic acid into 7,10-dihydroxy-8E-octadecenoic (7,10-DiHOME) acid with surfactant properties (Mercade *et al.*, 1988). The stereo configuration was later determined as two hydroxyl groups in S,S configuration (Knothe *et al.*, 1992) notably, the new compound maintained the unsaturation, indicating the enzyme was not a hydratase. *P. aeruginosa* strain 32T3 was reported to produce medium-chain hydroxy fatty acids (HFAs) such as 11-hydroxy-9E-octadecenoic acid and 9-hydroxy-10E-octadecenoic acid (Rodríguez *et al.*, 2001).The production of 7,10-DiHOME is a general characteristic of *P. aeruginosa* strains (De Andrés *et al.*, 1994; Parra *et al.*, 1990; Kuo and Nakamura, 2004). Other oxylipins, 10-hydroperoxy-8E-octadecenoic acid (10-H(P)OME) and 10-hydroxy-8E-octadecenoic acid (10-HOME), were also described as being produced by *P. aeruginosa* 42A2 (Guerrero *et al.*, 1997; Vidal-Mas *et al.*, 2005; Martinez *et al.*, 2010) and *P. aeruginosa* PR3 (Hou and Bagby, 1992).

The hydroxylation of unsaturated fatty acid is a widespread characteristic of 7,10,12-trihydroxy-8E-octadecenoic acids from ricinoleic acid (Kuo *et al.*, 2001) or 9,10,13-trihydroxy-11E-octadecenoic and 9,12,13-trihydroxy-10E-octadecenoic acids from linoleic acid (Kim *et al.*, 2000; Kim *et al.*, 2001). The complex stereochemistry of the resulting conversion, in which 16 compounds are described, indicates that some of these products are due to chemical autoxidation of linoleic acid (Kim et al., 2000). When cultivated on oily substrates (edible oils) as the carbon source, several oxylipins in *P. aeruginosa* strain 32T3 are reported to produce medium-chain hydroxy fatty acids (Rodríguez *et al.*, 2001), as in *P. aeruginosa* 42A2 NCIMB 40045 (Guerrero *et al.*, 1997; Martín-Arjol *et al.*, 2010). As shown in Figure 4, these products are accumulated in the supernatant (Martin-Arjol *et al.*, 2014).

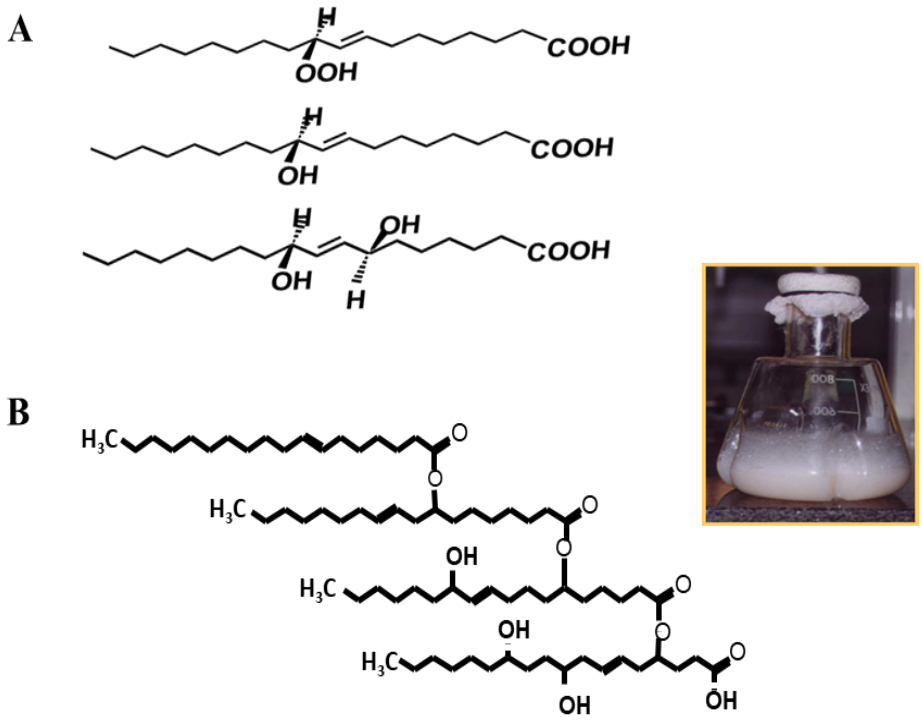

Figure 4. Hydroxy fatty acids and estolides produced by *Pseudomonas aeruginosa* grown on oily substrates (Martin-Arjol, 2014; Estupiñán *et al.*, 2015). (A) Oxylipins, (B) estolides.

At the same time, *P. aeruginosa* 42A2 produces and exports lipases to the culture medium, where the polymerization of the oxylipins (Fig. 4A) occurs (Peláez *et al.*, 2003). The new class of polymers (Fig. 4B) named estolides may be composed of different monomers. Later, *in vitro* synthesis using commercial lipases allowed the production of tailor-made estolides (Martin Arjol I, Busquets M, 2015).

1.4 Biocatalysis of fatty acids

Fatty acids play a major role as a source of energy because they can produce more ATP per gram than carbohydrates or proteins (Berg J M, et al. (2002) | SGD, n.d.). Fatty acids also have an important structural function in organisms, releasing molecules that can be used as building blocks or act as signaling molecules to trigger physiological change (Andeou and Feussner, 2009). The biological importance of oxylipins or oxygenated fatty acids as chemical mediators involved in the control of

numerous physiological processes has been reported in mammals, plants, fungi, and bacteria. They play key roles in inflammation, internal signaling, development and reproduction, motility, biofilm formation and virulence (Brash, 1999 ; Andeou and Feussner, 2009; Joo and Oh, 2012; Ellamar J B, Song K S, 2011).

HFAs have many biotechnological applications, notably as emulsifying agents in the food and cosmetics industries (Peláez *et al.*, 2003; Martín-Arjol *et al.*, 2010). Also, hydroxylated long-chain fatty acid products can act as biologically active antibacterial or antifungal substances (Kim *et al.*, 2000; Martín-Arjol *et al.*, 2010). However, the most important role of HFAs is as intermediates in the synthesis of fine chemicals and pharmaceuticals (Fig. 5) when they have a high amount of reactivity (Paul S, Hou HT, 2010; Ellamar J B, Song K S, 2011).

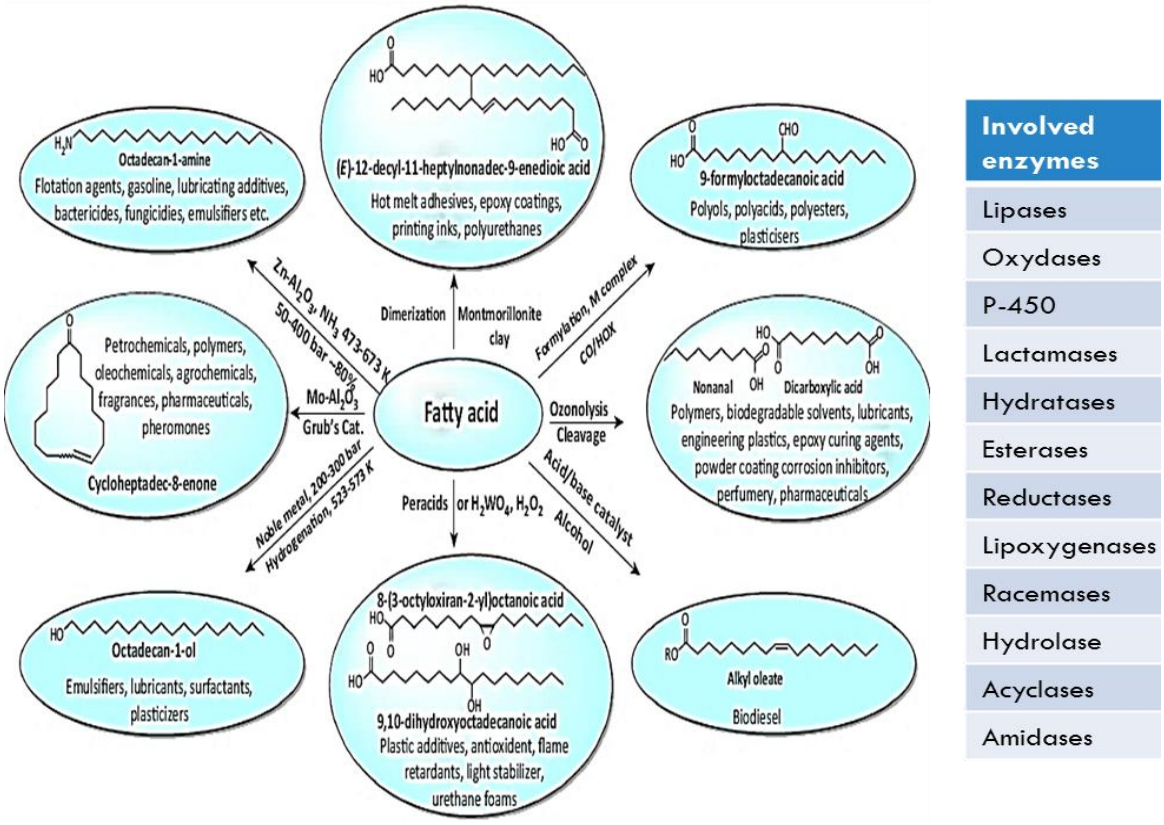

Figure 5. Biotransformation of fatty acids derived from food supply chain waste (Jin *et al.*, 2015).

1.4.1 Oxygenases

Oxygenases are the most important enzymes responsible for oxylipin synthesis (Mueller, 2004). Fatty acid oxygenases are a diverse enzymatic group, which can be generally classified in two major classes of enzymes:

1- Non-heme-containing enzymes such as lipoxygenases, cyclooxygenases, which produce hydroperoxy fatty acids (Hamberg, 1993; Funk, 2001).

2- Heme-containing mono-oxygenases, which belong to the cytochrome P450 superfamily (CYPs) and can oxidize double bonds, producing epoxides or secondary alcohols from saturated bonds (Guengerich, 1991) and di-oxygenases.

Fatty acid oxygenases are widely distributed and several enzymes, such as cytochrome P450 monooxygenases, prostaglandin H synthases, α-dioxygenases, linoleate diol synthases, and lipoxygenases, have been biochemically characterized, showing variations in their catalytic nature and in some cases, requiring the presence of cofactors (Burton, 2003).

1.4.2 Lipoxygenases

Lipoxygenases (LOXs) are found in animals, plants, and fungi (Liavonchanka and Feussner, 2006; Oliw, 2002). LOXs are described as non-heme, iron-containing enzymes that catalyze the stereoselective deoxygenation of polyunsaturated fatty acids with one or more 1Z,4Z structures (Oliw, 2002) (Fig. 6). By abstraction of the hydrogen on the carbon between the double bonds, a free radical is generated, and molecular oxygen is added at one end or other, leading to region or stereospecificity. This mechanism can release different oxylipins, according to the enzyme and substrate. LOX enzymes can oxygenate linoleic acid at three available positions (9R, 9S, or 13S) and arachidonic acid at 11 available positions (5R, 5S, 8R, 8S, 9R, 11R, 11S, 12R, 12S, and 15S) (Newcomer and Brash, 2015). *P. aeruginosa* LOX, the first bacterial LOX described, is active on arachidonic acid and can also convert linoleic acid to oxylipins (13S-HPODE and 9S-HPODE) (Garreta *et al.*, 2013).

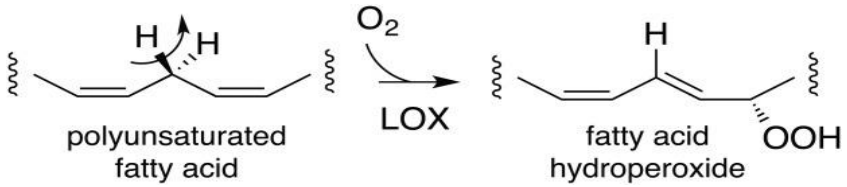

Figure 6. Lipoxygenase activity (Newcomer and Brash, 2015)**.**

In recent years, considerable effort has been dedicated to the characterization of bacterial LOXs (Hansen *et al.*, 2013). A notable achievement was the first crystallization of a bacterial LOX during the search for fatty acid oxygenases in prokaryotic organisms (Garreta *et al.*, 2011).

1.4.3 Heme-containing dioxygenases

Heme is a prosthetic group that can hold an iron molecule in the center of a porphyrin ring by four nitrogen atoms. Porphyrin consists of four pyrroles in a ring structure. One or two axial ligands complete the octahedral coordination around the iron ion. At least one of these ligands acts as a functional group of an amino acid of the protein to which it is bound, which has a strong effect on the reactivity of the heme group (Rydberg *et al.*, 2004; Frey and Hegeman, 2007) (Fig. 7).

Oxylipin-forming enzymes containing several groups include the heme-containing dioxygenases (DOX). Among them, the linoleate diol synthases (LDS) and 10R-DOX of filamentous fungi, and the α-DOX of plants and the prostaglandin H synthase (PGHS) of vertebrates have been characterized (Hörnsten *et al.*, 1999; Garscha and Oliw, 2009). Eukaryotes have the ability to oxygenate fatty acids by heme-dioxygenases, which usually occur with a cytochrome P450 for the transformation of the peroxide product (Brash *et al.*, 2014).

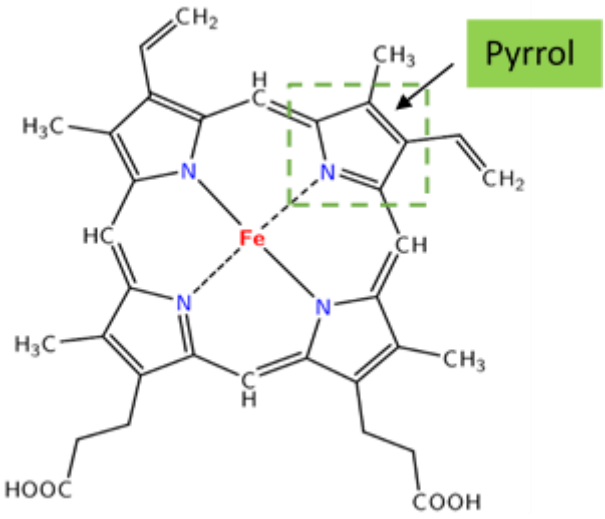

Figure 7. Heme structure

1.4.4 Cytochrome P450

Cytochromes are monooxygenases found in most living organisms, including animals, viruses, bacteria, fungi and plants (Guengerich, 1991). Cytochromes P450 (CYP) are hemoproteins characterized by absorbing light at a wavelength of 450nm (Omura and Sato, 1962).

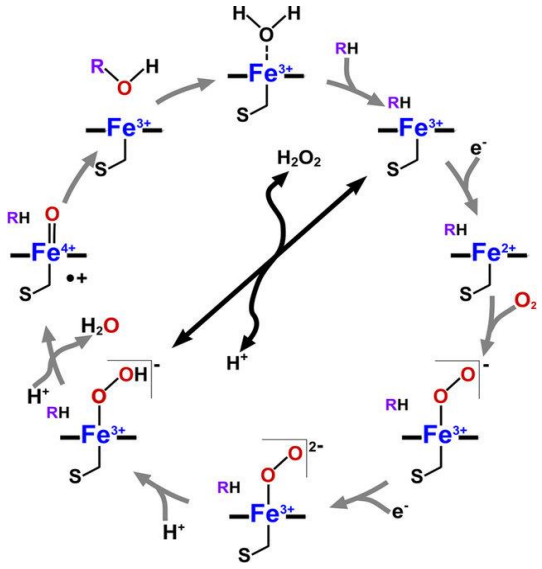

Figure 8. The catalytic cycle of cytochrome P450 (Belcher *et al.*, 2014).

After the CYP enzyme binds to a substrate, a water molecule is replaced. Then, before binding the oxygen, the ferric heme substrate is reduced to the ferrous state by electron transfer from NADPH (Brash, 2009). The first CYP described, using x-ray crystallography, was in P. putida (Fig. 8), which catalyzes the selective hydroxylation of the 5-methylene carbon of D(+)-camphor to form the exo-5-alcohol (Poulos et al., 1985).

1.4.5 Diol Synthases

Diol synthases (DS) catalyze the deoxygenation of unsaturated fatty acid to hydroperoxy fatty acids and the isomerization of released hydroperoxy fatty acid to fatty acid diols (Stahl and Klug, 1996). In 1992, Brodowsky and coworkers reported that the fungus *Gaeumannomyces graminis* has the ability to bioconvert linoleic acid into 8R-hydroperoxyoctadecadienoic acid (8*R*-HPODE) and, after isomerization, to 7S,8S-dihydroxyoctadecadienoic acid (7,8-DiHODE) (Brodowsky *et al.*, 1992; Hamberg *et al.*, 1994). The enzyme responsible for this bioconversion was purified and characterized as 7,8-LDS (Su, 1995). The mechanism of this enzyme starts with the oxidation of heme to form a tyrosyl radical. Pro-S hydrogen at C8 from linoleic acid can abstract the tyrosyl radical, and the subsequent antarafacial insertion of molecular oxygen leads to the formation of 8R-HPODE. The hydroperoxide (Fig. 9) can be converted to 7,8-DiHODE by abstraction of the pro-S hydrogen at C7 (Brodowsky et al., 1992; Hamberg et al., 1994).

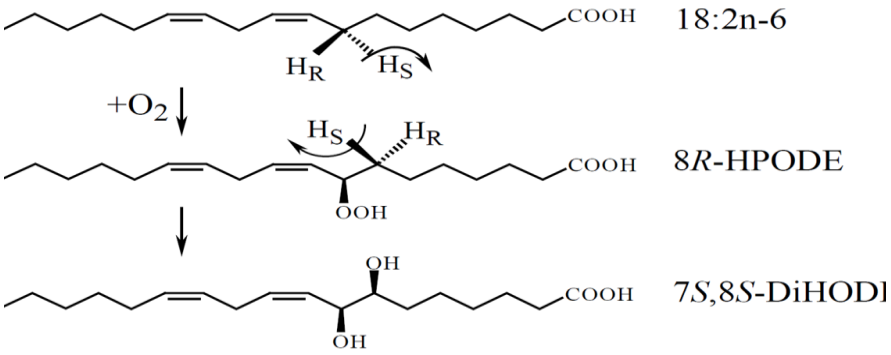

Figure 9. Catalytic reaction mechanism of 7,8-LDS (Hamberg *et al.*, 1994).

It was in 1996 when a new hemoprotein distinct from other fatty acid dioxygenases was described by Oliw et al in the phytopathogenic fungus *Gaeumannomyces graminis* (Su and Oliw, 1996) later on it was named the diol-synthase system (Garsha & Oliw, 2008).

The second report of homologous 7,8-LDS-encoding genes was in *Aspergillus* strains, including *A. clavatus*, *A. fumigatus*, *A. nidulans*, and *A. niger*, which can also produce 5,8- and 8,11-DiHODE from linoleic acid (Garsha and Oliw, 2007; Jernerén *et al.*, 2010). In 2008, Lee et al. proposed that cytochrome P450 is responsible for the hydroperoxide isomerase activity of 7,8-LDS, which the following year was confirmed by Brodhun and coworkers (F. Brodhun, C. Gobel, E. Hornung, 2009). The oleate-diol synthase pathway includes two sequential enzymatic reactions that act independently (Fig. 10): first, the preferred substrate oleic acid is converted into hydroperoxide 10-H(P)OME ((10*S*)-hydroxy(per)oxi-(8*E*)-octadecenoic acid) by a 10*S*-dioxygenase (10*S*-DOX) (PA2077) and second, the hydroperoxide is bioconverted into 7,10-DiHOME ((7*S*, 10*S*)-dihydroxy-(8*E*)-octadecenoic acid) by an 7,10-diol synthase (7,10-DS) (PA2078) (Martinez *et al.*, 2010; Estupiñán *et al.*, 2014).

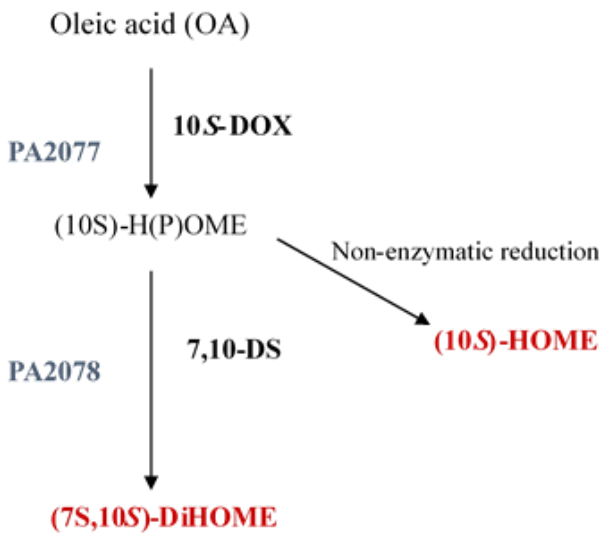

Figure 10. Mechanism of the oleic acid diol synthase of *P. aeruginosa* (PA2077 and PA2078) based on our results. Two characterized enzymes that are responsible for this pathway (adapted from Estupiñán *et al.*, 2014).

Oleate-derived oxylipins 10-H(P)OME, which is spontaneously reduced to 10-HOME ((10*S*)-hydroxy-(8*E*)-octadecenoic acid), and 7,10-DiHOME are synthesized in the periplasm of the cell and exported though ExFadLO outer-membrane transport to the extracellular medium, where they accumulate and act as bioactive compounds (Martínez *et al.*, 2013).

After the identification of these enzymes in *P. aeruginosa* strains, it was demonstrated that they are encoded by *PA2077* and *PA2078* genes, which constitute a fine-regulated operon belonging to the same metabolic pathway, known as the oleate-diol synthase route (Estupiñan *et al.*, 2014).

Bioinformatic analysis of diol-synthase enzymes has been classified as a new subfamily of enzymes, di-heme cytochrome c peroxidases (FadCCPs) (Estupiñán *et al.*, 2014), with two members so far, which can act as mono- and di-hydroxylating enzymes without cofactor supply. An overview of the entire metabolic pathway for oleic acid hydroxylation is presented in Fig. 11.

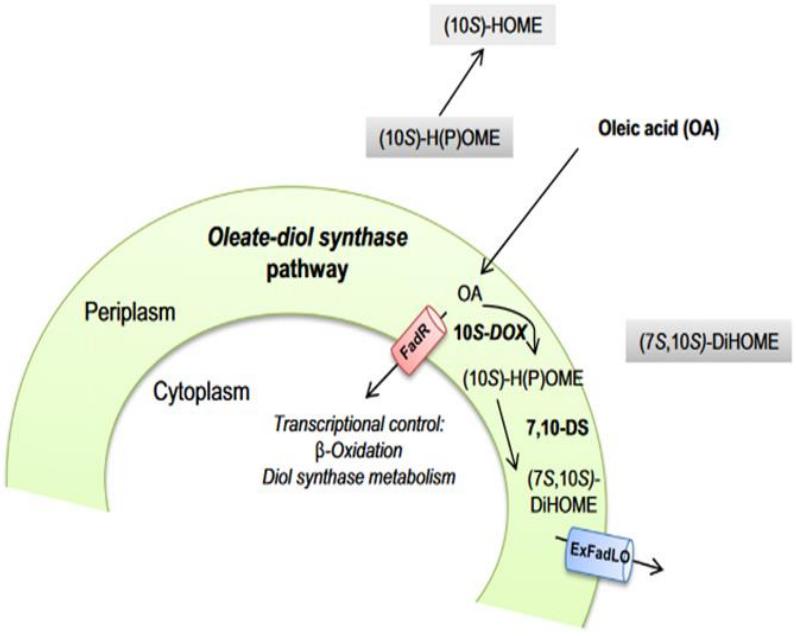

Figure 11. The metabolic pathway for oleic acid (adapted from Estupiñán *et al.*, 2014).

Oleic acid, a preferred substrate, induces transcription of fatty acid metabolism genes and is metabolized into 10-H(P)OME and sequentially to 7,10-DiHOME by

10*S*-DOX and (7S,10S)-DS enzymatic activities in the periplasm. The resulting oxygenated fatty acids are exported by the ExFadLO OM-transporter and are possibly involved in environmental adaptation.

The high similarity of FadCCP enzymes, including their catalytic core of 10*S*-DOX and 7,10-DS compound by two confronted heme-binding groups, allows them to be described as cytochrome c peroxidases (CCPs). Phylogenetic analysis revealed an extremely conserved transcriptional unit, suggesting that the enzymes could have originated from a genetic duplication event and underwent functional evolution through mutagenesis, acquiring different catalytic behavior (Estupiñán *et al.*, 2015).

1.5 Heterologous overexpression in *Escherichia coli*

One of the host microorganisms most frequently used to produce recombinant protein is *Escherichia coli*, which has been the model organism for basic and applied purposes. There are different reasons for choosing *E. coli* as a host microorganism: its genetics have been studied for decades, it is fast-growing, easy to manipulate and can host a large number of cloning vectors. In some cases, over-expression of heterologous protein in *E. coli* leads to the accumulation of the target protein in dense water-insoluble aggregates, known as inclusion bodies (IBs) (Baneyx, 1999; Qi *et al.*, 2015). It can be found in the cytoplasm or periplasm of the host *E. coli*, and electron microscopy reveals them as dense particles of aggregated protein.

1.5.1 Inclusion body formation

Formation of inclusion bodies (IBs) is the result of multiple factors provoking the misfolding of the polypeptide chain, which leads to protein aggregation. The occurrence of IBs might be due to weakening activity of chaperones during high-level expression and the subsequent formation of partially folded or misfolded protein intermediates in cytoplasm. Chaperones are protein acting as quality control mechanisms that protect protein during stressful conditions; for example, the chaperone sHsps can protect cellular proteins and accelerate IB solubilization. The

catalytic activity of the aggregate protein can be increased by chaperones sHsp, IbpA and IbpB after a small heat shock (Mogk *et al.*, 2003; Krauss *et al.*, 2017). A heat shock stress during protein expression, and the use of a strong inducer or promoter in vectors, which produces a high number of copies of the target gene, can also play a role in the formation of IBs (Singh *et al.*, 2015).

Another important parameter affecting protein aggregation is the amino acidic sequence; the presence of a hydrophobic amino acid sequence of protein might influence the aggregation when there is a high concentration of the heterologous protein (A1. Fig). The tendency of a polypeptide to undergo aggregation depends on the physicochemical characteristics of amino acids, such as hydrophobicity, charge, and propensity to secondary structure. AGGRESCAN program analyses have shown that factors like length, location, abundance, function, and conformation of proteins effect their aggregation (Ramón *et al.*, 2014; García-Fruitós *et al.*, 2011).

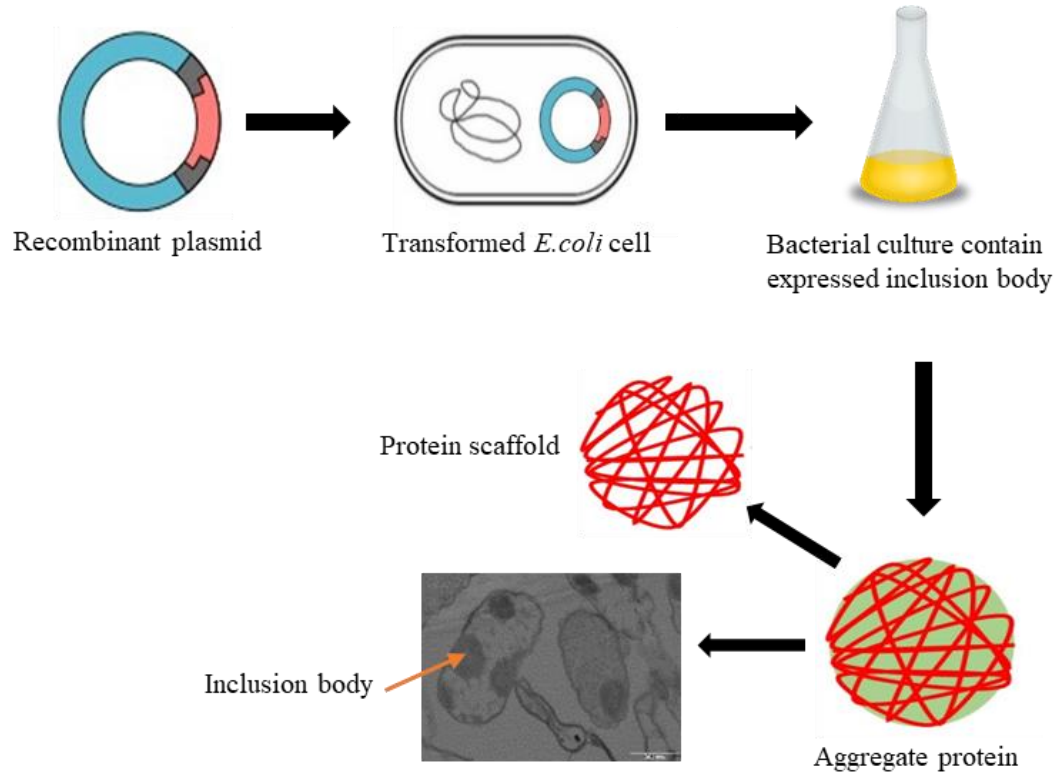

Figure 12. Production of an inclusion body (IB). Expression under stress of recombinant protein in *Escherichia coli* as an IB. Image: IB in the polar region of the *E.coli* cells surrounded by a protein scaffold.

IBs can be found in the pole or at both poles of rod-shaped *E. coli* cells as spherical or cylindrical particles ranging in size from 200 to 1200 nm that contain the 80-95% of aggregated proteins. The average buoyant density of *E. coli* cell lysates depends on the formation of IBs and can be 1,085 kg/m^3 (Krauss *et al.*, 2017) The difference of density between IB particles and soluble protein is enough to separate them by centrifugation. The presence of IBs at the polar end depends on macromolecular pressure in the nucleoid region, and whether the center of the cell is full of DNA (Fig. 12). The movement of IBs from the middle of the cell to the pole occurs does not require energy. DnaK and ClpB are two important disaggregating chaperones found at the poles (Ramón *et al.*, 2014; Rinas *et al.*, 2017).

1.5.2 Structure of inclusion body

IBs are globular proteins, oligomeric species, or polypeptides that are intrinsically disordered and form aggregates (García-Fruitós *et al.*, 2011). Such aggregations are formed by non-native intermolecular hydrophobic interactions between protein-folding intermediates (Vallejo and Rinas, 2004). When IBs are due to the overexpression of a cloned gene, the fine composition of such aggregates is not homogeneous. Different aggregated proteins can coexist with different conformational states; structural analysis has revealed a high level of protein secondary structure but also properly folded molecules and hence functionally active IBs. During aggregation, different polypeptides, especially proteins involved in protein folding, might be entrapped within IBs (Carrió *et al.*, 2000; Carrió and Villaverde, 2002).

As reported by Carrió *et al*., the intermolecular interactions driving aggregation might occur through homologous protein patches and be prone to organization into higher-order structures that fulfill all characteristics of amyloid which consist of aggregations of peptides made of native-like secondary structures. Amyloid fibrils and amyloid-like proto-aggregates in inclusion bodies can be characterized by β-sheet secondary structure and fibril morphology (Nilsson, 2004; Carrió *et al.*, 2005 Singh *et al.*, 2015). All amyloid structures have similar morphological

characteristics and are composed of protofilaments with cross-β-sheets that are parallel to the fibril axis, and each β-sheet contains β-strands that are perpendicular to the fibril axis (Fig. 13A). β-sheets are composed of polypeptide backbones that hold and connect tightly through short hydrogen bonds and are the main reason that Thioflavin-T(Th-T) and Congo red can bind to amyloid fibrils (de Groot *et al.*, 2009; García-Fruitõs *et al.*, 2011).

Fourier-transform infrared spectroscopy (FT-IR) is a powerful tool that can analyze the secondary structure of proteins; FT-IR can measure wavelength or intensity when infrared light is absorbed by the sample, allowing the basic structure to be determined (de Groot *et al.*, 2009).The sharp features of infrared spectra are characteristic of specific types of molecular vibration that are useful for sample identification. In the second derivative of the FT-IR spectra, nine characteristic vibrational bands arise from the amide groups of proteins. Among them, Amide I, due to the C=O stretch vibration of the backbone of the peptide chain, is the most useful probe for determining the secondary structure of proteins, providing a relative amount of different types of secondary structures for each protein. The protein spectra from the second derivative analysis yielded bands with frequencies characteristic of specific secondary structures that are essential for all the proteins (Dong *et al.*, 1990).

1.5.3 Protein recovery from IB

Recent studies have shown that IBs can have biological activity. When IBs are used as immobilized enzymes or perform other biological activities, they are known as catalytically active IBs (CatIBs). The formation of IBs with biological activity can be the result, of a self-assembling ionic peptide (Singh *et al.*, 2015). *E. coli* can produce CatIBs that contain the enzymes β-galactosidase and polyphosphate kinase. Purification of CatIBs is easy and chromatographic purification is not required (Krauss *et al.*, 2017). IBs are mechanically stable proteins that can be converted to a soluble form by solubilization and refolding methods (Rinas *et al.*, 2017).

A variety of methods may be used to solubilize IBs and render active protein, which is accomplished after refolding of the polypeptide. However, the efficiency of the overall process should be evaluated (De Bernardez Clark, 2001). Conversely, if active expressing proteins are in the form of IBs, this can be advantageous, as reflected by examples in literature because it may facilitate the recovery and purification of the IB in the first stages downstream, without any need to refold the protein. Also, the manipulation of culture media and expression conditions might facilitate the production of IBs (Worral and Gross, 1989; Tokatlidis *et al.*, 1991; García-Fruitós *et al.*, 2005; Jevševar *et al.*, 2005).

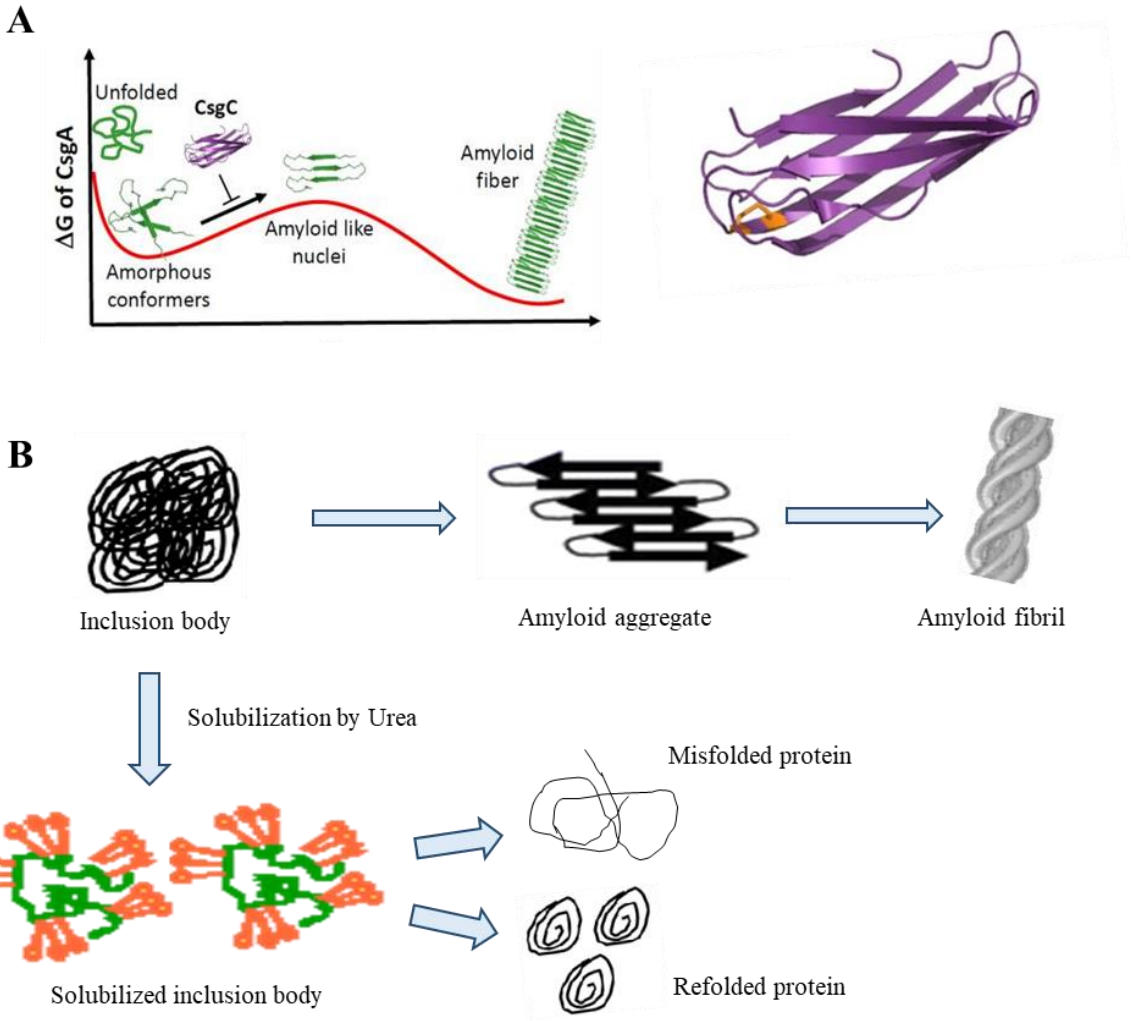

Figure 13. Scheme of IB structure and protein refolding. A, Presence of amyloid-like structures in the IB formation (Van Gerven *et al.*, 2015). B, Recovery of protein from IBs by solubilization of IB proteins using urea as a strong reagent.

There are different approaches to IB purification, one of the mildest being a combination of sonication, lysozymes, and filtration (Rodríguez-Carmona *et al.*, 2010). For recovery of bioactive protein from IBs by mild solubilization, a strong chaotropic agent like urea for producing solubilized enzymes is used (Fig. 13B), alternatively, the freeze-thaw method can be used for mild solubilization (Singh *et al.*, 2015). The recovery of active protein from IBs is usually low and inefficient, and each target protein should be matched by a specific method (de Groot *et al.*, 2009).

1.5.4 Inclusion body as mechanically stable

Mechanically stable IBs are characterized as nanoparticles that can be used for tissue engineering, acting as scaffolds, stimulators of cell proliferation and differentiation, and as a natural protein delivery system for a therapeutic effect. They can provide enhanced treatment with fewer side effects. The production of these biomaterials is economically affordable and they are polymeric materials that can be used as building blocks to obtain silk or protein fragments. Cano-Garrido and co-workers demonstrated the production of fully functional IB-like protein nanoparticles in lactic acid bacteria which developed a safe process of protein-based production with a wide range application for pharmaceutical. More research is still needed to develop new biomedical applications of IBs (Cano-Garrido *et al.*, 2016; Unzueta *et al.*, 2018).

2. AIMS

This research project is focused on the characterization of the enzymes involved in the oleate diol synthase pathway of *Pseudomonas aeruginosa.* The characterization of 10*S*-dioxygenase (10*S*-DOX) and 7,10 (*S*,*S*)-diol synthase (7,10-DS) of the FadCCPs subfamily is presented, as an initial step to deepen into their biotechnological and green-technology applications and their importance in the impact of host-pathogen interactions in insect and plants cells.

The specific aims are:

1. The *in vitro* production of 10-H(P)OME from oleic acid, the substrate of the 10*S*-DOX using a new recombinant *P. putida* KT2440 KT2440/pBBR-77.

2. The biochemical characterization of the 10S-dioxygenase (10*S*-DOX) and the 7S, 10S-diol synthase (7,10-DS).

3. The study of the structure, morphology and functional activity of the protein aggregates formed in *E.coli* as an inclusion body.

4. An experimental screening for 10*S*-DOX and 7,10-DS activities in other proteobacteria.

3. MATERIALS AND METHODS

3.1 Materials

Fatty acids (90-99%) were supplied by Merck. Stock solutions (20 mM) were prepared in absolute ethanol (Panreac) or dimethyl sulfoxide (DMSO) (Sigma-Aldrich) and stored at -20 ºC. A homemade standard containing oleic acid, 10-H(P)OME, 10-HOME, and 7,10-DiHOME (Martin-Arjol *et al.*, 2014) was used for the biochemical characterization of the enzymes. Isopropil-β-D-1-tiogalactopyranoside (IPTG) (Carl Rothe, Germany) was used as an inducer; Phenylmethanesulphonyl fluoride (PMSF), Proteinase K, Congo Red, and Thioflavine were supplied by Sigma-Aldrich (Merck, Darmstadt, Germany). Solvents for organic extractions and chromatography mobile phase for HPLC and LC/MS were from Panreac Applichem, Carlo Erba Reagents and Fisher Scientific. All the chemicals were of ACS grade quality.

3.1.1 Bacterial strains, plasmids and culture conditions:

The bacterial strains and plasmids used in this work are listed in Table 1. All recombinant strains were grown in TSB media (17 g casein peptone, 3 g soymeal peptone, 2.5 g glucose, 5 g NaCl, and 2.5 g KH_2PO_4, and when required 15 g/l of agar) at 30ºC, overnight on a rotary shaker at 150 rpm under aerobic conditions. Media were supplemented with antibiotics at the following concentrations: for *E. coli* DH5α chloramphenicol 20 µg/ml; for *Pseudomonas putida* KT2440 chloramphenicol 400 µg/ml and for *E. coli* BL21/pET28a-78 kanamycin 50 µg/ml. *Pseudomonas putida* KT2440 was cloned with the PA2077 gene inserted into the pBBRMCS1 plasmid (Sambrook *et al.*, 1989), the 10*S*-DOX expressed was used to produce 10-H(P)OME, the substrate for the enzyme diol synthase reaction.

Table 1. Plasmids and strain used in this work.

Strains	Relevant characteristics	Reference
E. coli DH5α	supE44ΔlacU169(ϕ80lacZΔM15)hsR1 RecA1 endA1 gyrA96thi-1relA1	Invitrogen
E. coli DH5α/pMMB-77	CmR, carrying *PA2077* gene (10-*dox*)	(Estupiñán et al., 2014)
E. coli DH5α pMMB-78	CmR, carrying *PA2078* gene (7,10-*ds*)	(Estupiñán et al., 2014)
P.putida KT2440	Wild type, GRAS (Generally Recognize as Safe) strain	(Estupiñán et al., 2014)
P.putida KT2440/pBB-77	CmR, carrying pBBR-77 (10-*dox*)	(Estupiñán, 2015 PhD)
P.aeruginosaPAO1(ΔDS)/pBB-77	CmR, ΔPA2078 mutant carrying pBBR-77 (10-*dox*)	(Estupiñán et al., 2014)
E. coli BL21Star(DE3)	F- ompT hsdSB (rB-mB-) gal dcm rne131 (DE3)	Invitrogen
E. coli BL21/pET28a -78	KanR, carrying *PA2078* gene (7,10-*ds*) in pET28a vector	This study

3.1.2 Cloning and expression of 10S-dioxygenase for *in vitro* production of 10-H(P)OME

Gene PA2077 was amplified from PAO1 genomic DNA as reported elsewhere (Estupiñan *et al.*, 2014). The amplified gene was cloned into *P. putida* pBBR-77, and PA2077 was expressed in the shuttle plasmid pBBRMCS1. Cultures of *P. putida* KT2440/pBBR-77 were grown on TSB overnight at 30ºC and 150 rpm; cells were harvested by centrifugation at 10,000 g for 20 min and 3-fold concentrated in buffer Tris-HCl 50 mM, pH 7. The cell suspension, adjusted by optical density at $O.D._{600nm}$=2.0, was sonicated (70% vibration amplitude and 3 cycles of 1 min; 0.5 s pulse rate, in ice) (Bandelin Sonopuls HD) and then centrifuged at 10,000 g for 15 min. The cell extract was incubated with 0.5 g/l of oleic acid for 1 h at 30 ºC in a rotary shaker at 150 rpm. Products were extracted and detected by TLC and/or HPLC for monitoring 10-H(P)OME production.

3.1.3 Expression of 10*S*-DOX and 7, 10-DS

Recombinant enzymes 10*S*-DOX and 7,10-DS were expressed in *E. coli* DH5α containing the plasmids pMMB-77 and pMMB-78, respectively (Estupiñán *et al.*, 2014). Recombinant *E. coli* DH5α/pMMB-10*S*-DOX and *E. coli* DH5α/pMMB-7,10-DS were grown in TSB supplemented with chloramphenicol (20 µg/ml) and incubated overnight at 30 ºC in a rotary shaker operating at 150 rpm. To obtain cellular extract, cells were collected by centrifugation at 10,000 g for 20 min, 20-fold concentrated in 50 mM Tris-HCl buffer pH 7.0, and frozen at -20 °C. After thawing in an ice jacketed bath, cells were sonicated at 70% vibration amplitude and 3 cycles of 1 min at 0.5 s pulse rate (Bandelin Sonopuls HD 3100). Clarified cell extracts were then recovered after ultracentrifugation at 40000 x g for 30 min, at 4°C (Beckman Coulter, Avanti J-20 XP, United States).

Protease inhibitor cocktail cOmplete™, Mini, EDTA-free (Sigma-Aldrich), was used in the cellular extract samples. Finally, samples were filtered twice with centrifuge filter 30K MWCO (15,000 g for 30 min) in double volume in 50 mM Tris-HCl buffer pH 8.0.

3.1.4 Expression of 10*S*-DOX and 7, 10-DS as inclusion bodies (IBs)

Cultures of *E. coli* DH5α/pMMB-77 and *E. coli* BL21/pET28a-78 strains were grown in TSB (17 g of casein peptone, 3 g soymeal peptone, 2.5 g glucose, 5 g NaCl, and 2.5 g KH_2PO_4). Media were supplemented with antibiotics at the following concentrations: for *E. coli* DH5α/pMMB-77 chloramphenicol 20 µg/ml; BL21/pET28a-78 kanamycin 50 µg/ml, incubated 3 h at 37 ºC on a rotary shaker operated at 130 rpm. Expression was induced during the exponential phase (O.D. 600_{nm}=0.7) with 1 M IPTG.

3.2 Inclusion Body purification

The culture of *E. coli* DH5α/ pMMB-77 and *E. coli* BL21/ pET28a-78 were taken 3 h after induction and cells were harvested by centrifugation, for 20 min at 15,000 g (Beckman Coulter, Allegra 25R, United States). The corresponding pellet was resuspended in 40 ml lysis buffer (20-fold concentrated) (Tris-HCl buffer 50mM, pH 8, containing 100mM NaCl and 1mM EDTA).

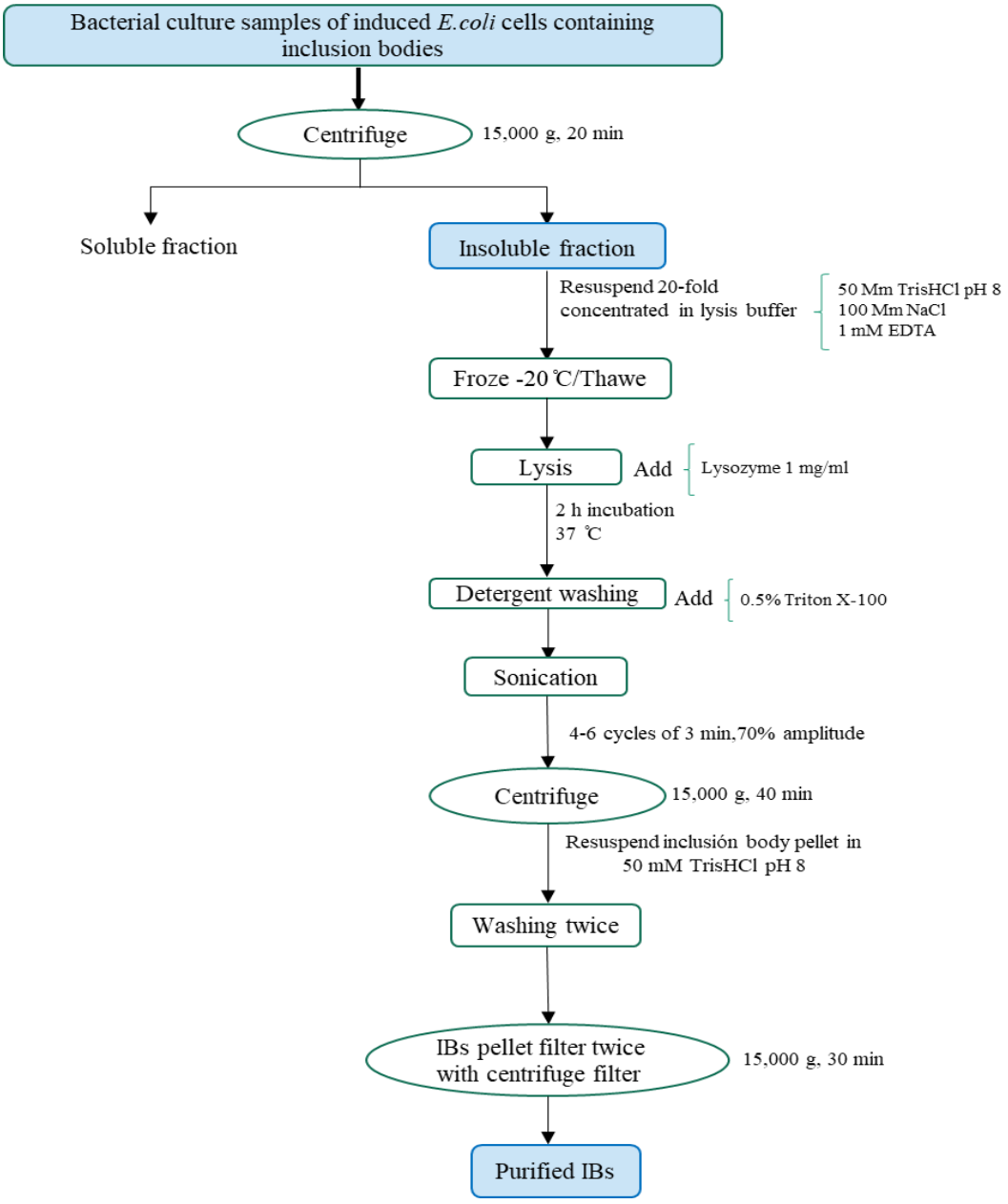

Figure 14. Scheme for purification of IBs.

The bacterial suspensions were frozen at -20 ^{0}C. Inclusion body (IB) purification was carried out by a modified protocol described by Rodriguez-Carmona (Fig. 14). After the bacterial suspension (5ml) was thawed from -20 ^{0}C, 1mg/ml lysozyme was added. After 2 h of incubation at 37 °C and 130 rpm, 0.5% Triton X-100 was added and the mixture was incubated at room temperature for 1 h at 130 rpm. The mixture was disrupted by sonication between 4-6 cycles of 3 min (70% vibration amplitude and 0.5 s pulse rate). Samples were centrifuged (15,000 g, 40 min) and the insoluble fraction, including IBs, was washed twice with the same volume in 50 mM Tris-HCl buffer, pH 8.0. Finally, samples were filtered twice with centrifuge filter 30K MWCO (15,000 g, 30 min) in double volume in 50 mM Tris-HCl buffer, pH 8.0. After final filtration, purity was controlled by SDS-PAGE. Pure IBs were stored at -20 °C (Rodríguez-Carmona *et al.*, 2010).

3.2.1 Solubilization and refolding of IBs

Solubilization of IBs was done with the freeze-thawing method (Qi *et al.*, 2015). Briefly (Fig. 15), induced recombinant cells (15 ml) were thawed at room temperature and centrifuged at 15,000 g for 20 min at 4ºC. The pellet was suspended with the same volume of PBS (10 mM, pH 8). Suspended cells were sonicated in 5 cycles of 1 min (70% vibration amplitude; 0.5 s pulse rate), and centrifuged again at 15,000 g for 20 min at 4ºC. The pellet from sonicated cells was resuspended in the same volume of washing buffer (20 mM Tris-HCl, 300 mM NaCl, 1 mM EDTA, 1% Triton X-100, 1 M urea, pH 8.0) and then centrifuged again at 15,000 g for 20 min at 4ºC. This washing step was repeated three times in order to purify IBs from the other cell components. The pellet obtained after these washings were suspended in the same volume in PBS (20 mM, pH 8) in order to eliminate excess detergent from the washing steps. The resuspended IBs were centrifuged at 12000 g for 20 min at 4ºC and collected in the same volume of solubilization buffer (20mM PBS, 2M Urea, pH 8.0). Finally, purified IBs were frozen at -20 ºC overnight, thawed at room temperature, and centrifuged at 12,000 g for 15 min at 4 ºC to obtain a clear supernatant. Supernatants were analyzed by SDS-PAGE to check the quality of

protein. The protein concentration of solubilized IBs and non-solubilized IBs (pellets) was determined by the Nanodrop and Bradford Assay, using bovine serum albumin (BSA) as the standard. The supernatant fraction was concentrated by filtration in Amicon®Ultra-15 10000 MWCO tubes, centrifuging the samples at 12000 g for 15 min at 4 ºC, to remove excess urea. The concentrated supernatant, which contained the protein refolded from IBs, and the non solubilized IB fraction, was taken to be quantified.

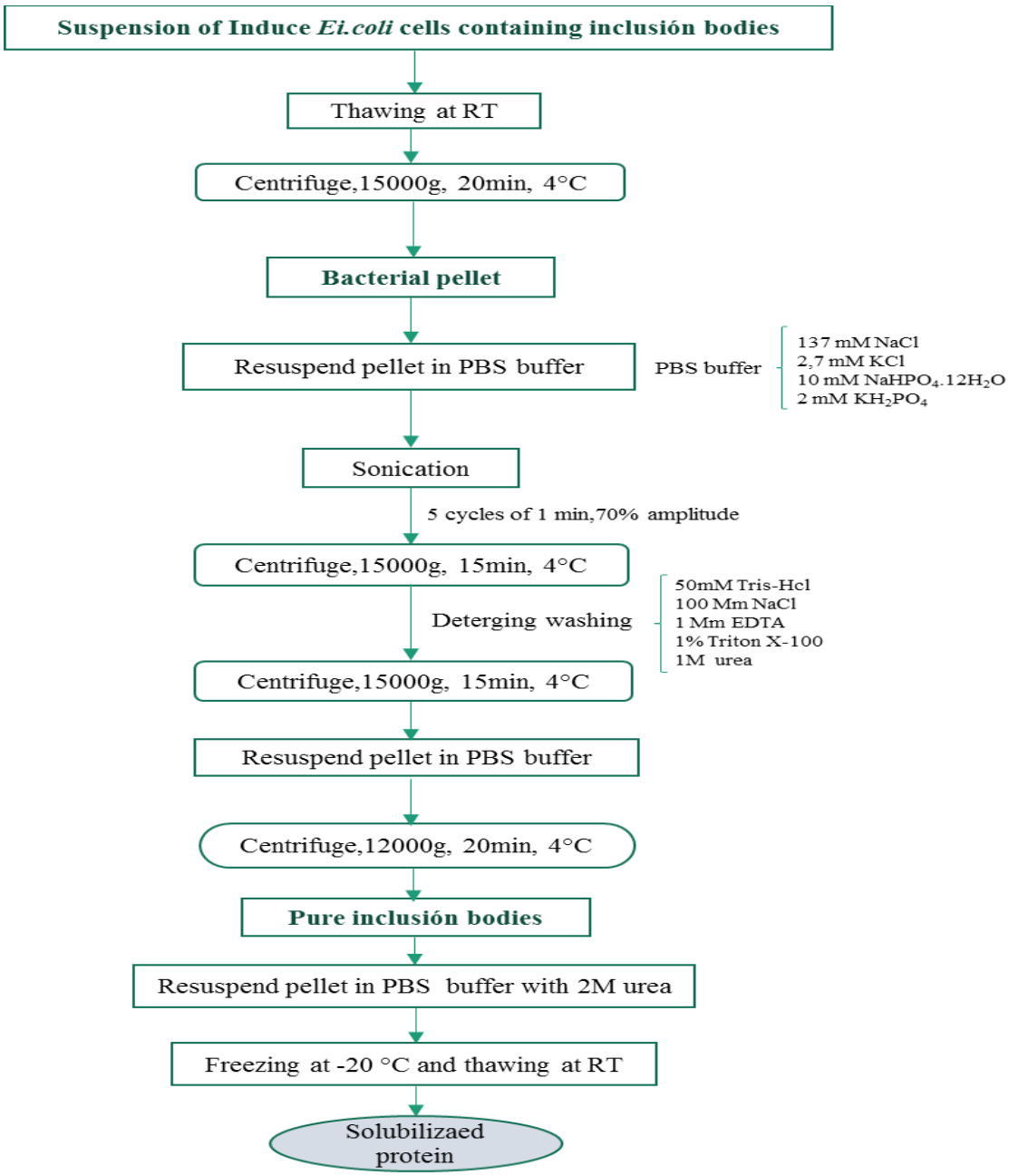

Figure 15. Scheme for the freeze-thawing method (Solubilization and refolding of IBs).

3.3 Protein determination

Protein concentration was measured by the micro-volume spectrophotometer Thermo Scientific NanoDrop 2000 (Wilmington, DE, USA) and/or determined by the Bradford method, using bovine serum albumin as the standard protein (Bradford, 1976).

3.3.1 SDS-PAGE

The estimated molecular mass of the recombinant enzyme was determined by SDS-PAGE with resolving (10%) and stacking gels (5%); standards and samples were heated at 99 ºC for 5 min. Electrophoresis was performed (about 1 h) at a 130 V along with standard molecular mass markers (MW 14.4 kDa to 116 kDa). After migration, gels were fixed and proteins were stained with Coomassie Brilliant Blue following the procedure of Laemmeli (Laemmli, 1970). Gels were calibrated for molecular mass with a wide range of protein standards, Fermentas PageRuler^{TM} Prestained Protein Ladder (SM0671, MW 10-170 kDa; Fisher Scientific, Waltham, MA, USA). The content of the recombinant proteins was determined by densitometric analysis of Coomassie-stained gels using a BioRad imaging densitometer and bovine serum albumin (BSA) as the standard.

3.4 *In vitro* biotransformation assays

Fatty acids used as substrates in the biotransformation assays were prepared from fresh stock solutions; for oleic acid (OA) (20mM) and 10-H(P)OME (1.6 mM) in 50 mM Tris-HCl buffer, pH 7, adjusted to the final concentration of 0.2 mM for OA and 0.8 mM for H(P)OME, unless otherwise stated. The enzyme reaction consisted of 500 µl of the corresponding substrate solution and 100 µl of protein solution for soluble enzymes (16 mg /ml for 10S-DOX or 13,2 mg/ml for 7,10-DS) to a final volume of 1 ml in a 50 mM Tris-HC buffer, pH 7. In the case of inclusion bodies, 100 µl of IBs-77 (192 µg /ml) or IBs-78 (257 µg /ml) was added to 500 µl of substrate solution to a final volume of 1 ml in a 50 mM Tris-HC buffer, pH 7.

The reaction mixture was routinely incubated (in a 2 ml Eppendorf tube) at 30 °C, for 15 min (10*S*-DOX or 7,10-DS) and 20 min (IBs-77 or IBs-78) in a thermoblock (Labolan, Spain) with shaking at 750 rpm.

All biotransformation assays were conducted in the same conditions, including a negative control, and were done in triplicate. The reaction was quenched by acidification to pH 2 with 0.5 M HCl. Products were extracted twice with ethyl acetate (v/v) and strong vortexing. Organic phases were recovered, collected after centrifugation (9,000 g for 2 min), evaporated at 30 °C until dryness, and recovered in methanol. Qualitative detection of fatty acid and oxylipins was performed in precoated TLC plates (0.25-mm Silica Gel 60A, 20 × 20 cm) (Macherey Nagel™ Aluminum Sheets Alugram SIL G), Phosphomolibdic acid hydrate (Fluka Analytical) 10% (w/v) in absolute ethanol (Panreac), as described elsewhere using pure home made standards, before HPLC analysis (Estupiñan *et al.*, 2014).

3.4.1 Substrate specificity

Substrate specificity of 10*S*-DOX was determined using palmitoleic acid, 16:1 *cis*-9 (99%); methyl oleate (99%), oleic acid, 18:1 *cis*-9 (99%);18:1 elaidic acid, *trans*-9 (99%), petroselenic acid, 18:1 *cis*-6 (99%); cis-vaccenic acid, 18:1 *cis*-11 (99%); ricinoleic acid, 18:1 *trans*-12OH (99%); linoleic acid, 18:2 (*cis*-9, 12) (99%); γ-linolenic acid, 18:3 (*cis*-6, 9, 12) (99%) and (12*S*)-HOME (99%) and 10-HOME (100%) as substrates (Table 2). Products were analyzed by RP-HPLC-MS/MS.

Table 2. Range of substrates used for characterization of the substrate specificity of 10*S*-DOX enzyme.

Substrate	Abbreviations	Formula
Oleic acid	OA	(9*Z*)-Octadecenoic acid
Ricinoleic acid	RA	(9*Z*,12*R*)-12Hydroxyoctadecenoic acid
Elaidic acid	EA	(9*E*)-Octadecenoic acid
Palmitoleic acid	POA	(9Z)-Hexadecenoic acid
Linoleic acid	LA	(9*Z*,12*Z*)-Octadecadienoic acid
methyl-oleate acid	mOA	Methyl-(9*Z*)-Octadecenoate acid
y-Linoleic acid	y-LA	(6*Z*,9*Z*,12*Z*)-Octadecatrienoic acid
cis-vaccenic acid	cVA	(11*Z*)-Octadecenoic acid
Petroselinic acid	PA	(6*Z*)-Octadecenoic acid

3.5 Biochemical characterization of 10*S*-DOX and 7, 10-DS

Activity assays for 10*S*-DOX and 7,10-DS were carried out in 50 mM Tris-HCl buffer, pH 7 at 30 ºC or other temperatures as stated in the text, with the appropriate concentrations of substrates, OA or 10-H(P)OME, respectively. The effect of pH on enzyme activity was determined in 20 mM Britton-Robinson buffer over a pH range of 5 to 10 at 30 ºC. Optimal temperature was also evaluated in standard assay conditions over a range of 20 to 50 °C at intervals of five degrees. Thermal stability was determined by incubating cell extracts in the corresponding buffer at different temperatures from 25 to 70 °C for 15 min, in sealed vials. All the samples were immediately chilled in ice and the enzyme activity was measured under standard assay conditions at the optimum temperature. Assays were done in triplicate.

The effect of divalent cations on the enzyme activity was determined by addition of the corresponding metal salts to the reaction mixture to obtain a solution with a final concentration of 1mM. A 100 mM stock solution of the following compounds was used: $CoCl_2 \cdot 6H_2O$; $CdCl_2$; $NiCl_2 \cdot 6H_2O$; $HgCl_2$; $MnCl_2 \cdot 2H_2O$; $CaCl_2 \cdot 2H_2O$; $SnCl_2 \cdot H_2O$; $FeCl_2$; $MgCl_2 \cdot 6H_2O$; $ZnCl_2$; $CuCl_2 \cdot 6H_2O$. All compounds were dissolved in bidistilled water, except $SnCl_2 \cdot H_2O$, which was diluted in 96% ethanol. Enzyme activity was measured by the RP-HPLC method. The residual activity was

calculated and expressed as a percentage of the activity obtained in the absence of the metal ion. Kinetic parameters were determined over a range of concentrations of OA (0.05 to 1mM) and 10-H(P)OME (0.2 to 1.8mM), at 30 ºC in 50 mM Tris-HCl, pH 7 buffer. All determinations of enzyme activity were performed in triplicate and represented values correspond to the average ± standard deviation.

3.5.1 Determination of the active site metal

The active site metal of 10*S*-DOX and 7,10-DS was determined by CCiT (Scientific and Technological Centers) of the University of Barcelona on an ICP-MS (inductively coupled plasma mass spectrometer), an AGILENT 7500ce model (Santa Clara, CA, USA). For the assay, 1 ml (3 μg/ml) of the sample was placed in a Teflon reactor with 1 ml of HNO_3 (15 %) and 1 ml H_2O_2 for 48 hours at 90 °C, and then 22 ml of Milli-Q water was added.

3.6 Screening for oxylipin producer strains

In order to detect new prokaryotes with diol-synthase activity, bacteria belonging to the genera *Aeromonas, Shewanella, Thauera, Ensifer* and *Pseudomonas* spp. other than *P. aeruginosa* were screened (Table 3). The following bacterial cultures preserved at -80 °C were grown in 50ml of suitable media for 24h and 48h as follows: *Aeromonas allosaccharophila* CECT 4220, *Aeromonas bivalvium* 868E, *Aeromonas caviae* CECT 4226, *Aeromonas hydrophila* CECT 839, *Aeromonas salmonicida* CECT 894, *Pseudoalteromonas antarctica* DSM151318, *Pseudomonas fluorescens* CECT 844, *Pseudomonas fragi* DSM 3456, *Pseudomonas lundensis* DSM 6252, *Pseudomonas taetrolens* DSM 21104, *Shewanella vesiculosa* CECT 7339, and *Shewanella putrefaciens* ATCC 8071; all strains were incubated at 30 °C except *S. vesiculosa* at 20 °C in TSB (g/l): casein peptone (17), soymeal peptone (3), glucose (2.5), NaCl (5), and KH_2PO_4 (2.5). *Pseudoalteromonas aliena* DSM16473, and *Shewanella hanedai* ATCC 33224 were incubated at 20 °C (except *S. woodyi* at 30 ºC) in Marine broth (MB) medium (g/l):

peptone (5), yeast extract (1), ferric citrate (0.1), NaCl (19.45), $MgCl_2$ (5.9), $MgSO_4$ (3.24), CaCl (1.8), KCl (0.55), $NaHCO_3$ (0.16), and BrK (0.08). When required, 15g/l agar was added. *Ensifer fredii* DSM 5924 was incubated at 30 ºC in TY medium (g/l): tryptone (5.0), yeast extract (3.0), and $CaCl_2 \cdot 6$ H2O (1.3), and when required 15g/l agar was added. *Thauera aminoaromatica* DSM 25461 was incubated at 30 ºC in Stoke's medium (g/l): polypeptone (5), $MgSO_4 \cdot 7H_2O$ (0.2), $FeNH_4SO_4$ (0.15), sodium citrate (0.1), $CaCl_2$ (0.05), $MnSO_4$ (0.05) and $FeCl_3 \cdot 6H_2O$ (0.01).

Table 3. Bacterial strains used in the experimental screening for the detection of diol synthase activity.

Bacterial Strains	Growth media	Growth Temperature
A. allosaccharophila CECT 4220	Trypticase soy broth (TSB)	30ºC
A. caviae CECT 4226		30ºC
A. bivalvium 868E		30ºC
A. hydrophila CECT 839		30ºC
A. salmonicida CECT 894		30ºC
P. fluorescens CECT 844		30ºC
P. fragi DSM 3456		30ºC
P. putida ATCC 12633		30ºC
P. lini DSM 16768		30ºC
P. oleovorans ATCC 8064		30ºC
P. lundensis DSM 6252		30ºC
P. taetrolens DSM 21104		30ºC
P. tolassi ATCC 33618		30ºC
P. psychrophyla DSM 17535		30ºC
S. vesiculosa CECT 7339		20ºC
S. putrefaciens ATCC 8071		30ºC
P. antarctica DSM 15318		30ºC
P. aliena DSM16473	Marine broth (MB)	20ºC
P. atlantica CECT 579	Marine broth TY agar	20ºC
S. hanedai ATCC 33224		20ºC
S. woodyi DSM12036		30ºC
Ensifer fredii DSM 5924		30ºC
Thauera. aminoaromatica DSM 5461	Stocke's medium	30ºC

After autoclaving, the following solution was added to a final concentration (mg/l): vitamin B12 or cyanocobalamin (0.5), thiamine hydrochloride (0.4) and biotin (0.4). The medium was supplemented with 15g/l of bacto-agar when required. After growing on the corresponding media, cells were harvested and centrifuged at 10.000 g. The pellet was sonicated and the cell extract was clarified as previously described. The cellular extract was incubated with 0.5-1% of oleic acid for 30 min at 30 ºC and 150 rpm in order to detect oxylipin production.

3.7 Bioinformatics tools

DNA and amino acid sequences were obtained from The Pseudomonas Genome Database (www.pseudomonas.com). Blast searches were performed for nucleotide and amino acid sequence analysis in order to retrieve identity and similarity percentages by pairwise alignment. NCBI (http://www.ncbi.nlm.nih.gov) was used for multiple sequence alignment (MSA) (Altschul *et al.*, 1997). Phylogenetic analysis was conducted via the neighbor-joining method, using MEGA 7 software. A bootstrap consensus tree was performed after 1000 repeats.

3.8 Liquid Chromatography analysis

Enzymatic activity was determined by RP-HPLC (reverse-phase liquid chromatography), quantifying the amount of reduction of the substrate compared with the control substrate without enzyme. The analysis was carried out using a Shimadzu LC-9A Chromatograph (Shimadzu, Japan) and Tracer Exel column 120 C8 (150 mm × 4.6 mm, 5 µm) (Teknokroma, Spain) coupled to a Sedex 55 light-scattering detector (Sedere, France). Optimal separation was achieved with a gradient elution using A: acetonitrile (0.1% v/v acetic acid) and B: water (0.1% v/v acetic acid) at the flow rate of 1 ml/min or 2.5 ml/min and a gradient (min, %A): (0, 50), (15, 100), (25, 100), (27.5, 50), (30, 50). The volume of injection was 50 µl. Retention times of fatty acid and hydroxylated fatty acid were established using an inhouse standard (Martin-Arjol *et al.*, 2014). One unit of enzyme activity was

defined as the amount of enzyme required for the conversion of 1 μmol of substrate per minute under the assay conditions used.

3.8.1 Liquid chromatography/mass spectrometry (HPLC-MS/MS)

Liquid chromatography coupled mass spectrometry was performed with a quaternary MS Accela pump system (Thermo Scientific) and with an analytical silica column Tracer Excel 120 C8 (150 mm × 4.6 mm, 5 μm) (Teknokroma, Spain), which was eluted usually at a flow-rate of 0.6 ml/min with A: acetonitrile (0.1% v/v acetic acid), B: water (0.1% v/v acetic acid). The eluent was exposed to electrospray (ESI) for monitoring negative ions in an LTQ-Orbitrap (Thermo Scientific) ion mass spectrometer. The electrospray voltage was set at 3.5 kV and the temperature of the heated capillary was 400 °C. Data acquisition was carried out with Xcalibur software (Thermo Scientific). Identification of compounds was performed as previously described. Briefly, a full scan of the total ion current (TIC) from *m/z* 100-800, MS^2 analysis of *m/z* 297.2 and *m/z* 313.2, MS^3 analysis of *m/z* 313.2→*m/z* 295.2 was used for 7,10-DiHOME and 10-H(P)OME discrimination (Estupiñán *et al.*, 2014).

3.9 Proteolytic digestion of inclusion bodies

Fresh pure IBs were treated as described above. Briefly, after thawing, IBs were suspended in phosphate-buffered saline (PBS) and sonicated to obtain a homogeneous suspension. The IBs were diluted to 1 OD at 350 nm. Proteolytic digestion of IBs was initiated by adding proteinase K to 0.02 mg/ml final concentration and incubated at 25 °C for 30 min. A control suspension without protease K was run in parallel. Samples were taken every 7 min, and 1mM protease inhibitor (PMSF; Sigma) was added to stop the digestion before samples underwent SDS-PAGE analysis (Cano-Garrido *et al.*, 2013).

3.9.1 IB identification of the amyloid structure

Two diagnostic dyes, Congo red (CR) and Thioflavin-T, were used to identify the IB structure by means of spectrophotometer analysis.

Congo Red test: Pure IBs were diluted in phosphate-buffered saline (PBS) at 20 µg /ml final protein concentration and 10 µmol CR. Absorbance spectra were collected together with negative control solutions of dye in the absence of protein and protein samples in the absence of dye from 400 nm using quartz cuvettes 10 mm light path (Carrió *et al.*, 2005).

Thioflavin-T (Th-T) has been described as a specific fluorescent marker that can detect amyloid structures (Upadhyay *et al.*, 2012). The fluorescence emission spectra of purified IBs (20µg/ml) were recorded using an excitation wavelength of 440nm at 25 °C, 30 min on a Spectronic Unicam AB2 Luminescence Spectrometer (Carrió *et al.*, 2005). Samples used in these experiments were diluted in phosphate-buffered saline (PBS) containing 65 µmol Th-T and 0.02 mg/ml PK, adjusted to a final volume of 1 ml.

3.9.2 Fourier Transformed Infrared (FTIR) spectroscopy

The FTIR spectra of the dry samples of purified IBs were analyzed using a Thermo Scientific FTIR spectrometer. Each spectrum consisted of 124 independent scans, measured at a spectral resolution of 2 cm^{-1} within the 1500-1700 cm^{-1} range. The background spectrum was collected before each measurement.

With the aim of studying the structure of the aggregates formed during the expression of *E. coli* harboring DH5α (pMMB-77) and BL21 (pET 28 a-78), whole cells and purified inclusion bodies were lyophilized before the FT-IR analysis to reduce water interference in the infrared spectra.

3.9.3 Transmission Electron Microscopy (TEM)

Native cells, induced cells, and pure IBs-77 (200 µg/ml), and IBs-78 (335 µg/ml) were analyzed. The pellet was fixed in 1 ml of 2.5 % glutaraldehyde with 0.1 M phosphate buffer (PB) and incubation was performed twice at room temperature, for

30 min under agitation. After centrifugation (2000 rpm, 5 min) the pellet was washed four times with PB (at 4 ºC) for 10 min. Thereafter, samples were infiltrated, polymerized, sectioned and mounted as reported in Colomer et al. (Colomer *et al.*, 2002). 20 ultrathin sections were observed in a JEOL 1010 microscope (EM); 80Kv images were acquired using a CCD Megaview 1kx1k.

Fresh observations were performed for the analysis of IBs-77 and IBs-78. A drop of purified inclusion bodies (20 µg) after 30 min incubation with PK (0.02 mg/ml) was placed on a copper grid and observed after 22 min. The grids were stained with 2% (W/V) uranyl acetate for two minutes, completely dried out and viewed with a JEOL 1010 microscope using accelerating voltage.

3.9.4 Atomic force microscopy (AFM)

For analysis of the biological samples, a purified IB suspension in sterilized bi-distilled water was prepared. A drop (5-10µl) of the suspension solution was placed onto freshly cleaved mica or glass cover slips. After adsorption at room temperature, samples were blow-dried with nitrogen compressed air. FM studies were conducted in air at room temperature using an extended multimode AFM head with a Nanoscope controller (Bruker, Germany). All AFM images were recorded in peak force tapping mode with triangular SNL silicon cantilevers (normal radius of 6-8 nm) at a scan rate of 1 Hz.

4. RESULTS & DISCUSSION

4.1 Biochemical characterization of the recombinant 10*S*-dioxygenase and the 7,10 diol synthase

Hydroxy fatty acids, produced by the activity of different enzymes, lipoxygenases. hydratases, P450 monooxygenases, diol synthases (Kim and Oh, 2013), are common constituents of living systems (animals, plant, fungi, and prokaryotes) with functional or structural roles. Some dihydroxy fatty acids act as precocious sexual inducer (psi) factors because for their ability to regulate the sexual and asexual life cycles of filamentous fungi (Seo *et al.*, 2016).The biological role of hydroxy-fatty acids, named also oxylipins, has been known for years due to the relevance of the well-known lipoxygenases. Hydroxy fatty acids can be an intermediate in a pathway like jasmonic acid in plant signaling and leukotriene or lipoxin synthesis in vertebrate animal also as end product such as 12-HETE that can act as single signaling molecules. Oxygenation of unsaturated fatty acids esterified in triglycerides can be used as a fuel source for the developing embryo (Brash, 1999). Monohydroxy, di-hydroxy or poly-hydroxy fatty acids (Seo *et al.*, 2014), are very important and used in the food, cosmetic industry focused on the skin care products; and in the chemical industry, in the synthesis of plastics, biopolymers, and polyurethanes it can be used in the production of polyurethanes (Kim and Oh, 2013; Kim *et al.*, 2017b) .

In 1988 a new feature was found by our group, when *P. aeruginosa* 42A2, isolated from oil-contaminated water when cultivated with oleic acid (OA), transformed in 7,10 (S,S)-dihydroxy-8E-octadecenoic acid found in the culture medium (Mercadé *et al.*, 1988; Bosch *et al.*, 1988). Subsequent studies on this biotransformation led to the description of a new operon in *P. aeruginosa*, carrying a novel enzymatic system: the diol synthase system (Fig. 16). This operon contains two genes, *PA2077*, and *PA2078*, contiguously located in the genome (Estupiñán *et al.*, 2014).

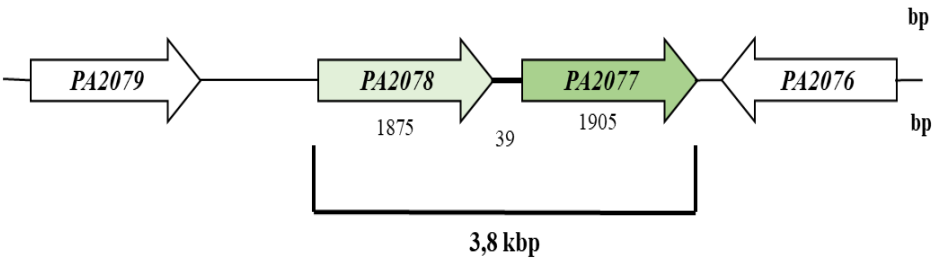

Figure 16. Genomic organization of ORFs PA2077 and PA2078 (adapted from Estupiñán *et al.*, 2014).

After gene cloning and recombination, it was demonstrated that OA was converted to the hydroperoxide 10-H(P)OME by a 10*S*-dioxygenase (10*S*-DOX) (PA2077). Using 10-H(P)OME as a substrate, the dihydroxylated compound 7,10-DiHOME was released by 7,10-hydroperoxide-diol synthase (7,10-DS) (PA2078), and the enzymes were classified in the FadCCPs subfamily (Fig. 17) (Estupiñán *et al.*, 2014).

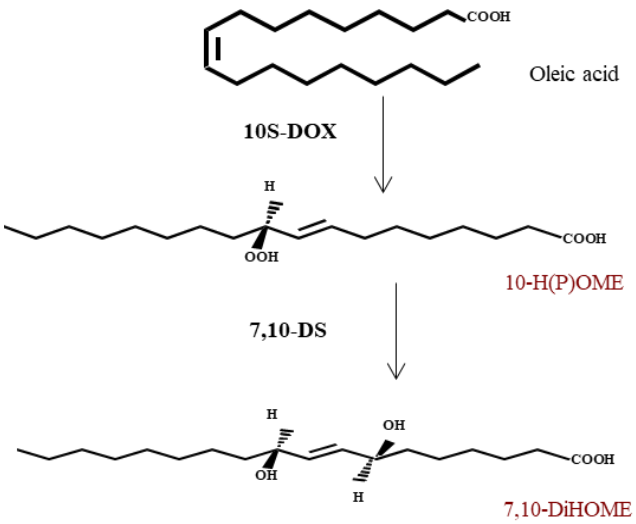

Figure 17. Biochemical pathway of the conversion of oleic acid into (S)10 -hydroperoxy-8(E)-octadecenoic acid (10H(P)OME) by 10*S*-diol synthase (10*S*-DOX) and (7,10-DiHOME) *(S*,S)7.10-dihydroxy-8(E)-octadecenoic acid by 7,10(*S*,*S*)-dioxygenase. (7,10-DS (adapted from Estupiñan, M Ph.D., 2015).

4.1.1 Expression of the recombinant enzymes

Once the singular activity of the two enzymes was established, 10*S*-DOX and 7,10-DS were expressed and produced in a heterologous host, *Escherichia coli* DH5α, carrying pMMB-77 or pMMB-78 constructs (Estupiñan *et al.*, 2014), for their biochemical characterization. During the time course of cell extract purification through conventional methods such as ionic, hydrophobic chromatography or gel filtration it was found that the enzyme activity of both enzymes decreased (results have not shown). Therefore these results led to the use of clarified cell extract that is more stable than a purified enzyme. Cell culture was harvested and cells were centrifuged and sonicated. The total protein concentration of the supernatant was 20.5 mg/ml for 10*S*-DOX and 16.5 mg/ml for 7,10-DS. After clarification by filtration the final protein concentration was 16.0 mg/ml for 10*S*-DOX and 13.2 mg/ml for 7,10-DS. A similar observation was found that using the recombinant cell for conversion of unsaturated fatty acids was more stable than the use of the corresponding purified enzyme, due to the loss of the great part of its activity during purification process (Jeong *et al.*, 2015; Kim *et al.*, 2017a).

In the present study, we justified the oleate diol synthase activity of *Pseudomonas aeruginosa* that using OA as a preferred substrate and the biochemical characterization of 10S-dioxygenase (10*S*-DOX) and 7S,10*S*-diol synthase (7,10-DS) involved in the oleate diol synthase activity (Fig. 17) that before never characterized among bacteria. For years the diol synthase system was restricted to fungi; *Aspergillus nidulans* (Brodhum et al 2010), *A. fumigatus* (Jenéren et al, 2010; Jenerén & Oliw, 2012); an excellent revision of the presence of the diol-synthase system remarked the in other fungi such as *Laestisaria arvalis*, *Magnaporthe grisea* or *M. oryzae* and different species of *Aspergillus* have been reported to bear the diol synthase system (Kim and Oh, 2013). In recent years Gardner and Hou reported similar from other *Pseudomonas* strain; *P. aeruginosa* PR3 (Gardner and Hou, 1999) later different hydroxy-fatty acids were described from ricinoleic acid (Kuo *et al.*, 2001), γ-linoleic acid (Lang *et al.*, 2008), palmitoleic acid (Bae *et al.*, 2010) however the biochemical mechanism was not known. It was until 2010 when the first attempt on the description of the biochemical pathway was suggested in a

similar way than in fungi that the conversion was due to 10-dioxygenase and a hydroperoxide isomerase (Martinez *et al.*, 2010).

The convenient working concentration, in the case of 10*S*-DOX, was stablished as being 0.20 mM for the substrate (OA) and 1.6 mg protein/100 µl of clarified cellular extract from of *E. coli* DH5α/ pMMB-77. Whereas for 7,10-DS it was 0.8 mM for the substrate (10-H(P)OME) and 1.3 mg protein/100 µl for of the respective cellular extract from of *E. coli* DH5α/ pMMB-78. Different reaction conditions were optimized (substrate, time, pH, temperature, thermal stability, metal cations Km) for enzyme characterization.

4.1.1.2 Molecular weight and active site metal ion

A band corresponding to the predicted molecular weight was determined by SDS-PAGE with known standards, as being 66 kDa for 10*S*-DOX and 65 kDa for 7,10-DS (Molecular Weight Estimation, Bio-Rad). 10*S*-DOX activity of *P. aeruginosa* 42A2 was reported to be 50 kDa molecular mass (Martinez *et al.*, 2010) however, in this case, it was supposed to be a unique enzyme, RoxA from *Xanthomonas sp.* 35Y show 71.5 kDa molecular mass (Jendrossek and Reinhardt, 2003) that is similar to molecular mass of PA2077 and PA2078 (Estupiñán *et al.*, 2015) also linoleate 10S-dioxygenase from cyanobacteria has molecular mass of 63kDa (Brash *et al.*, 2014) and similar to the recombinant 10S-dioxygenase from *Nostoc punctiforme*, 70.63 kDa (Kim *et al.*, 2017b), The molecular mass found in the case of the fungal diol synthase of *Aspergillus nidulans* has fungal diol synthase activity and after expressing its proteins show 120 kDa molecular mass (Seo *et al.*, 2014), similar molecular mass was reported for 8S,11S diol synthase from *Penicillium chrysogenum*, 120 kDa (Shin *et al.*, 2016) or in the case of that from *Glomerella cingulate* being 127 kDa (Seo *et al.*, 2016), that is about double amount of molecular mass of PA2077 and PA2078.

Inductively coupled plasma mass spectrometry indicated that 10*S*-DOX and 7,10-DS contained Fe^{+2} bound to the heme group as a prosthetic group at a Fe^{2+} concentration of 0.95mol (10*S*-DOX) and 1.18 mol (7,10-DS) per mol of protein.

Su & Oliw reported 2.8 mol per mol of the enzyme in the case of the 8-Dioxygenase of *Gaeumannomyces graminis* (Su and Oliw, 1996). In 2004 Braaz and co-workers indicated that the purified rubber oxygenase (RoxA) contained 1.9 mol of heme per mol of the 65-kDa protein (Braaz *et al.*, 2004). Crystallized RoxA shows nearest protein structure to 10*S*-DOX and 7,10-DS. The presence of iron in the active center is a common feature of other oxylipin-producing enzymes such as diol synthases P450, lipoxygenases, cyclooxygenases, and dioxygenases (Brash *et al.*, 2014; (Garreta *et al.*, 2013a Hansen *et al.*, 2013a) and contrasts with the 9S-lipoxygenase-bearing manganese, found in the rice pathogen fungus *Magnaporthe salvinii* (Wennman and Oliw, 2013; Wennman *et al.*, 2015).

Bacterial production of hydroxy-fatty acids such that from *Nostoc punctiforme*, described as linoleate 10-dioxygenase (Kim *et al.*, 2017b) or that from a cyanobacterial strain (Brash *et al.*, 2014) and *P. aeruginosa* (Estupiñan *et al.*, 2014) demonstrated 10-dioxygenase activity at the N-terminal domain and hydroperoxide isomerase activity at the C-terminal domain converted oleic acid to 7,10-dihydroxy-8(E)-octadecenoic acid (7,8-DiHOME) (Seo *et al.*, 2015).

4.1.1.3 Substrate specificity of 10*S*-DOX

It was known that the preferred substrate of 10*S*-DOX is OA when incubation is performed using the whole cell extract of *Pseudomonas aeruginosa* 42A2 (Martinez *et al.*, 2010). Now, we used individual recombinant *E. coli* that express 10*S*-DOX. On the knowledge that the first step on the conversion of oleic acid as preferent substrate for 10*S*-DOX a range of unsaturated fatty acids were selected: ricinoleic acid, (9*Z*,12*R*)-12 hydroxyoctadecenoic acid; elaidic acid,(9*E*)-octadecenoic acid; palmitoleic acid, (9Z)-hexadecenoic acid; linoleic acid, (9*Z*,12*Z*)-octadecadienoic acid; methyl-(9*Z*)-octadecenoate acid; γ-linolenic acid, (6*Z*,9*Z*,12*Z*)-octadecatrienoic acid; cis-vaccenic acid, (11*Z*)-octadecenoic acid; petroselinic acid, (6*Z*)-octadecenoic acid.

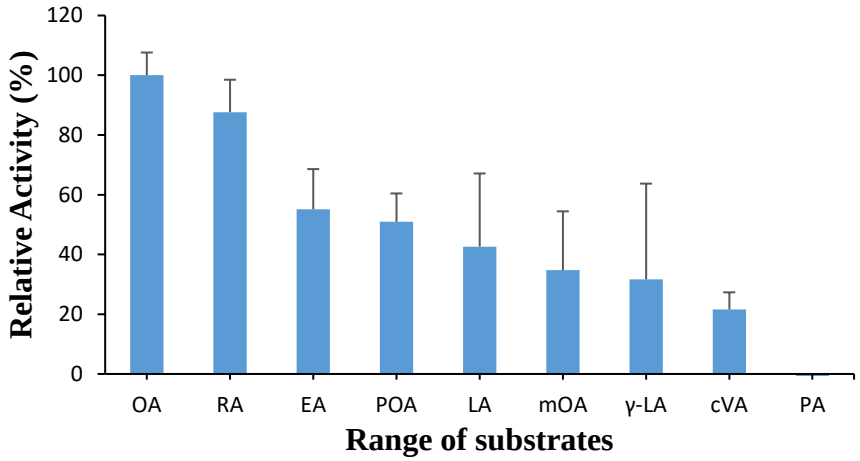

Figure 18. Substrate specificity of 10*S*-DOX. The rate of biotransformation of each substrate is expressed relative to the rate of OA transformation (100%); RA: ricinoleic acid; EA: elaidic acid; POA: palmitoleic acid; LA: linoleic acid; mOA: methyl-(9*Z*)-octadecenoate acid; γ-LA: gamma-linolenic acid; cVA: cis-vaccenic acid; PA: petroselinic acid. Activities were determined as described in Material and methods using *E. coli* DH5α/pMMB as a control.

It was previously reported by the whole cellular extract of *P. aeruginosa* 42A2, containing both enzymes, transformed along with oleic acid, another fatty acid with different positions of the unsaturated bond or poly-unsaturated fatty acids; the results suggested the double bond position affected the conversion of the substrate, being more favorable at position 9,10 however no quantitative preferences were reported (Martinez *et al.*, 2010). In the present work, the affinity of the first enzyme to was studied taking into account this is the first step on natural habitat. As can be observed in Fig. 18, the different affinity of the first acting enzyme, 10*S*-DOX (*E. coli* DH5α/pMMB-77) was assayed. As known oleic acid shoved the highest affinity, similar than that of *N. punctiforme* which was also active on linoleic and α-linolenic acid (Kim *et al.*, 2017b). In the case of study, ricinoleic acid was the second most favorable substrate with 88% of the relative activity compared with the OA. The affinity with linoleic acid was 42.6%, indicating that the new enzyme differs from the so-called cyanobacterial diol synthase (Lang *et al.*, 2008). Which differs also from fungal diol-synthases reported, having linoleic acid as the preferential substrate (Su and Oliw, 1996; Li *et al.*, 2009; Jeneren *et al.*, 2010; Kim *et al.*, 2017a;

Shin *et al.*, 2016; Seo *et al.*, 2016; Choi *et al.*, 2015; Jeong *et al.*, 2015). It was also demonstrated that neither the *cis/trans* configuration, the position of the double bond (C9-C11-C12) were an impediment for enzyme conversion. The remained activity with elaidic acid was 55.14%, with linoleic acid, 42.6 % and with γ-linolenic acid, 31.7%. Whereas the position of the double bond in C11 did reduce the activity to 15.77%. It is noteworthy the activity of 10*S*-DOX on methyl-oleic acid with 40% of the activity compared with oleic acid, suggesting the relative importance of the free carboxyl head. As expected, OA was the preferential substrate and was used for further characterization assays of the 10*S*-DOX enzyme and for the production of 10-H(P)OME, required for the biochemical characterization of 7,10-DS.

4.1.2 Production of 10*S*-H(P)OME as a substrate for 7,10-DS characterization

It was formerly established that the substrate for 7,10-DS is 10*S*-H(P)OME (Figure 17); this product is not commercially available, it was produced *in vitro*. In order to produce 10S-H(P)-HOME recombinant *P. aeruginosa* bearing (ΔDS/pBBR-77) was used. In Fig. 19 different time conversion were compared with the aim to get a substrate with a high content of 10*S*-H(P)-HOME.

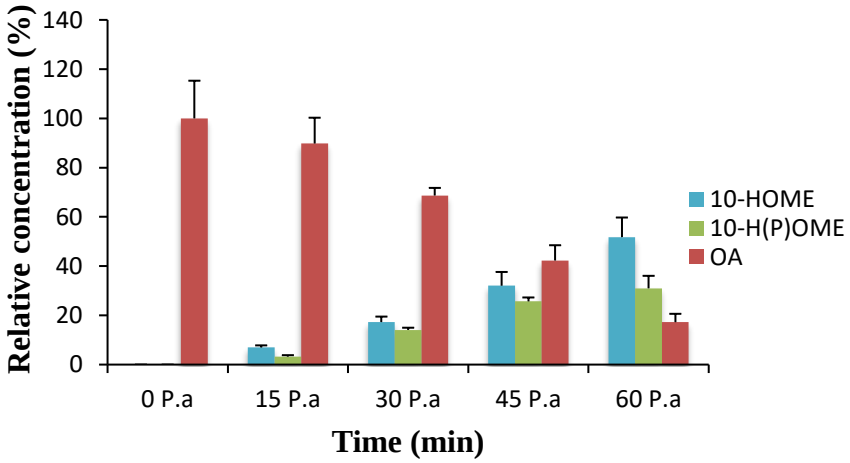

Figure 19. Production of 10*S*-H(P)OME at different incubation times (min). (Plot giving % of relative production of H(P)OME with *P. aeruginosa* (ΔDS/pBBR-77).

As shown although the oleic acid decreased along the incubation time, most of the hydroperoxide formed was converted to 10*S*-HOME (52%) and poor 10S-H(P)-HOME content, about 31% was obtained in the final mixture. With the aim to optimize the production of the needed substrate, another alternative was designed as reported earlier (Estupiñan, M Ph.D., 2015): 10*S*-DOX was cloned and expressed in a recombinant GRAS strain, *P. putida* KT2440 After extraction, the DNA with the fragment containing PA-2077 was subcloned into the vector pBBR and then transformed into *P. putida* KT2440 (see Materials and methods). A positive clone of *P. putida* KT2440/pBBR-77 producing 10S-H(P)-HOME from OA that could analyze by HPLC.

P. putida KT2440 showed promise as a microorganism host for the functional expression of *10S-dox* for biotechnological procedures requiring high conversion yields, mild temperatures, and shorter bioconversion rates, allowing the production of hydroperoxide derivatives from a broad range of long-chain fatty acids, as shown above. The expression of 10*S*-DOX in *P. putida* KT2440/pBBR-77 offers other advantages: *P. putida* is a GRAS organism, whereas *P. aeruginosa*, the native species (*P. aeruginosa* ΔDS/pBBR-77), is not.

In the present work was designed the process of producing 10-H(P)OME from *P. putida* (pBBR-77) by 10*S*-DOX (Fig. 20): the first culture on a nutrient broth of *P. putida* (pBBR-77) was cultivate to obtain biomass. In this step, it was demonstrated that by changing the single experimental factor the aeration by using Erlenmeyer flask, during incubation, *P. putida* (pBBR-77) concentration could be increased. After recovering the biomass, the pellet obtained was concentrated x3 times in Tris-HCl buffer, then the cell suspension was incubated with OA for 10*S*-DOX biotransformation under standard conditions (refer to material and methods). At the end of the incubation time no 10-H(P)OME could not be found in the supernatant.I suggesting that the needed no transport system was present in *P.* putida in contrast with the ExFaDLO system for the export of hydroxy-fatty acids found in *P. aeruginosa* (Martinez et al, 2013). It was necessary to break the cells by sonication to obtain a cell extract before to be incubated with OA at 30 ºC and 150 rpm.

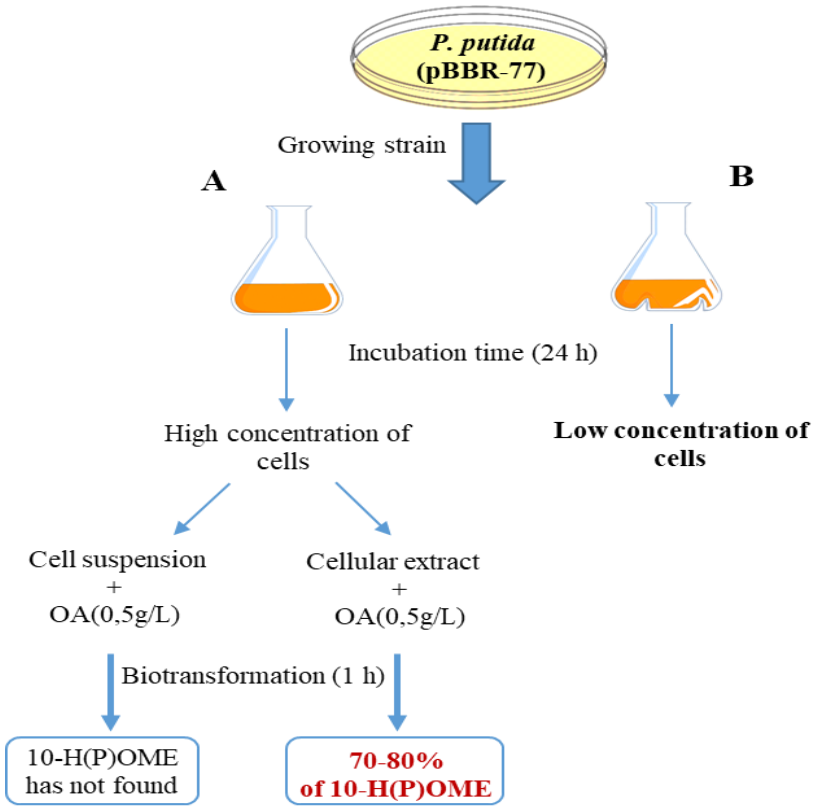

Figure 20. Scheme of the production of 10-H(P)OME from *P. putida* (pBBR-77) by differents methods. As shown 50-80% of 10-H(P)OME produced by cellular extract after biotransformation under standard conditions (refer to material and methods).

As shown in Fig. 20 standard Erlenmeyer flask or baffled flask (see to material and methods); after cultivation, cells were recovered by centrifugation and the biomass contained was higher in those flask incubated in the standard flask (13.60 mg/ml) (Fig. 20A) than in the baffled flask (9.4 mg/ml) (Fig. 20B). These results show the amount of transfer oxygen has a direct effect on the cell growth of *P. putida* (pBBR-77) in the nutrient broth culture.

P. putida (pBBR-77) using an OA concentration of 0.5 g/l produced the maximum amount of 10-H(P)OME and was used to monitor the bioconversion of OA; the 10-H(P)OME relative concentration increased steadily from 30 minutes up to 1 hour (Fig. 21). Small scale (1 ml) of time course 10-H(P)OME production from *P. putida* is presented in Fig. 21, the maximum production was achieved at 60 min (A2. Fig), when a 52% (w/w) conversion yield was achieved and a 30% which was spontaneously reduced to 10*S*-HOME. Products were quantified by HPLC (Fig. 21).

High amount of production of 10-H(P)OME was obtained when the volume of biotransformation was increased (25ml), achieving concentration in the range of 50-80% (Fig. 22).

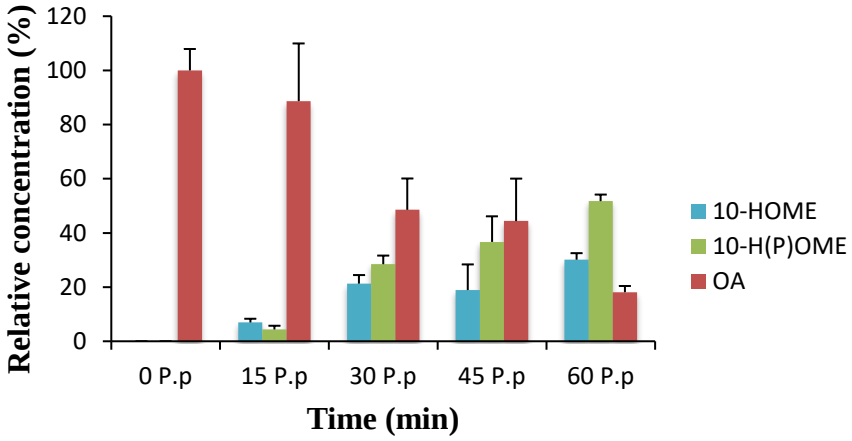

Figure 21. Production of 10*S*-H(P)OME at different incubation times (min). (Plot giving % of relative production of H(P)OME with *P. putida* (pBBR-77)).

The aforementioned benefits might be due to the cellular redox environment of the *P. putida* KT2440 extract, which allows greater stability of 10-H(P)OME than in the homologous host. Previously, *P. putida* KT2440 was evaluated for 10-H(P)OME, 10-HOME and 7,10-DiHOME production by biotransformation assays of OA and using inhouse-produced 10-H(P)OME as a negative control for the presence of 10*S*-DOX and 7,10-DS or other oleate-derived oxylipin-forming enzymes.

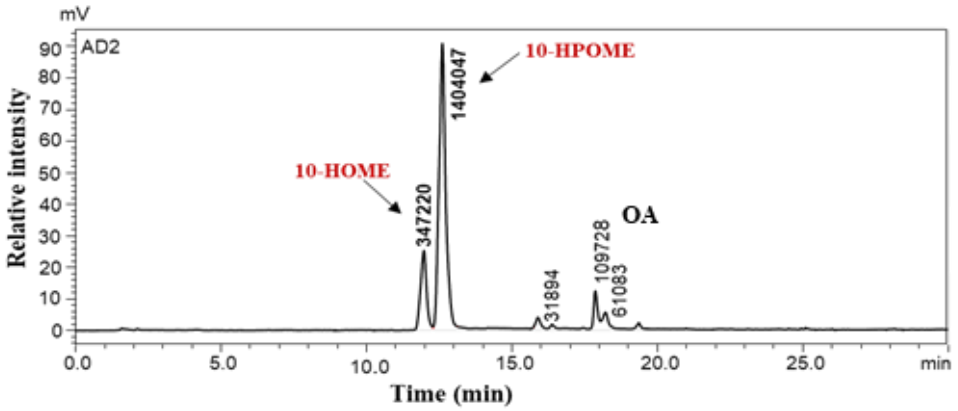

Figure 22. RP-HPLC of H(P)OME production of *P. putida* (pBBR-77) under standard conditions (1 h at 30ºC and 150 rpm).

4.1.3 Biochemical characterization of 10*S*-DOX and 7,10-DS

Activity assays for 10*S*-DOX and 7,10-DS were carried out in 50 mM Tris-HCl, pH 7.0 buffer at 30ºC or other temperatures as stated in the text, with the appropriate concentrations of substrates, OA or 10-H(P)OME, respectively. Expression assays of *E. coli* DH5α/pMMB-10*S*-DOX and *E. coli* DH5α/pMMB-7,10-DS were carried out without any induction at optimal temperature 30 ºC.

4.1.3.1 Time course reaction for 10*S*-DOX activity

The time reaction for the activity of 10*S*-DOX was performed in 50 mM Tris-HCl buffer (pH 7.0) at 30 ºC with a final concentration of 0.4 mM OA. The reaction time between 5-30 min was assayed. The results in Fig 23 indicated the activity of 10*S*-DOX reaching its maximum after 15 min of incubation and enzyme activity decreased after 20 min of incubation. The maximum production of 10-H(P)OME was achieved at 15 and 20 min. In this experiment investigated reaction time of 10*S*-DOX activity, to proceed with forthcoming assays.

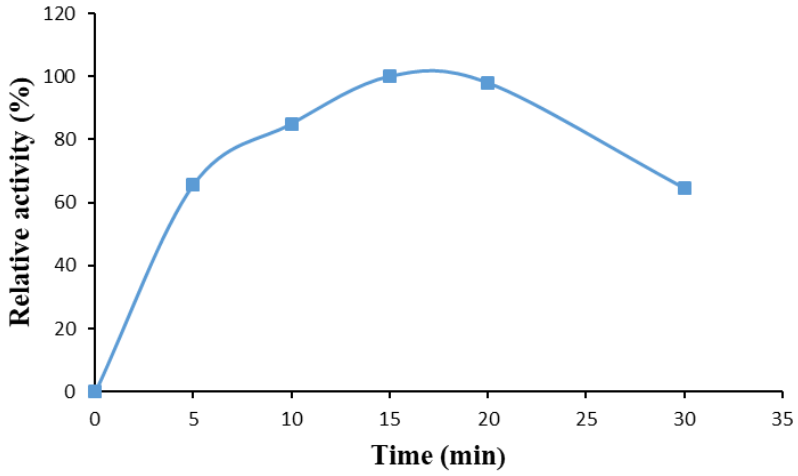

Figure 23. Effects of time reaction on 10*S*-DOX activity at 30 ºC in 50mM Tris-HCL buffer pH 7. The experiment was done by triplicate.

4.1.3.2 Effect of pH on enzyme activity

The effect of pH on enzyme activity was determined at 30ºC at different pH ranging from 5.0 to 10.0 (Fig. 24). The buffer used was Britton-Robinson buffer (20 mM) adjusted to different pH values (5-10) (Britton, 1952). The pH profile changes for 10*S*-DOX are similar pH profile changes for 7,10-DS. Our results also demonstrated that both enzymes have plateaux covering a wide range of pH with maximum activity, from neutral to basic (pH 7.0 to 10.0), demonstrated that pH 7.0 enzyme reached more than 80% of its activity. Below this range, the enzyme activity decreased.

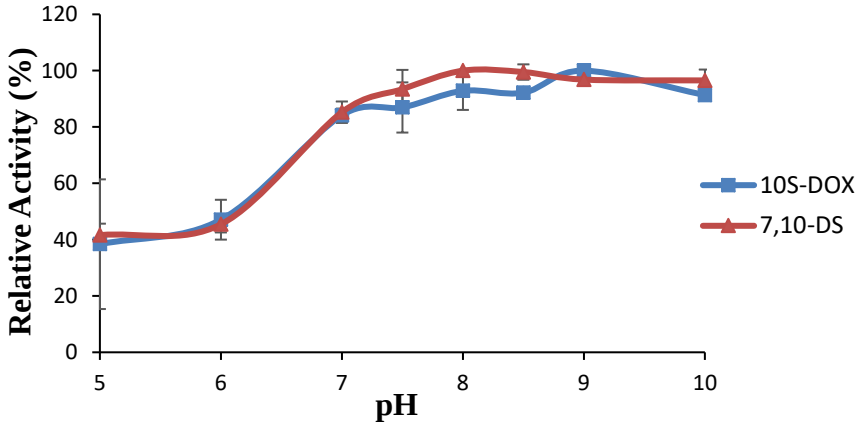

Figure 24. Effect of different pH values of the reaction on 10*S*-DOX and 7,10-DS activity in 20mM Britton-Robinson buffer, pH 5-10.

The similar pH profiles observed for 10*S*-DOX and 7,10-DS might be due to their localization in the same cellular compartment, the periplasm (Martínez *et al.*, 2013). Previous studies have shown optimum pH for most of fungal diol synthase enzymes is between a range of pH 7.0-9.0; the diol synthase of *Glomerella cingulate* with a maximum activity between pH 6.5-7.0 (Seo *et al.*, 2016) or that of *Penicillium chrysogenes*, in dimethyl sulphoxide (DMSO) as solvent pH 8.0-8.5 (Kim *et al.*, 2017b) in the case of the diol synthase of *Aspergillus nidulans* reached optimum pH was 7.0-7.5 (Seo *et al.*, 2014) .

4.1.3.3 Effect of temperature on enzyme activity

The optimal temperature for enzyme activity was determined at a different temperature from 20 to 50 ºC, results indicated enzymes were active at a wide range of temperature. As shown in Fig. 25, The maximum activity of 10*S*-DOX appears as a distinctive peak, whereas for 7,10-DS it is a platform in the range of 30-40 ºC.

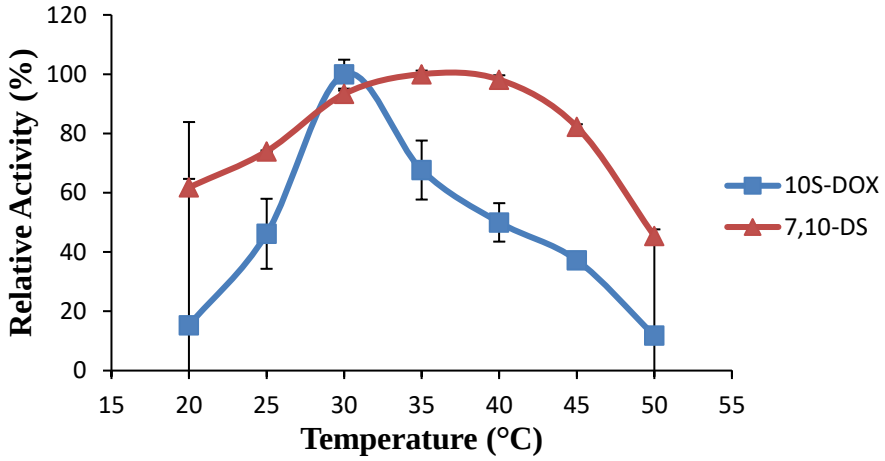

Figure 25. Effect of different reaction temperatures on 10*S*-DOX and 7,10-DS activity.

Whereas 10*S*-DOX activity clear maximum activity at 30 ºC, while no preferred temperature was observed for 7,10-DS in the range of 30-40 ºC. It is noteworthy mention that the relative activity of the 7,10-DS is higher than that of the 10*S*-DOX and at 40 ºC the relative activity of the 7,10-DS is double than in case of the 7-DOX (98% and 49% respectively). The 45% of activity of the 7,10-DS still remained at 50 ºC compared with the relative activity of the 10*S*-DOX at the same temperature (17%). Many studies have shown the maximal conversion rates of the substrate for enzymes that have diol synthase activity at ranging from 25 to 40 ºC: poor information is found in literature from prokaryote dioxygenase or diol synthase; in the case of the 10*S*-DOX, that from *Nostoc punctiforme* and that from *Stenotrophomonas nitrireducens* the optimal temperature is 35 ºC (Kim *et al.*, 2017b; Choi *et al.*, 2015). In eukaryote organism slightly different temperatures are reported, depending on the substrate for the recombinant 8,11-linoleate diol synthase

of *Penicillium chrysogenum, in the case of* oleic acid was 30 ºC (Kim *et al.*, 2017a) in the case of the diol synthase of *Aspergillus nidulans*, the optimal temperature is 35ºC (Seo *et al.*, 2014) while for a recombinant variant, named 8-dioxygenase of *A. nidulans* was 27 ºC (Jeong *et al.*, 2015) and 20 ºC is the maximum activity reported by the 8-dioxygenase of *Glomerella cingulate* (Seo *et al.*, 2016). The highest optimal temperature reported so far is for the 7,8 linoleate diol synthase from *G.* cingulate , 40-45 ºC (Seo et al., 2016) and most of the enzyme losing activity after this range (Seo et al., 2015; Kim et al., 2017).

4.1.3.4 Enzyme stability

To determined thermostability of enzyme, the enzyme activity was analyzed at pH 7.0 by quantification of the residual enzyme activity after pre-incubation of the samples at temperatures ranging from 25 to 60 ºC for 10 min (Fig. 26). As shown, the thermal stability of 7,10-DS is higher than of 10*S*-DOX especially at 25 ºC with 24% more stable than the 10*S*-DOX, at higher temperature treatment the remained activity is about 10% higher.

Both enzymes were unstable over 50ºC and lost about 50% of activity (10*S*-DOX 49.2% and 7,10-DS 54.8%) when they were incubated for 20 min at 30ºC. 10*S*-DOX was more thermostable than 7,10-DS when incubated for 10 min at 25 ºC. Both enzymes of the oleate-diol synthase system were completely inactivated at 70 ºC.

The different profile was reported for the 7,8-linoleate diol synthase and the derived 8-DOX from *G. cingulate*; the later enzyme kept about the 95% of the residual activity until 40-45 ºC whereas the 7,8-linoleate diol synthase exhibited 72% of residual activity (Seo *et al.*, 2016). This could be a critical point for applying the enzymes in industrial processes with harsh conditions.

The thermal instability observed in 10*S*-DOX and 7,10-DS could be because they are intracellular enzymes that have evolved to be active at cellular temperatures in mesophilic hosts such as *P. aeruginosa*. After comparing these results with results of the effect of temperature, indicated in both assays results show the decreasing

activity of enzyme after reaching to 50 ºC, also demonstrated 10*S*-DOX is less stable than 7,10-DS during increasing temperature.

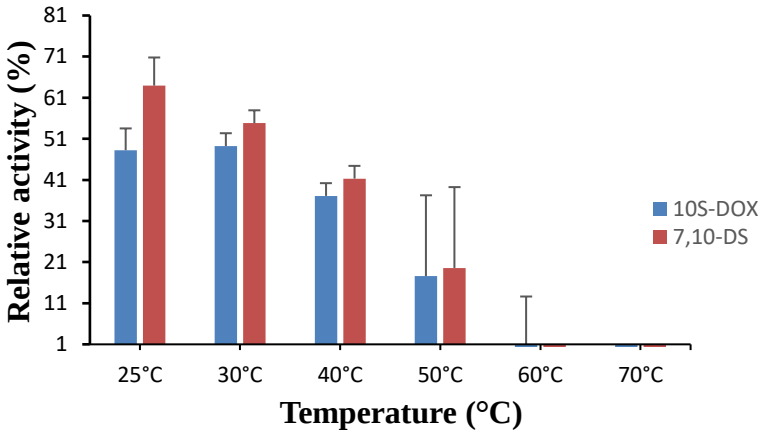

Figure 26. Thermal stability was analyzed by incubating the enzymes (10*S*-DOX and 7,10-DS) at 25-60ºC in 50mM Tris-HCL buffer pH 7. The control refers to non-treated cell extract was measured at 30ºC and represents 100% of enzymatic activity.

4.1.3.5 Effect of divalent cations on enzyme activity

The enzymes 7,10-DS and 10*S*-DOX are di-heme proteins containing two heme prosthetic groups. The heme groups contain an oxidized iron atom Fe^{2+} in the center of a highly hydrophobic planar porphyrin ring that serves as a catalyst in 10*S*-DOX and cytochrome P450s and cytochrome c oxidases (Estupiñán *et al.*, 2015). The potentiating or inhibiting effect of different metal ions on the activity of both enzymes was investigated by adding 1mM concentration of selected metals to the reaction mixture that can act as possible inhibitors or activators of the enzymes.

Under the optimized conditions effect of different divalent cations on enzyme activity were determined (Fig. 27). The results demonstrated most of the metal ions showed different effect on every (10*S*-DOX or 7,10-DS) enzyme activity, in this regard 10*S*-DOX in the presence of Co^{+2}, Hg^{+2} or Zn^{2+} inhibited 6.7, 10.9 and 13.3%, respectively, of its total activity, followed by 21.4% for Ca^{2+}, 26.58 for Mg^{2+} and 29.73 for Ni^{2+}. Whereas in the presence of Fe^{2+} and Mn^{2+} enzyme activity was reduced by approximately to 61.8 and 51.6 %, respectively, the addition of Sn^{+2} reduced enzyme activity to 39.9 %. The activity of 7,10-DS was enhanced (%) by

the addition of Mg^{2+} (27.8%), Sn^{2+} (9.5%), Cd^{2+} (3.2%) and Ni^{2+} (9.0%) and barely affected by Co^{2+} (93.2%) or Fe^{2+} (92.7%). In the case of Ca^{2+} activity remained at 86.4% and was reduced to 54.9% by the addition of Hg^{2+}.

The effect of ions on the enzyme activity was different; 10*S*-DOX activity did not improve in the presence of any of the cation used, compared with the control, whereas the behavior of 7,10-DS varied, Cd^{2+}, Ni^{2+}, Sn^{2+}, and Mg^{2+} enhancing activity being relevant the increase of activity in presence of cadmium and magnesium (Fig. 27) and no ion acting like a complete inhibitor.

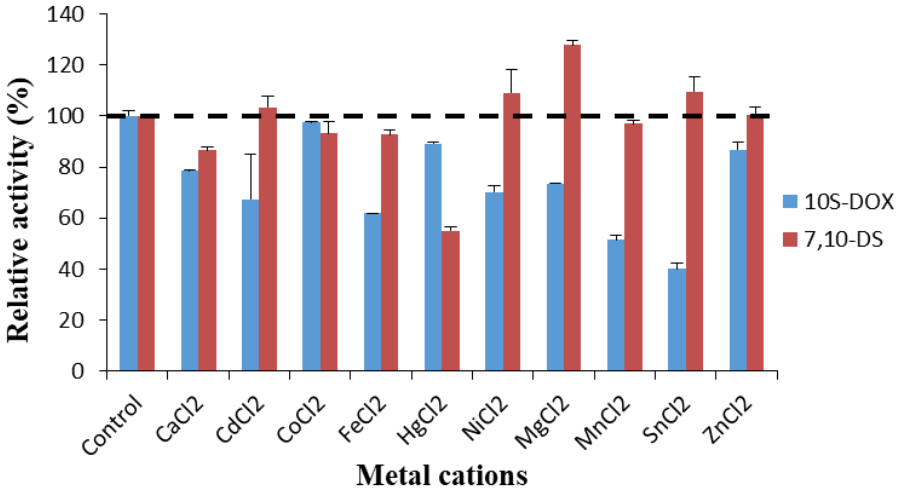

Figure 27. Effect of cations on the activity of 7,10-DS and 10*S*-DOX enzymes. The control was incubated at optimal conditions with no cation addition and is referred to like 100% of enzymatic activity.

4.1.3.6 Kinetics study

Kinetics parameters of both enzymes were determined under suitable conditions of pH and temperature. 10*S*-DOX activity was obtained from clarified cells extracted from *E. coli* DH5α/pMMB-77 in 50mM Tris-HCL buffer pH 7 at 30 ºC at different OA ranging from 0.05-0.35 mM. As depicted in Fig. 28, when the OA concentration was higher than 0.3 mM, the enzyme activity was inhibited by an excess of the substrate and decreased by more than 50% (data not shown).

The Lineweaver-Burk constant, Km, and maximum velocity, V_{max}, of 10*S*-DOX were obtained directly from the linearization of the Lineweaver-Burk equation and their values were 0.89 ± 0.22 mM and 14.7 ± 0.26 Ug^{-1} min^{-1}, respectively.

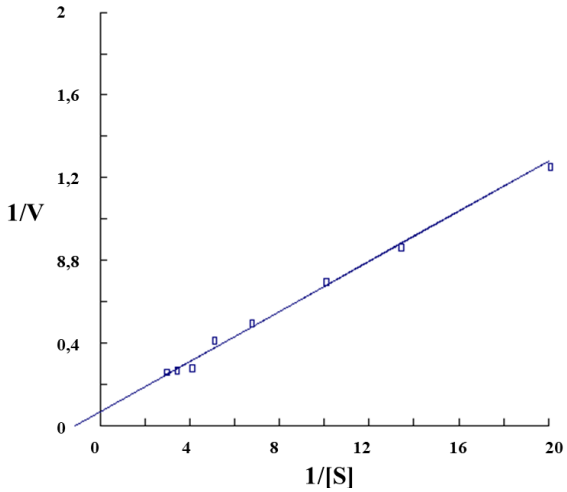

Figure 28. Lineweaver-Burk plot for Km and Vmax values of the 10*S*-DOX enzyme at 30ºC. Assay condition was pH 7 in the presence of different concentrations of OA (0.05-0.35 mM).

For 7,10-DS, obtained from *E. coli* DH5α/pMMB-78, the activity determined at different substrate concentrations (10*S*-H(P)OME) in the range of 0.2-1.2 mM in 50mM Tris-HCl buffer pH 7 at 30 ºC gave a typical Lineweaver-Burk plot, as shown in Fig 29. Kinetic constants were determined from Lineweaver-Burk equation plots in the standard assay conditions (pH 7) with a Km and V_{max} of 3.26 ± 0.31 mM and 54 ± 0.38 Ug^{-1} min^{-1}, respectively.

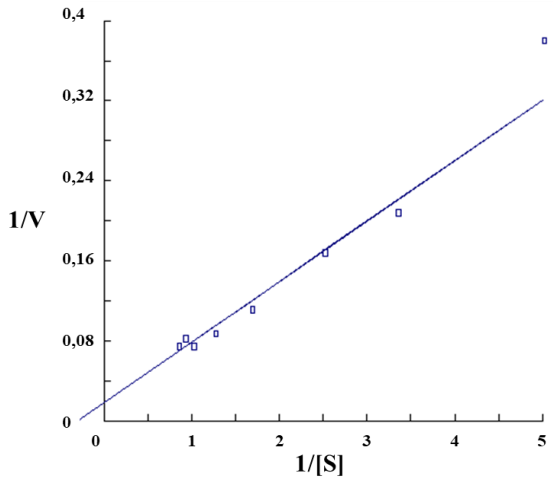

Figure 29. Lineweaver-Burk plot for Km and Vmax values of the 7,10-DS enzyme at 30ºC. Assay condition was pH 7 in the presence of different concentrations of 10-H(P)OME (0.2-1.2 mM).

4.1.4. Screening for oxylipin-producing bacteria

The phylogenetic tree of orthologous diol synthase-encoding genes present in *P. aeruginosa* revealed that the diol synthase operon could be due to a gene duplication event in a common ancestor maintaining an adjacent location, although one of the genes evolved a new function (Estupiñán *et al.*, 2014; Lynch and Katju, 2004). A similar disposition of related genes has been described in cyanobacteria: a cyclooxygenase (10*S*-dioxygenase) that works in tandem with a catalase-related protein, rendering 10S-hydroperoxide lyase activity (Brash *et al.*, 2014), and a bifunctional enzyme, a lipoxygenase with diol synthase activity from the cyanobacteria *Nostoc*, generating (10*E*,12*E*)-(9,14).dihydroxy-(10,12)-octadecenoic acid from linoleic acid (Lang *et al.*, 2008). Considering hydroxy fatty acids are constitutive components of living organisms with structural and functional roles (Senger *et al.*, 2005), and with the aim of studying the scope of diol synthase activity in the bacterial kingdom, 23 different species of environmental proteobacteria belonging to 6 genus with similar habitats; water, soil and plant interaction were tested using oleic acid as substrate (A3-A4.5 Fig). Some of the bacteria screened were selected based on the phylogenetic proximity with *P. aeruginosa* (Fig. 30) and others have previously given positive distant matches

(*Thauera aminoaromatica* and *Ensifer fredii*) (Estupiñán *et al.*, 2014). Amino acid sequence alignment of PA2077 and PA2078 proteins in *P. aeruginosa* identified several significant motifs or specific residues related to heme/iron-binding sites or relevant in oxygenation reaction (Estupiñán *et al.*, 2015), multiple amino acid sequence alignment of PA2077 and PA2078 among this 6 genus could find similar consensus motif such as concerved heme sequences (CXXCH), ferrous ion union (EGR), P450 motifs (EXXR) and the essential histidine of oxidases (MauG) that in *Shewanella, Pseudoalteromonas, Ensifer and Pseudomonas* as identified before in *P. aeruginosa* (A5-A5.3. Fig).

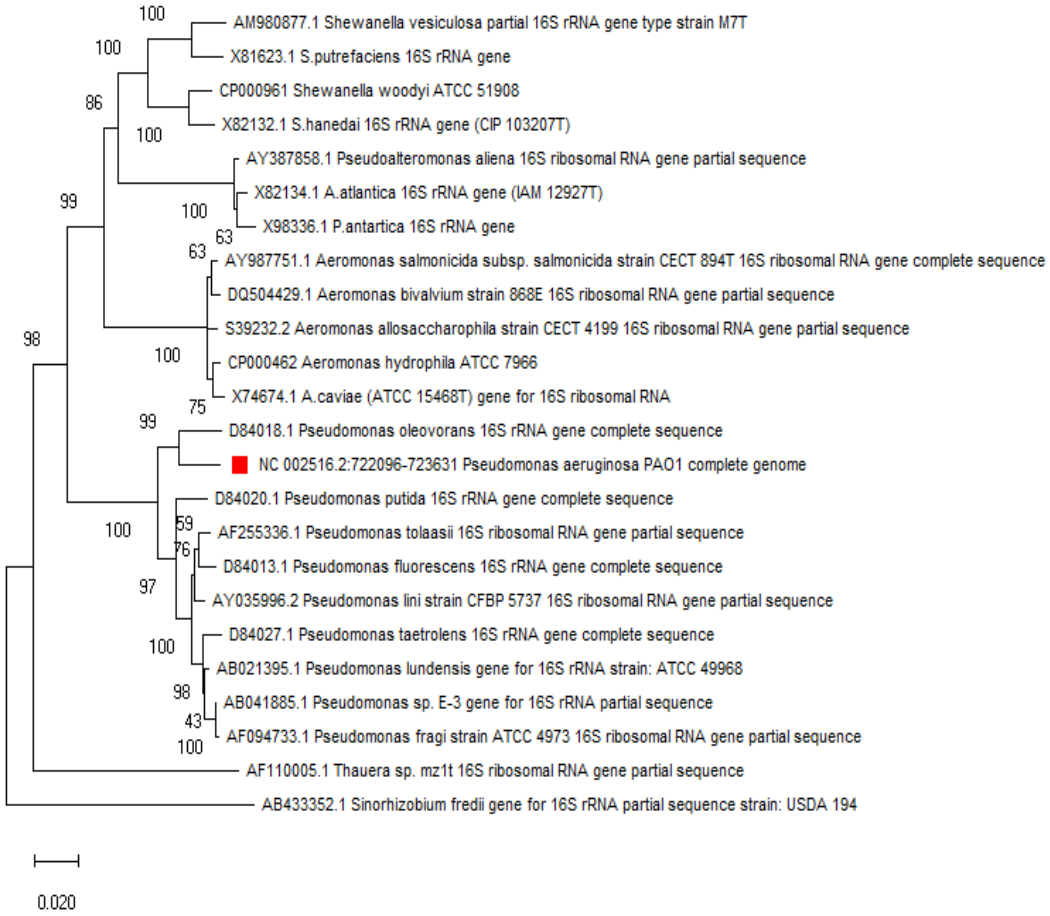

Figure 30. Phylogenetic tree of the related strains screened for oxylipins production. Phylogeny reconstruction in the 16S rRNA region. *Pseudomonas aeruginosa* (labeled in red) as control species.

After grown under suitable conditions (see material and methods section), analysis of the organic extract by RP-LC-MS/MS revealed that whether these bacteria have

the putative ability to produce the same oxylipins (10-H(P)OME and 7,10-DiHOME) from OA as found in *P. aeruginosa*. In Table 4 is shown the first report so far of bacterial strains assayed to detect the diol synthase pathway. As observed most of the bacterial assayed 10*S*-hydroxy-8E-octadecenoic acid (10-HOME) was detected; as mentioned above that product is a side compound from the spontaneous reduction of 10-H(P)OME. *Pseudomonas putida* and *P. psycrophyla* although grown on suitable conditions, could not transform oleic acid into the selected oxylipins. Briefly, after a full scan of the total ion current (TIC) from *m/z* 100-800, in the MS^2 analysis *m/z* 297.2 and *m/z* 313.2, and in the MS^3 analysis (*m/z* 313.2→*m/z* 295.2) were selected for 7,10-DiHOME and 10-H(P)OME discrimination (A6-A6.6. Fig), the strains that appeared in Table 4.

Table 4. Products detected in the supernatant due to the transformation of oleic acid by selected proteobacteria. H(P)OME: 10S hidroperoxid-8E-octadecenooic acid; HOME: 10S-hydroxy-8E-octadecenoic acid; DiHOME: 7,10dihydroxy-8E-ocatadecenoic acid.

Strains	H(P)OME	HOME	DiHOME
Aeromonas allosaccharophila CECT 4220	-	**x**	**x**
Aeromonas caviae CECT 4226	**x**	**x**	**x**
Aeromonas bivalvium 868E	**x**	**x**	**x**
Aeromonas hydrophila CECT 839	-	**x**	**x**
Aeromonas salmonicida CECT 894	**x**	**x**	**x**
Pseudoalteromonas atlantica CECT 579	**x**	**x**	**x**
Pseudoalteromonas aliena DSM16473	-	**x**	**x**
Pseudoalteromonas antarctica DSM151318	**x**	**x**	**x**
Shewanella woodyi DSM12036	**x**	**x**	**x**
Shewanella putrefaciens ATCC 8071	-	**x**	-
Shewanella vesiculosa CECT 7339	**x**	**x**	-
Shewanella hanedai ATCC 33224	**x**	**x**	**x**
Pseudomonas lini DSM 16768	-	**x**	**x**
Pseudomonas tolassi ATCC 33618	-	**x**	**x**
Pseudomonas taetrolens DSM 21104	-	**x**	**x**
Pseudomonas fluorescens CECT 844	**x**	-	**x**
Pseudomonas fragi DSM 3456	-	**x**	**x**
Pseudomonas lundensis DSM 6252	-	**x**	-
Pseudomonas oleovorans ATCC 8064	-	-	-
Pseudomonas psychrophyla DSM 17535	-	-	-
Pseudomonas putida ATCC 12633	-	-	-
Thauera. aminoaromatica DSM 25461	**x**	-	-
Eisinfer fredii DSM 5924	**x**	-	**x**

Using *P. aeruginosa* as a positive control, the activity of 10*S*-DOX was determined by the analysis of the spectrum of the released product. The MS^2 spectrum of 10-H(P)OME from the OA conversion produced signals at *m/z* 155.279 (Fig. 31A) and the MS^3 spectrum of 10-H(P)OME gave predominant signals at *m/z* 155.179; 51.277 (Fig. 31B).

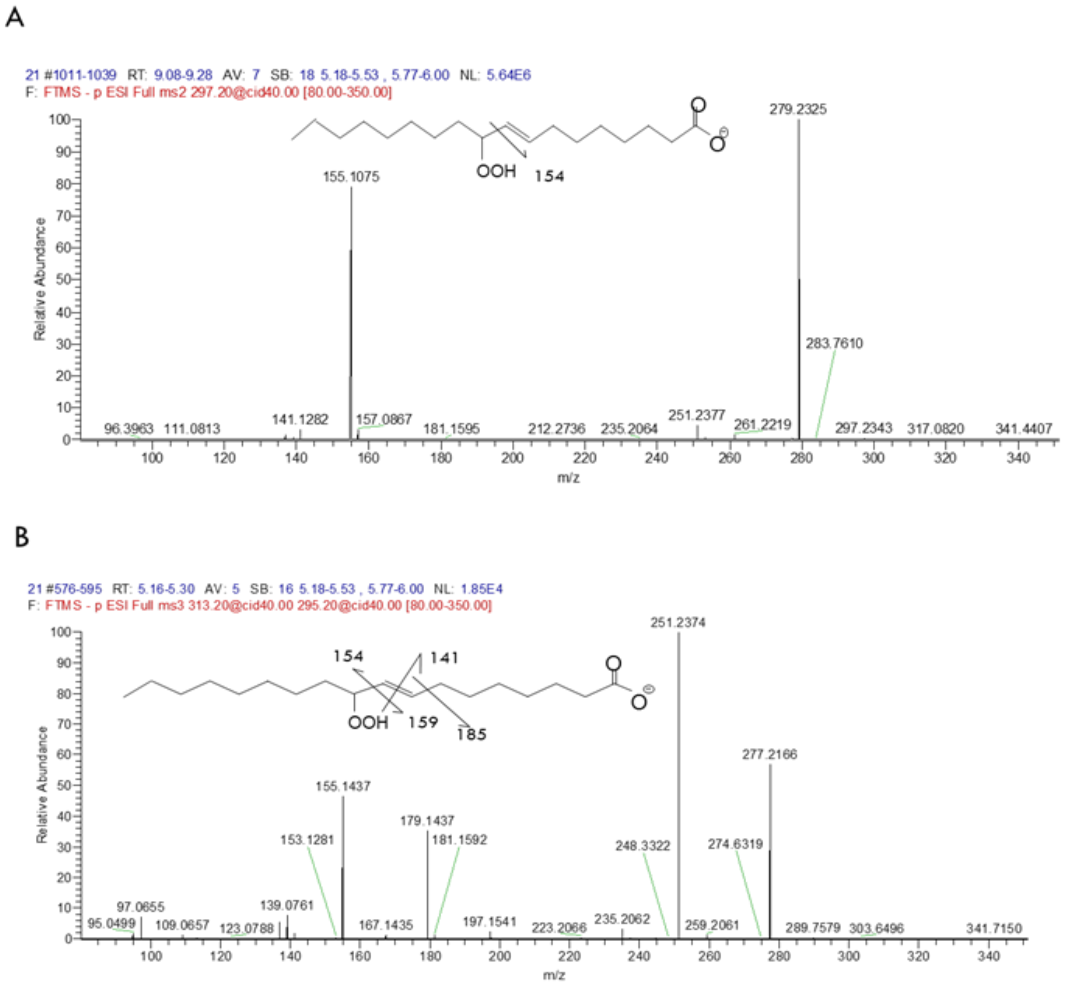

Figure 31. LC-MS/MS spectra of 10-H(P)OME produced by *P. aeruginosa*. (A) MS^2 spectrum producing signals at *m/z* 155.279. (B) MS^3 spectrum producing signals at *m/z* 155.179 and 251.277.

The corresponding ions of 7,10-DiHOME obtained from the conversion of 10-H(P)OME from MS^2 spectra were found at *m/z* 251, 293, 295, and 314 (Fig. 32A) and prominent signals from the 7,10-DiHOME MS^3 spectrum were found at *m/z* 155,

179, 251, and 277 (Fig. 32B). All spectrographic analyses match the data obtained previously for these compounds (Nilsson *et al.*, 2010).

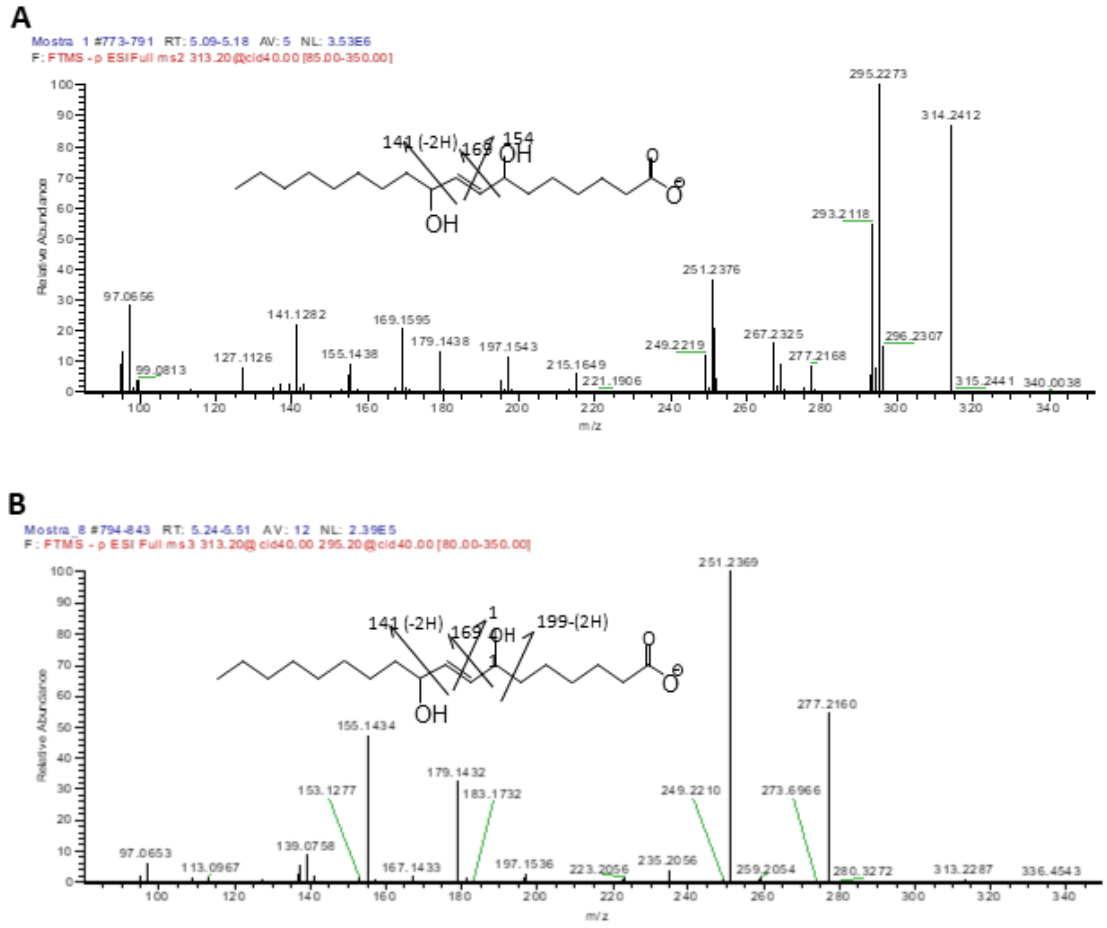

Figure 32. LC-MS/MS of 7,10-DiHOME obtained from the diol synthase activity of *P. aeruginosa*. (A) MS^2 spectrum with fragments at *m/z* 251.293 and 251.314. (B) Signals of MS^3 found at *m/z* 155, 179, 251 and 277.

Diol synthase activity was also found in other species of *Pseudomonas.* As shown in Fig. 33A, when the cell extract of *P. tolassi* or *P. taetrolens* was incubated with OA, 10-H(P)OME) was found in the supernatant, being the catalytic product of 10S-dioxygenase. In the case of *P. lini* or *P. fluorescens*, the LC-MS-MS spectra of the products revealed 10-H(P)OME and 7,10-DiHOME (Fig. 33). The MS^2 spectra of 10-H(P)OME (m/z 313→full scan) (Fig. 33A) and the MS^3 spectra of 7,10-DiHOME (m/z 313 full scan →295) (Fig. 33B) suggest the presence of the functional proteins of 10S-,dioxygenase (10*S*-DOX) and 7,10-diol synthase (7,10-

DS). Although the incubation of the cellular extract of *P. fragi* or *P. lundensi* with OA rendered only 7,10-DiHOME, the complete diol synthase system was active in these strains considering the reaction sequence.

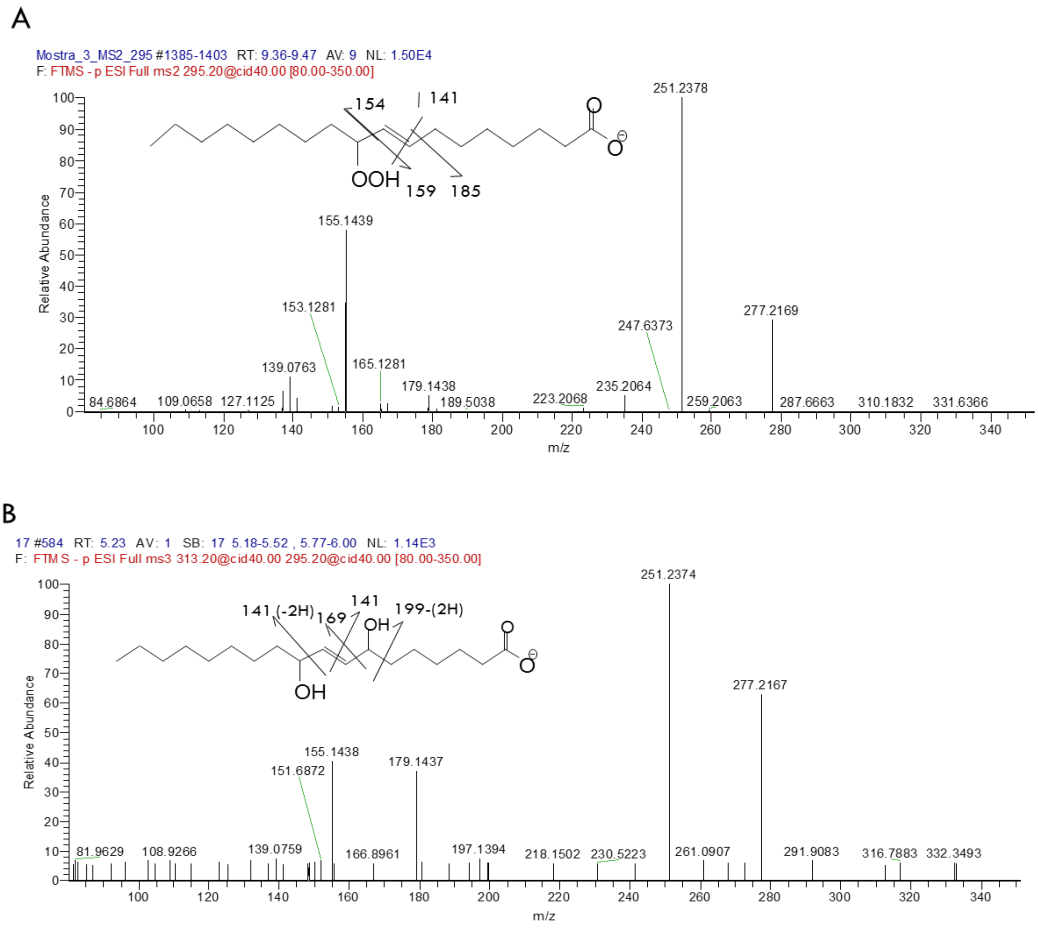

Figure 33. LC-MS/MS spectra of 10-H(P)OME and 7,10-DiHOME in the products found when the cellular extract of *Pseudomonas fluorescens*, *P. lini*, *P. taetrolens* and *P. tolassi* were incubated for 30 min with oleic acid.

Several species of *Aeromonas* were also screened for diol synthase activity. Cellular extracts of *A. allosaccharophila*, *A. bivalvium*, *A. caviae*, and *A. salmonicida* were incubated with OA for 30 minutes, and two oxylipins derived from OA,10-H(P)OME and 7,10-DiHOME were detected in the supernatant. The corresponding spectra are shown in Fig. 34. H(P)OME (m/z 313→full scan) was identified after analysis of the MS^2 (Fig. 34A) and 7,10-DiHOME (m/z 313 full scan →295) after analysis of the MS^3 (Fig. 34B). In the supernatant of *A. hydrophila* and *A.*

allosacchariphila only 7,10-DiHOME was detected, although there were indications that the complete functional diol synthase system was present, since as stated earlier the substrate for 7,10-DS is the product of the first reaction catalyzed by 10*S*-DOX.

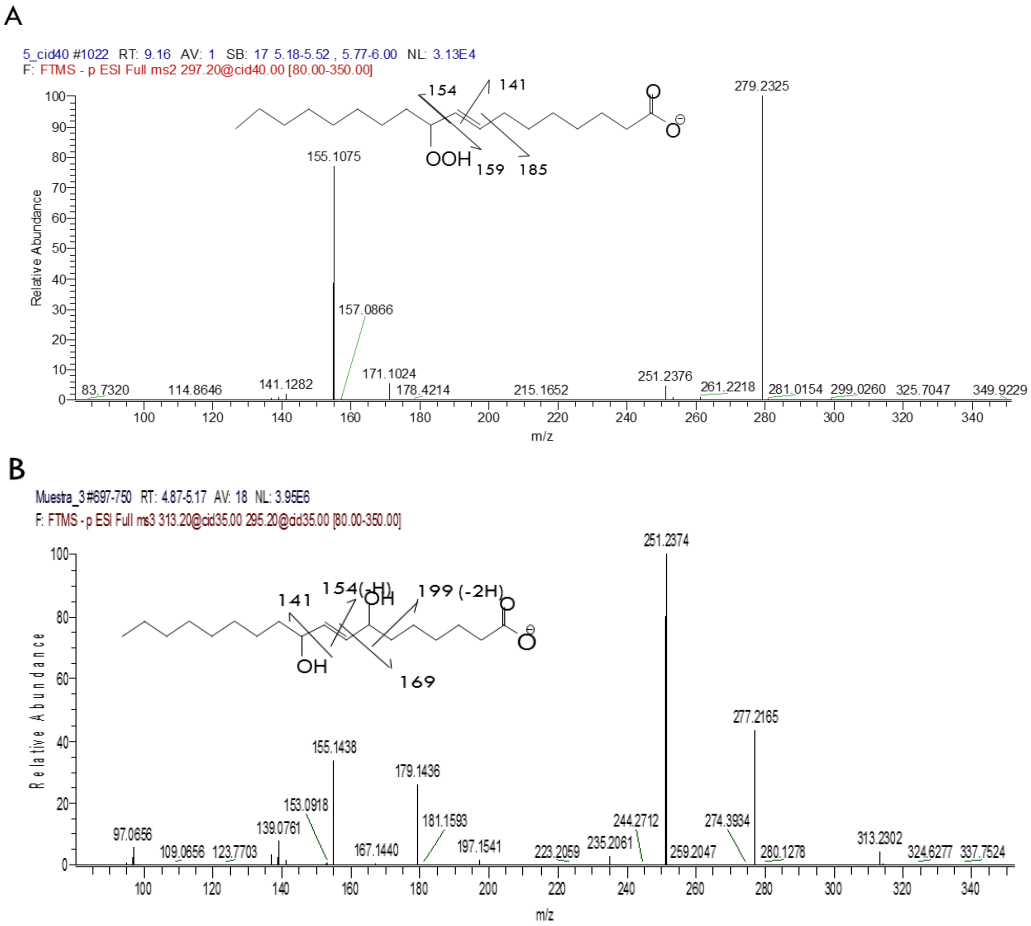

Figure 34. LC-MS/MS of 10-H(P)OME and 7,10-DiHOME obtained from the diol synthase activity of different *Aeromonas:* (A) MS^2 spectrum of H(P)HOME with fragments at *m/z* 155 found with the cell extracts of *A. allosaccharophila* and *A. hydrophila*; (B) MS^3 signals of 7,10-DiHOME found at *m/z* 155, 179, 251, and 277 for *A. bivalvium, A. caviae, A. salmonicida.*

The diol synthase system was detected in the screened cellular extracts of *Pseudoalteromonas*, since 10-H(P)OME and/or 7,10-DiHOME were found. Products from the cellular extract of *Pseudoalteromonas antarctica* grown in TSB at 20 ºC showed the MS^2 spectra of 10-H(P)OME (m/z 313→full scan) (Fig. 35A), whereas in the case of *P. aliena* and *P. atlantica* the product released displayed the MS^3 spectra of 7,10-DiHOME (m/z 313 full scan →295) (Fig. 35B).

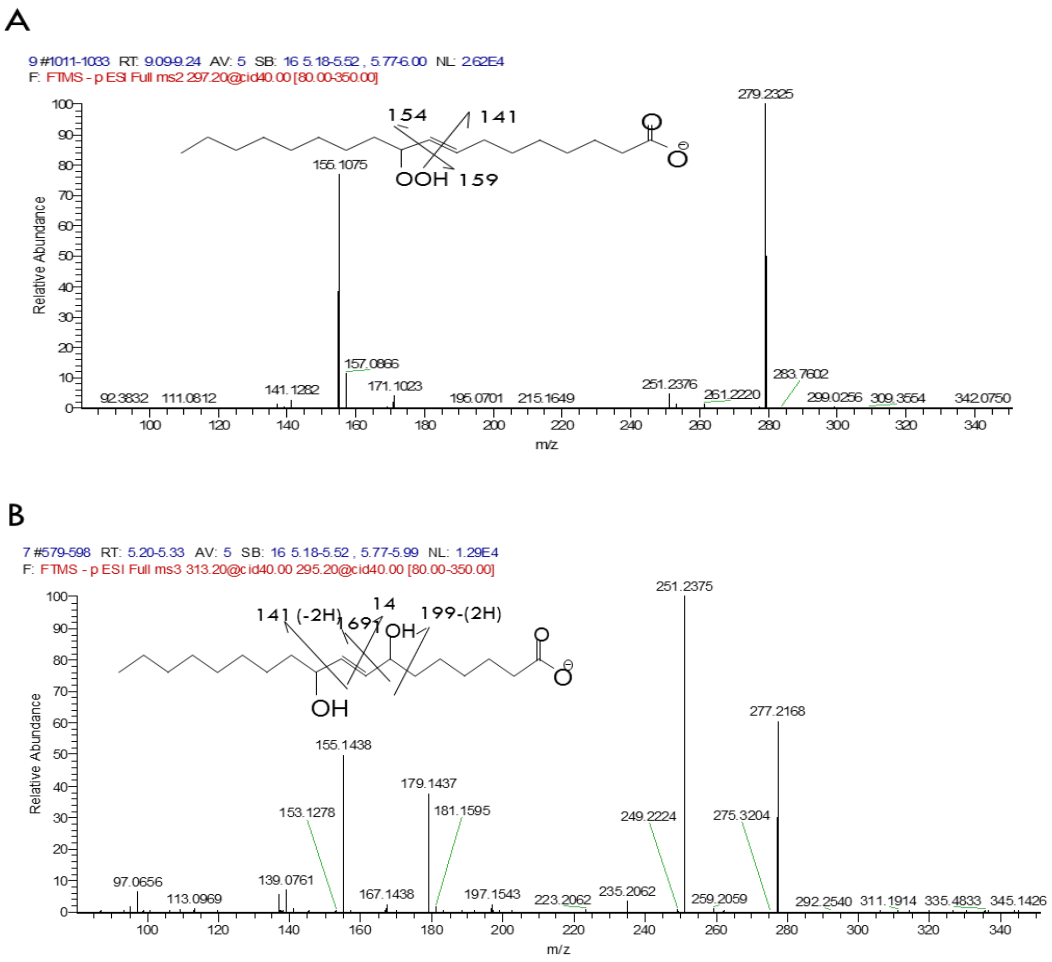

Figure 35. LC-MS/MS spectra for the products obtained by *Pseudoalteromonas antarctica* and *P. aliena*. A) MS^2 spectra of 10-H(P)OME obtained from *P. antarctica.* B) MS^3 spectra of 7,10-DiHOME obtained from *P. atlantica.*

A different range of products was found when assaying species of *Shewanella.* After incubation, the cell extracts of *S. woodyi and S. hanedai* released 10-H(P)OME and 7,10-DiHOME.The MS^2 spectra for H(P)OME (m/z 313→full scan) are shown in Fig. 36A and the MS^3 spectra for 7,10-DiHOME (m/z 313 full scan →295) in Fig. 36B. With *S. vesiculosa* and *S. putrefaciens* only H(P)OME was detected (Fig. 36A).

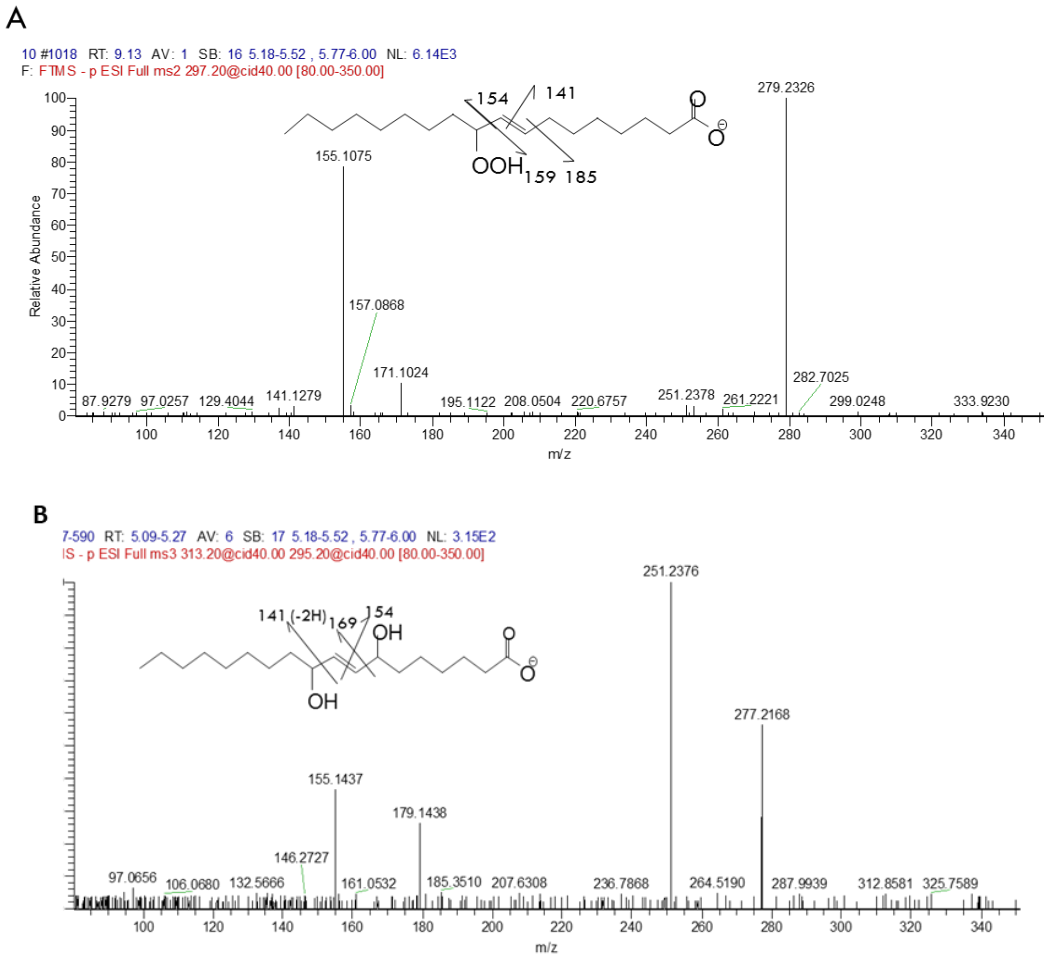

Figure 36. LC-MS/MS spectra for the products obtained by *Shewanella* species assayed. A) MS^2 spectra of 10-H(P)OME obtained from *S. woodyi* and *S. hanedai*, *S. vesiculosa* and *S. putrefaciens.* B) MS^3 spectra of 7,10-DiHOME obtained from *P. atlantica.*

In the *Ensifer fredii* cell extract incubated with OA, both (H(P)OME and 7,10-DiHOME) were detected. The MS^2 spectra of 10-H(P)OME (m/z 313→full scan) are depicted in Fig. 37A and MS^2 spectra of 7,10-DiHOME (m/z 313→full scan in Fig. 37B.

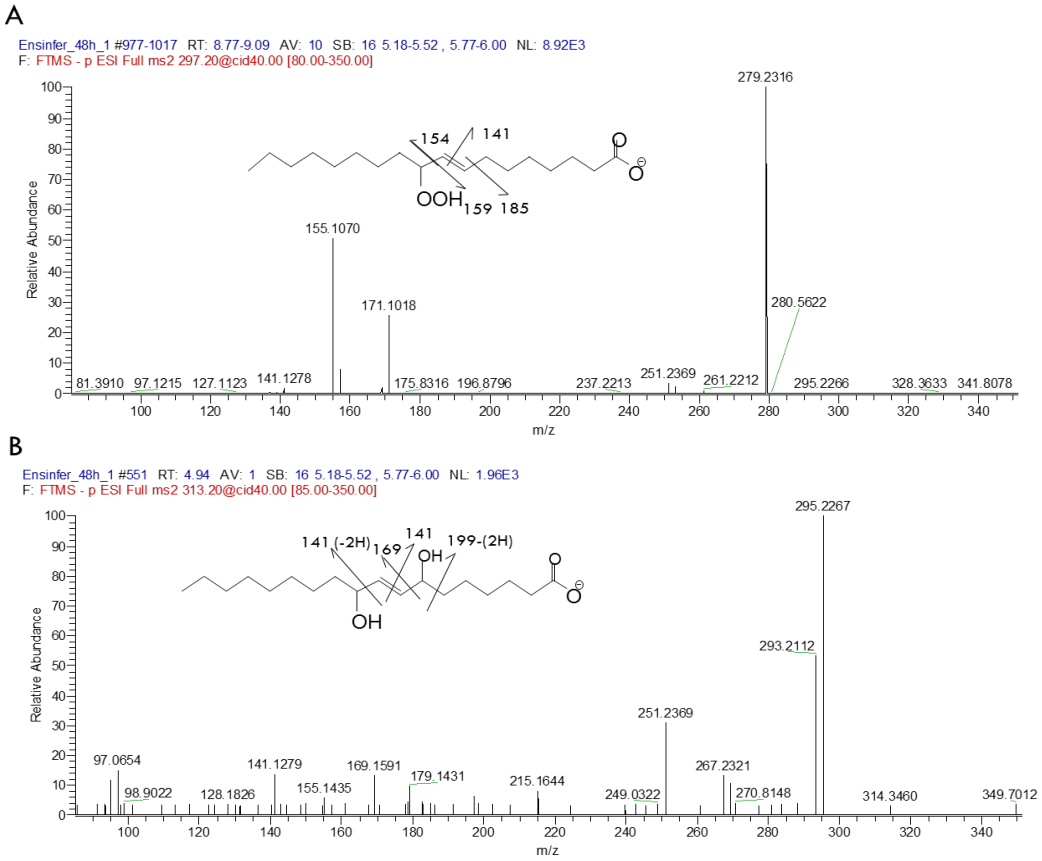

Figure 37. LC-MS/MS analysis of A) 10-H(P)OME and B) 7,10-DiHOME obtained by *Enifer fredii.*

It has also been reported that the diol-synthase activity might have evolved from a common ancestor (orthologs) or by lineage-specific duplication (in paralogs). It was predicted that in the β-proteobacteria *Thauera aminoaromatica*, with a similar relation to the ORF PA2078-PA2077 of *P. aeruginosa*, also a γ-proteobacteria was detected (Estupiñán *et al.*, 2014). As shown in Fig. 38, the incubation of the cell extract of *T. aminoaromatica* rendered (10-H(P)OME).

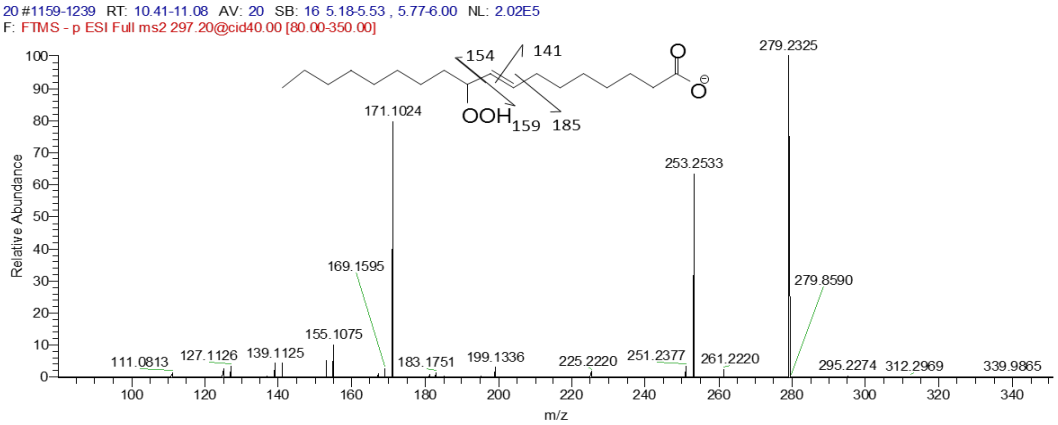

Figure 38. MS^2 spectrum of the 10-H((P)OME released by *Thauera aminoaromatica.*

For the first time, an experimental screening demonstrated the presence of an enzymatic system producing same hydroxyl-fatty acids than the oleate diol synthase pathway first described in *Pseudomonas aeruginosa*, consisting in two single enzymes, 10S-Dioxygenase (10*S*-DOX) which catalyse oleic acid (OA) into 10S-hidroperoxid-8E-octadecenoic acid H(P)OME and a second enzyme a 7,10 (*S*,*S*) Diolsynthase converting the hydroperoxide H(P)OME into 7,10-DiHOME. This results demonstrated that the diol synthase system is not restricted to *Pseudomonas aeruginosa.*

4.2 Functional and structural characterization of the inclusion body produced by over expression of 10*S*-DOX and 7,10-DS

In our previous studies, recombinant soluble enzymes (10S)-dioxygenase (10*S*-DOX) and 7,10-hydroperoxide-diol synthase (7,10-DS), which belong to the oleate-diol synthase metabolic pathway, were expressed in *E. coli* DH5α/ pMMB-77 and *E. coli* DH5α/ pMMB-78.When gene *PA2077* and *PA2078* corresponding to the enzymes (10S)-dioxygenase (10*S*-DOX) and 7,10-hydroperoxide-diol synthase (7,10-DS), were cloned in *E. coli* DH5α (pMMB-77) and *E. coli* BL21 (pET 28a-78) and induced by IPTG, the recombinant enzymes were over-expressed as inclusion bodies (Estupiñan, M Ph.D., 2015).

Here we studied the kinetics of IB formation by different techniques. Structure and morphology were characterized by transmission electron microscopy (TEM), size distribution analysis by atomic force microscopy (AFM), hydrolyzing structure of amyloids by proteolytic degradation (PK), Fourier- Transform Infrared spectroscopy (FT-IR) and Congo Red (CR) and Thioflavine (Th-T) dye binding assays were used to detect β-sheets in amyloids.

4.2.1 Occurrence and protein activity

The formation of heterologous proteins requires a great deal of cellular machinery, including cellular proteases and chaperones (Tyedmers *et al.*, 2010; García-Fruitó *et al.*, 2011). Additionally, cultural conditions such as environmental factors (temperature, pH), solution (buffers, ionic strength) or processing (expression, purification) may result in inclusion body (IB) formation (Wang *et al.*, 2010). A high rate of expression of a heterologous protein produces a stressful situation for the host cell, with high transcription or translation rates creating a bottle neck, although the response of the bacterial cell might be determined by the characteristics of the newly formed protein (Gasser *et al.*, 2008). The heterologous production of *E. coli* DH5α/pMMB-77 produced a fraction of 10*S*-DOX expressed as an insoluble protein (IBs-77); the 7,10-DS expressed in *E. coli* BL21-pET28a-78, the enzyme, 7,10-DS was also found mostly in IBs (IBs-78) (Fig. 39 lanes 1,2 respectively).

For a long time, IBs were considered to be inert deposits of inactive protein. The first evidence of enzymatic activity of IBs (Worrall and Gross, 1989) was a β-galactosidase expressed in *E. coli* and soon after it was discovered that IBs are reversible (Carrió and Villaverde, 2001; Carrió and Villaverde, 2002; Peternel and Komel, 2011; Rinas *et al.*, 2017). Moreover, IBs are fully stable for a long period at -20 ºC or at room temperature. These discoveries have prompted a growing research focus on IBs, therefore, attention was focused on the new IBs (IBs-77 and IBs-78) found.

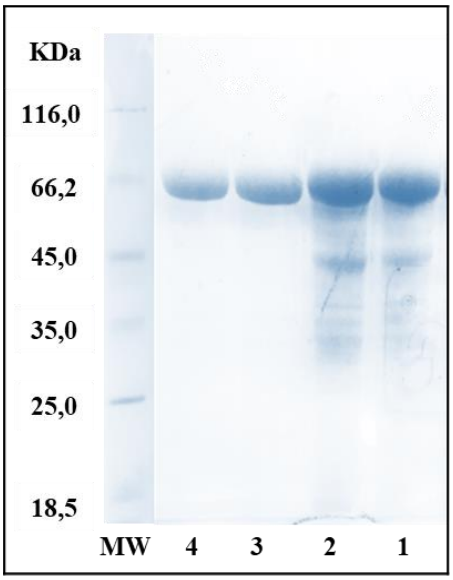

Figure 39. The SDS-PAGE analysis of DH5α (pMMB-77) and BL21 (pET 28a-78) overexpression in E. coli. Lane 1, crude IBs-77; lane 2, crude IBs-78; lane 3, refolded IBs-77; lane 4, refolded IBs-78 in PBS buffer containing 2M of urea. MW, molecular weight marker.

The aggregate protein formation depends on several parameters, such as the nature and overloading of the protein and the diffusion–limited process, and the amount of misfolded protein varies considerably. A foot-and-mouth disease virus protein (VP1-GFP) was reported to represent 80% of the cytosolic protein (Morell *et al.*, 2008), which is far higher than the 1.5-3% reported for *E. coli* (Tyedmers *et al.*, 2010). The amount of protein found as IBs was about 77% for IBs-77 and 75% for

IBs-78. The specificity in protein aggregation means IBs can be a source of highly pure enzymes and are therefore enriched in the recombinant protein itself. However, truncated peptides and/or other proteins or fragments of nucleic acids might be entrapped in the aggregates. On the other hand, the particulate particles favour the extraction of the heterologous protein (Gasser *et al.*, 2008).

After the purification of crude IBs which consisted of several steps, including lysozyme cell lysis, detergent washing and sonication followed by centrifugation and washing (see Materials and methods), only 14.6% and 21.78% of the protein was recovered for 10*S*-DOX and 7,10-DS, respectively; that is 6.9 and 4.6 fold. As seen pure IBs-77 represent 11.15% of the total cellular protein and IBs-78 the 16.43% (Table. 5).

Table 5. Protein concentration obtained in the production of inclusion bodies.

	IBs-77	**IBs-78**
Total protein (mg/ml)	7.8	8.52
Soluble protein in supernatant	1.8	2.12
Crude IBs (mg/ml)	6.0	6.4
Pure IBs (mg/ml)	0.87	1.39
Fraction of pure IBs protein (%)	11.15	16.43
Refolded protein (mg/ml)	0.33	1.33

As shown in Table 6, the specific activity of the supernatant after cell lysis due to soluble enzyme was very low in both cases (0.8×10^{-3} UI/mg). Most of the activity was recovered in the crude IBs: 1.55 UI/mg in IBs-77 and 1.00 UI/mg for IBs-78; as shown, (Table 6) IBs-77 lost part of the activity during the purification process since the specific activity of pure IBs-77 decreased after purification to 1.0 UI/mg whereas for Bs-78, the specific activity of pure IBs-78 increased to 2.2 IU/mg for IBs-78. After solubilization and refolding 4.7% of the activity was recovered in the case of IBs-77, although most of the aggregates were recovered as soluble enzyme while no activity was recovered in the case of refolded IBs-78.

Table 6. Enzymatic activities of the 10S-dioxygenase and 7,10 (S,S)-diol synthase, inclusion bodies.

Functional protein	**Refolded protein/IBs (%)**	**Specific activity UI/mg**				**Recovered activity (%)**
		Supernatant soluble protein	crude IBs	Pure IBs	Refolded protein	
10S-DOX	38.0	0.8×10^{-3}	1.55	1.05	0.05	4.7
7,10-DS	95.6	0.8×10^{-3}	1.00	2.2	nd*	0

* not detected

These activities reflect that the protein inactivation during *in vivo* protein aggregation is only moderate and aggregation does not necessary compromise the active center of the enzyme (García-Fruitós *et al.*, 2005). The formation of IBs appeared soon after induction hydrated deposits of protein (95%) with small amounts of cellular material (DNA, RNA, truncate peptides and lipids) (García-Fruitós *et al.*, 2009). From the structural point of view, the activity found in IBs is due to the kinetics of the aggregate formation and the nature of the protein; IBs consist partly of misfolded protein and partly of properly folded protein, biologically active but trapped in the network formed by the aggregate polypeptides (Peternel and Komel, 2011). As stated elsewhere, the aggregation-disaggregation occurs simultaneously in side cells as a dynamic event (García-Fruitõs *et al.*, 2011).

On the premise of this plasticity and the advantage that inclusion bodies are almost pure proteins as shown in Fig. 39, IBs-77 and IBs-78 were refolded and checked for enzyme activity. There are a diversity of methods to solubilize IBs to a stable, native, folded active protein; the rate might depend on the effects of ionic strength, dialysis, high hydrostatic pressure, and cation exchange resin for solid-phase extraction (Ramón *et al.*, 2014). The freeze-thawing method was chosen as it allows efficient and mild solubilization of IBs, which preserve native-like secondary structures of proteins, and improves the recovery of bioactive proteins from IBs (Qi *et al.*, 2015). As shown in Table 6, although the refolded protein of the IBs-77 accounted for 38% of the aggregated protein, but very low activity was detected (0.05% UI/mg). In the case of IBs-78, although 95.6% of the complete solubilized protein was achieved,

no activity was found, the refolding and the recovery of the activity seems to be a complex affair, and different parameters and strategies are required for an optimal recovery (Vallejo and Rinas, 2004; Villaverde *et al.*, 2015).

4.2.2 "*In vivo, in vitro"* Morphology of inclusion body

Thin slides of cell cultures were observed by transmission electron microscopy (TEM) to locate the aggregates within the cell and to measure their size and morphology. As can be seen in Fig. 40, the protein aggregates of IBs-77 appear as dark dense regions in the periphery of the cell, and more than one IB can be observed (Fig. 40A-C); the size ranged between 214.28 nm and 460.5 nm. Although IBs are predominantly located at the cell poles (Wu *et al.*, 2011), the position of IBs in the prokaryote cell is not completely understood (Tyedmers *et al.*, 2010; Zhou *et al.*, 2012), aggregates found in the middle of the cell located in near of the septation will occur (Rinas *et al.*, 2017).

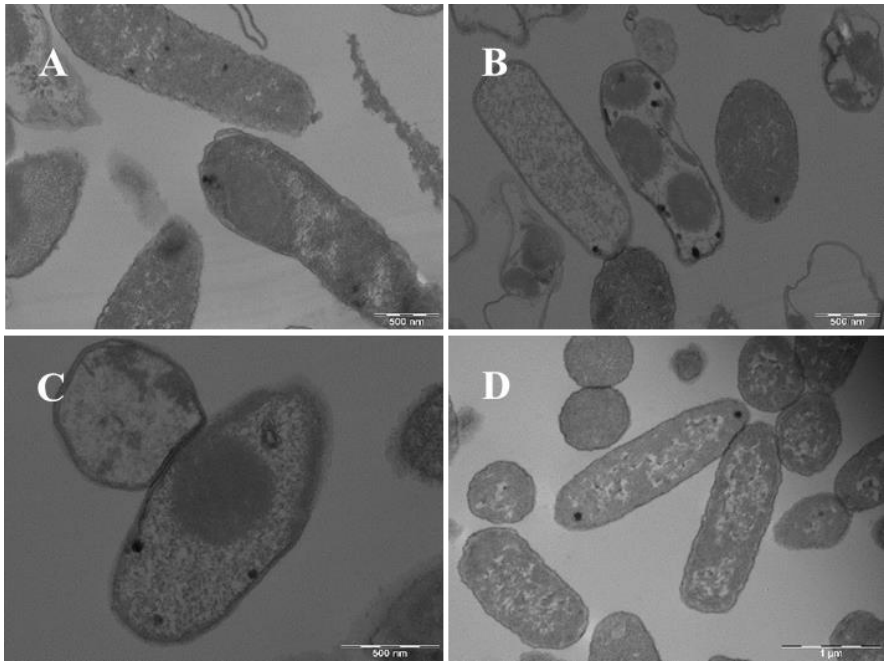

Figure 40. (A, B, C) Transmission electron microscopy images of induced cells of DH5α (pMMB-77) and (D) non-induced native cells of DH5α (pMMB-77).

The prokaryote cell is devoid of compartments and proteins are synthesized in multiple locations; it seems that the growth of the nucleation seed is quick and when it is saturated, new ones are formed. The aggregation mechanism varies according to the expressed protein (Upadhyay *et al.*, 2012; Peternel and Komel, 2011).

The *in vivo* IBs-78 (Fig. 41) appeared more compact and darker than the IBs-77 and occupied most of the cytoplasm. This might be due to their large size, ranging from 294 nm to 529 nm; a similar size was reported for *Lactobacillus* IBs (Cano-Garrido *et al.*, 2016). It was observed that most of the host cells were lysed, suggesting that the nature of the 7,10-DS differs from that of 10*S*-DOX and thus the effect on the host cell is also different.

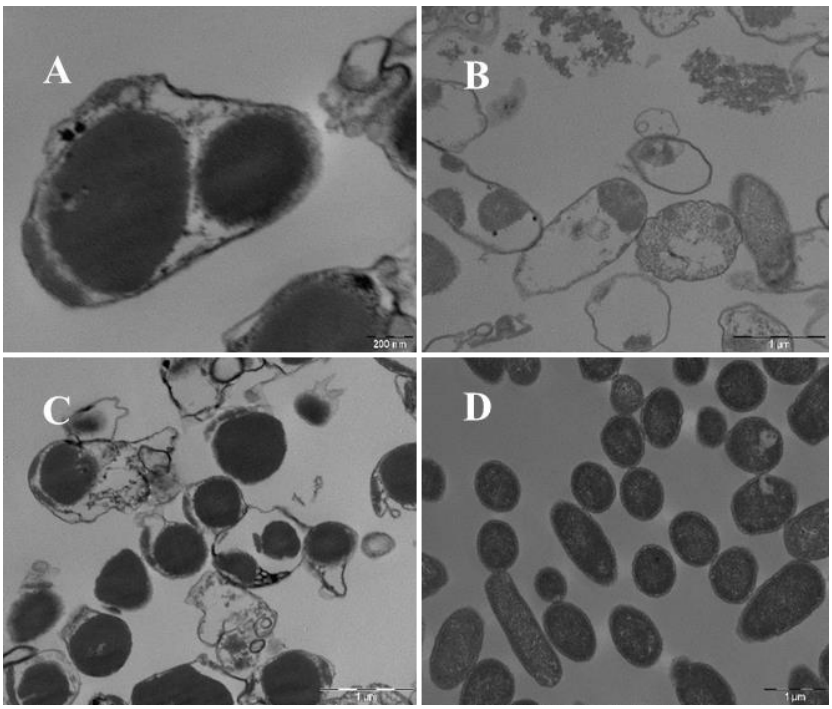

Figure 41. (A, B, C) Transmission electron microscopy images (TEM) of induced cells of BL21 (pET 28a-78), and (D) non-induced native cells of BL21 (pET 28a-78)

It has been reported that the number and the size of the aggregates reflect the kinetics of the IB formation; it is a self-assembling process in which misfolded intermediate aggregates fuse together in an IB, which continues to grow to form a larger inclusion, with properly folded proteins included within and a network with an

amyloid structure (Upadhyay *et al.*, 2012; Peternel and Komel, 2011). For a more in-depth study of the structure of the aggregates, IBs-77 and IBs-78 were isolated and purified as described above (Fig. 14 in Material and Methods). When purified, the IBs appeared as ovoid amorphous aggregates (Figure 42). The IBs-78 aggregates (Fig. 42B) were more intensely stained, suggesting the material was more hydrophobic and denser than that of IBs-77 (Fig. 42A), which appeared to be less compact.

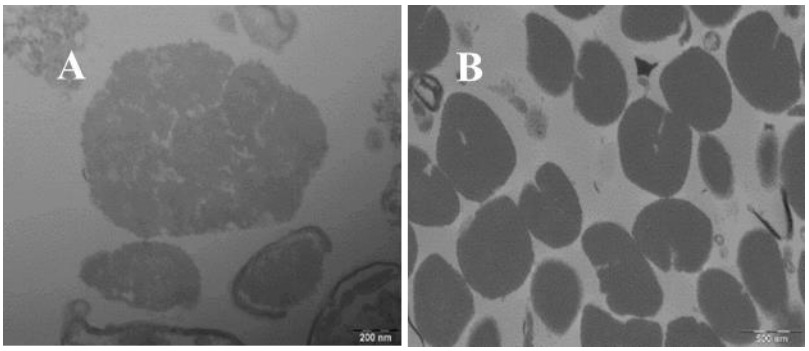

Figure 42. Transmission Electron Microscopy of purified inclusion bodies after fresh staining with uranyl acetate 2%. (A) IBs-77, (B) IBs-78.

4.2.3 Determination of the amyloid structure of inclusion bodies

The most common techniques to study the fine structure of IBs are Fourier-transform infrared spectroscopy (FT-IR), Congo red (CR) binding and Thioflavin T fluorescence (ThT). The first approach concerned the fine structure of the protein aggregates is to study, in this case, whether IBs-77 and IBs-78 have the amyloid structure frequently found in IBs in prokaryote or eukaryote cells (Nilsson, 2004; Ami *et al.*, 2005; Carrió *et al.*, 2005; García-Fruitós *et al.*, 2005; Morell *et al.*, 2008; de Groot *et al.*, 2009; Villaverde *et al.*, 2015; Cano-Garrido *et al.*, 2016). The amyloid structure is due to an ordered aggregation of misfolded protein; these protein aggregates are characterized by the presence of intramolecular β-sheets and a native-like structure (Carrió *et al.*, 2005). Infrared spectrometry (FT-IR) is currently used for the chemical characterization of proteins based upon the repeated unit, the peptide group. The resulting spectra of the second-derivative analysis yield

bands with frequencies characteristic of specific structures that are essentially the same for all proteins; nine characteristic vibrational bands of group frequencies arising from the amide groups of the polypeptide chains have been identified (Dong *et al.*, 1990). Among them, the most relevant for the present work are the bands of Amide I (1600-1700 cm^{-1}), which corresponds to the carbonyl peptide bond group and thus is used as a marker of the protein secondary structure, Amide II (about 1500-1550 cm^{-1}), is due to the protein-peptide bond vibrations (Dong *et al.*, 1990; Ami *et al.*, 2006). The most relevant band for assessing the amyloid structure of IBs by FT-IR was Amide I of the second-derivative spectra, one of the main bands of the protein infrared spectrum (Morell *et al.*, 2008) or the self-deconvolutaed spectrum, to avoied the noise of the second derivative spectrum (Vazhnova and Lukyanov, 2013).

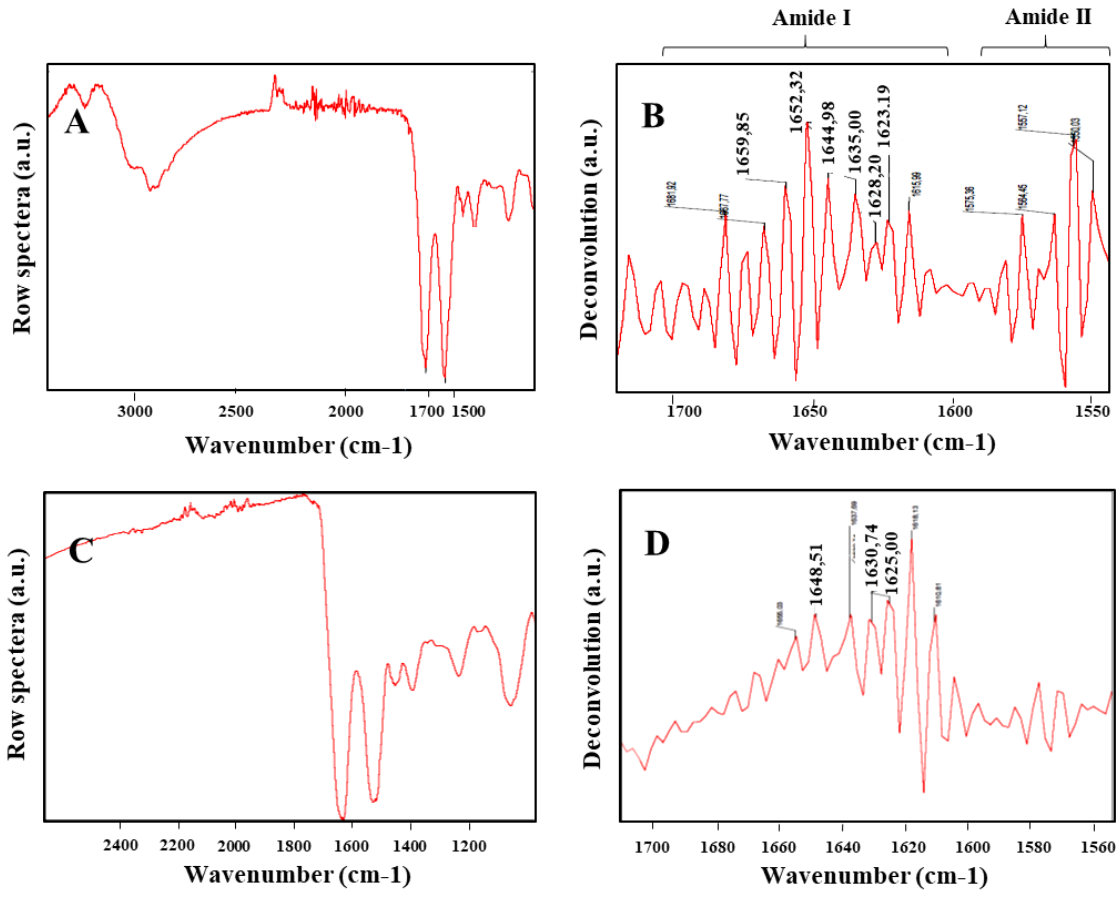

Figure 43. (A) Row spectra of control cells and (B) deconvoluted spectra of native cells. (C) Row spectra of purified IBs-77 and (D) deconvoluted spectra of purified IBs-77.

It is associated with a stretching vibration of the C=O that depends on the conformation of the backbone and has a frequency ranging between 1600 and 1700 cm^{-1} (Krimm and Bandekar, 1986). The Amide I band corresponding to the induced cells was clearly larger than that of the fresh cells (Fig 43A, C). As shown in the deconvoluted spectra in control cells (Fig 43B), the band corresponding to Amide I has two well-resolved components: it is possible to distinguish the frequency of aggregates or β-sheet structures near 1625-1629 cm^{-1} and the frequency of α-helix at about 1652-1656 cm^{-1} (Ami *et al.*, 2005; Ami *et al.*, 2006). The self-deconvoluted spectrum of the IBs-77 Amide I band is composed of a peak at 1630 cm^{-1} corresponding to β-sheets (aggregates) and a minor peak at about 1648 cm^{-1} corresponding to the α-helix (Fig. 43D).

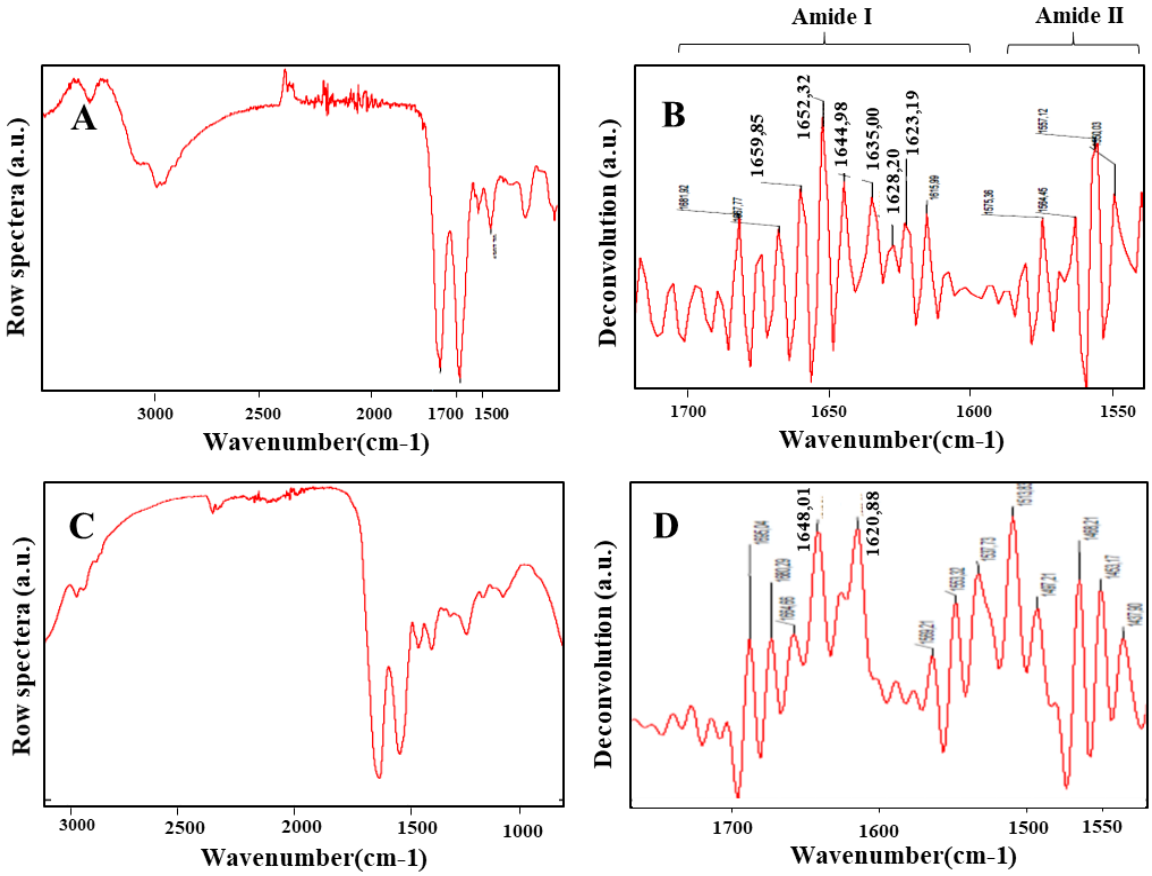

Figure 44. (A) Row spectra of control cells and (B) deconvoluted spectra of native cells. (C) Row spectra of purified IBs-78 and (D) deconvoluted spectra of purified IBs-78.

Similarly, the infrared response of the protein aggregates formed by the heterologous 7,10-DS (IBs-78) produced by recombinant *E. coli* BL21(pET 28 a-78) was examined by FT-IR spectrometry in intact cells (Fig. 44). The second-derivative spectrum enabled the secondary structure of IBs-78 to be determined by the analysis of Amide I (Ami *et al.*, 2006). The resulting spectrum represents the absorption of the recombinant protein within the intact cells. As shown, the Amide I band has a strong absorbance (Fig. 44B).

A similar spectrum to IBs-77 was obtained for IBs-78 spectrum (Fig. 44C, D) with a slightly different peak position at 1630 cm^{-1} compared with about 1620 cm^{-1} for the IBs within the cell. The complex appearance of the Amide I band can be analyzed in the deconvoluted spectrum in more detail; it can be seen that much of the structure of the IBs (Fig. 44D) is formed by aggregated protein.

Finally, the comparison of the subtracted deconvoluted spectra of control and induced cells, expressing 10*S*-DOX (Fig. 45A) and 7,10-DS (Fig. 45B), revealed the inclusion bodies within the induced cells, in which the main band corresponding to β-sheets at 1630-1635 cm^{-1} is clearly observed and the α-helix appears at 1652 cm^{1}.

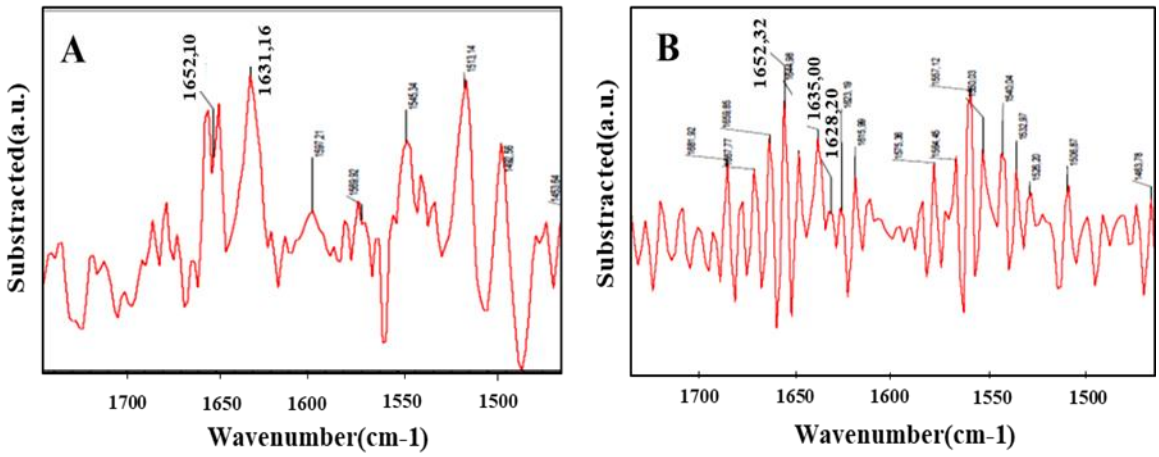

Figure 45. Substracted deconvoluted spectra of control cells and induced cells A) induced cells expressing 10*S*-DOX and B) induced cells expressing 7,10-DS.

4.2.4 Amyloid structure and dye binding

The aggregation of proteins is due to the intrinsic physicochemical characteristics of the amino acid sequence, their hydrophobicity, secondary structure, and charge (García-Fruitõs *et al.*, 2011). It has been suggested that the formation of amyloids is due to the amino acid sequence (Carrió *et al.*, 2005). Thus, protein aggregation might be understood as an anomalous type of protein-protein interaction; the specificity of such contact makes it possible to identify the aggregation-prone regions with Congo red or Thioflavin T.

4.2.4.1 Congo Red binding

In the 1920s, Benhold and Divry established that Congo red (CR) binds to amyloid structures in tissue sections and demonstrated its characteristic yellow-green birefringence under crossed polarizers (Khurana *et al.*, 2001). Since then, this birefringence has been used as a diagnostic tool for amyloid fibrils; the chemical structure of CR suggests that binding to protein could occur through a combination of both hydrophobic and electrostatic interactions. CR is a long and flat molecule with both apolar and polar parts (Fig. 46).

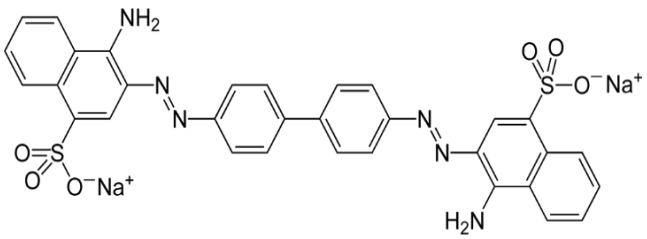

Figure 46. Structure of Congo red

The apolar part is comprised of a biphenyl group at the center and is extended by a diazo and two flanked naphthalene groups. The polar amino group and the negatively charged sulphate group are linked to a naphthalene ring. CR formed by both hydrophobic and hydrophilic groups binds to amyloid fibrils and induces

green-yellow birefringence under polarized light. Two binding modes have been proposed. One mode is *β*-sheet-specific in which the CR molecules are aligned along the fibril axes. In this mode, the CR molecules are thought to be stabilized either by the electrostatic interactions between the negatively charged sulphate groups of CR and the positively charged amino acid residues of proteins or by the hydrophobic effect of inserting CR into the grooves on the *β*-sheet surface. The other mode is *β*-strand-specific in which a CR molecule is parallel to the *β*-strand and is thought to intercalate between two *β*-strands in the antiparallel *β*-sheets. However, the specificity and the stabilities of these binding modes and their roles in amyloid fibril detection and inhibitions remain elusive (Wu *et al.*, 2007).

Upadhyay and co-workers (2012) reported that CR can not be bound in other proteins that lack the β-sheet structure (Upadhyay *et al.*, 2012). After binding to amyloid fibrils the spectra of CR shift due to change of its absorbance (Glenner *et al.*, 1972; Morell *et al.*, 2008; Wang *et al.*, 2008; Wang *et al.*, 2008; Capitini *et al.*, 2014).

As shown in Fig. 47, CR exhibits an absorbance peak at 490 nm, whereas the negative control IBs do not (Fig 47A, C). In the presence of an amyloid structure CR binds directly to the ordered β-sheets of IBs with a concomitant shift of absorbance between 508 nm at about 550 nm, depending on the nature of the protein; the shift of IBs-77 was at 500 nm and in for IBs-78 was 555 nm (Fig 47B, D). In the case of HET-s fungal prion it was reported to be 508 nm (Sabaté *et al.*, 2009), and 565 nm for asparaginase or human growth hormone (Upadhyay *et al.*, 2012). Considering that the amount of protein in both cases was 20μg/ml, as observed in Fig. 46D, the shift of absorbance for IBs-78 was higher (32%) than that observed for IBs-77 (Fig. 47B). In both cases, the spectra indicate that amyloid-like structures were present in the IBs, and the difference in the absorption of CR binding suggests differences in the hydrophobicity of the fibrils.

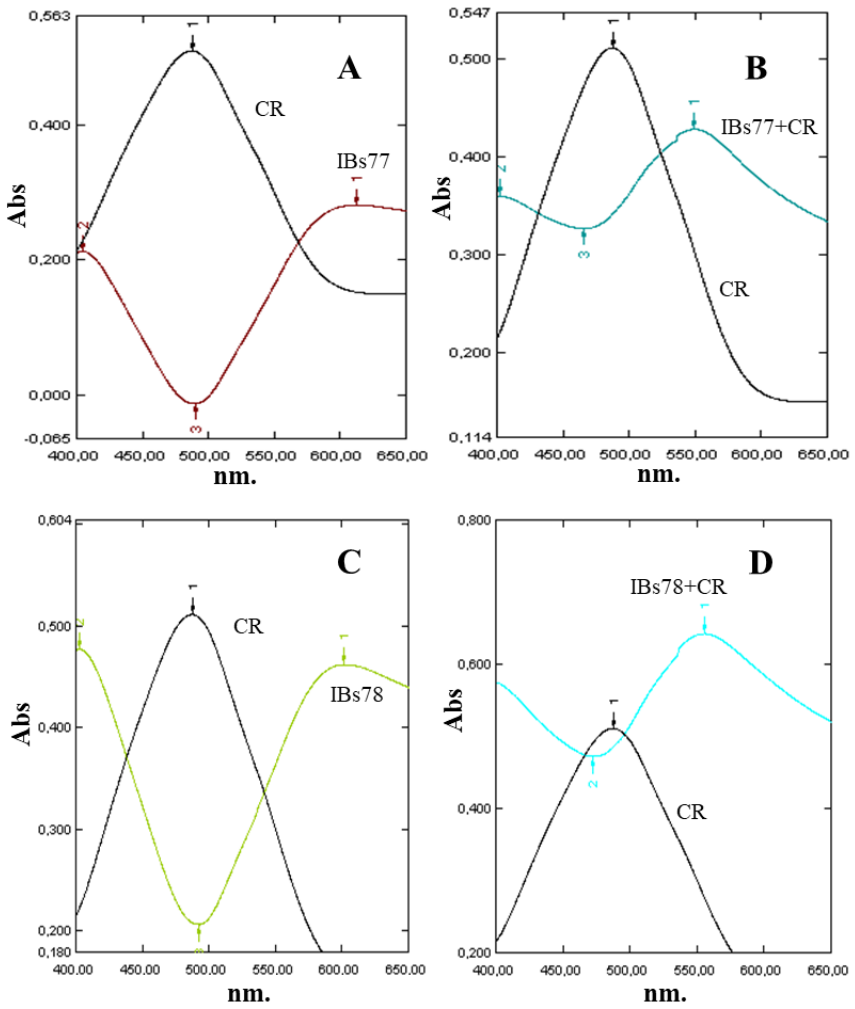

Figure 47. Congo red binding of pure IBs. Absorbance spectra of A: Congo red (black line), IBs-77 (brown line). B: Congo red (black line), IBs-77+CR (blue line). C: Congo red (black line), IBs-77 (brown line). D: Congo red (black line), IBs-77 (blue line).

4.2.4.2 Thioflavin T binding florescence

Although Thioflavin T (ThT) (Fig. 48) fluorescence is not considered one of the defining criteria for amyloid fibrils, it is accepted as an indicator of their presence (Nilsson, 2004).

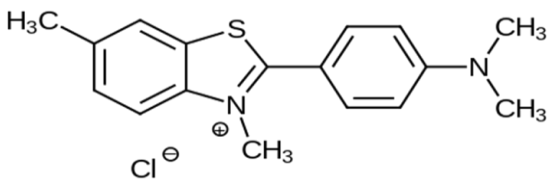

Figure 48. Chemical structure of Thioflavin T.

Fluorogenic compounds become highly fluorescent only when they are bound to a particular molecular entity, and thus they offer a set of highly sensitive and convenient techniques for detecting cellular components and structures beyond those observable with direct dyes. Naiki and LeVine (Naiki *et al.*, 1990; LeVine, 1995) were among the first who thoroughly characterized the fluorescence spectra and binding properties of ThT. It was demonstrated that, upon binding to fibrils, Th-T displays a dramatic shift of the excitation maximum (from 385 nm to 450 nm) and the emission maximum (from 445 nm to 482 nm) and that ThT fluorescence originates only from the dye bound to amyloid fibrils. The dramatic increase in ThT fluorescence results from the selective immobilization of a subset of ThT conformers. In solution, a low-energy barrier allows the benzylamine and benzathiole rings of ThT to rotate freely about their shared carbon-carbon bond. This rotation rapidly quenches excited states generated by photon excitation, causing low fluorescence emission free ThT. In contrast, rotational immobilization of ThT preserves the excited state, resulting in a high quantum yield of fluorescence. By extension, amyloid fibrils are likely to present a ThT-binding site that sterically "locks" the bound dye, thus leading to an enhancement of Th-T fluorescence (Biancalana and Koide, 2010).

For all the above reasons, and due to the special characteristics of ThT, which does not bind to precursor polypeptide monomers or amorphous aggregates of peptides and proteins digestion should be done to release fibrils (Upadhyay *et al.*, 2012). Moreover, the shift of ThT fluorescence might be due to a low number of aromatic amino acids, since ThT may have a certain preference for aromatic side chains (Lindberg *et al.*, 2015). The Thioflavin-T assay is the most commonly used method to check for the presence of cross-β-structures in amyloid-like proteins.

IBs-77 and IBs-78 in the presence of PK (to generate protein fibrils) and ThT were excited at 450 nm (Fig. 49) and increased in fluorescence at about 480-485 nm. ThT fluorescence underwent a shift at 487 nm with eighter for the fibrils of IBs-77 and 78, the maximum shift of absorbance of 50 units (IBs-78) occurred when most of the digestion was done, with an increase of 30 units, to the fluorescence of IBs-77 at 486 nm for an equal concentration of protein. Similar behavior has been found

with different proteins, such as prions (Upadhyay *et al.*, 2012). The TH-T assay showed that the IBs have an amyloid-like structure.

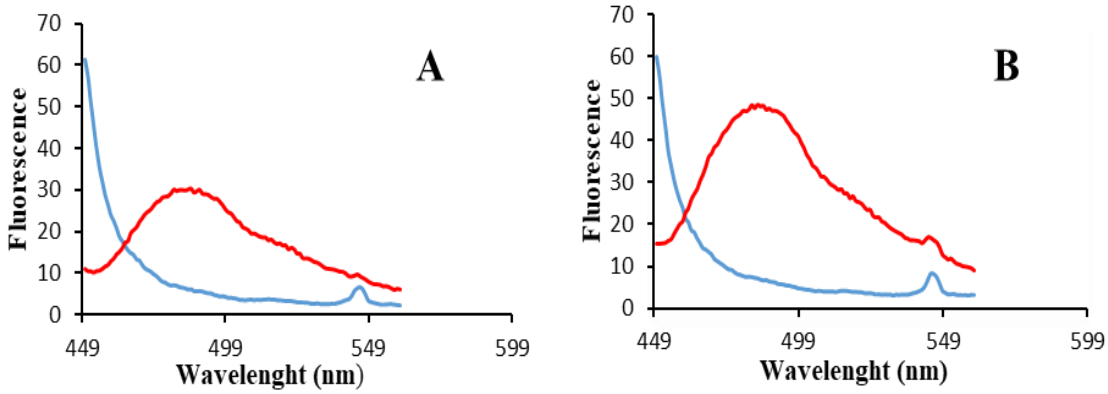

Figure 49. Fluorescence emission spectra of IBs-77 A: control (blue line) digested protein without ThT; ThT in the presence of digested IBs-77 (red line). Fluorescence emission spectra of IBs-78. B: control (blue line) digested protein without ThT; ThT in the presence of digested IBs-78 (red line). Absorbance units are arbitrary.

4.2.5 Digestion with Proteinase K

For an insight into the fine structure of IBs-77 and IBs-78, digestion with proteinase K (PK) was carried out with the purpose of releasing amyloid fibrils to be combined with binding dye Thioflavin T. Proteinase K is a subtilisin-related serine protease that hydrolyses peptide bonds at the carboxylic sides of aliphatic, aromatic or hydrophobic amino acids. This protease is currently used for mapping the core of amyloid fibrils because it has high activity against globular domains or disordered proteins but shows low activity against packed backbones in amyloid β–sheet structures (de Groot and Ventura, 2006).

We added 0.02 mg/ml PK to a suspension of IBs-77 (20 μg) or IBs-78 (25 μg) and monitored the decrease of turbidity spectra over time due to the solubilization of the protein. Further analysis was done using SDS-PAGE. As depicted (Fig. 50A, B), the absorbance value of turbidity (OD 350 nm) decreased critically over 20 min of incubation: 78.0% and 78.5% for IBs-77 and IBs-78, respectively. This indicated the digestion of the aggregates, and the pseudo-solubilization of the emerging fibrils

suggested the aggregates were sensitive to the PK. In the case of IBs-77 (Fig. 50A), a sharp decrease in turbidity was observed in the first 10 min of reaction, followed by a slow decrease until the end of the reaction (30 min), when only 7 μg/ml remained resistant to PK (35%). Whereas in the case of IBs-78 (Fig. 50B), a decline in turbidity was observed over the incubation time, indicating the different nature of this protein, and the PK-resistant fraction accounted for 32%. In parallel, samples were taken to follow the kinetics of the digestion in SDS-PAGE analysis (Fig. 50C, D) of the IBs protein after digestion.

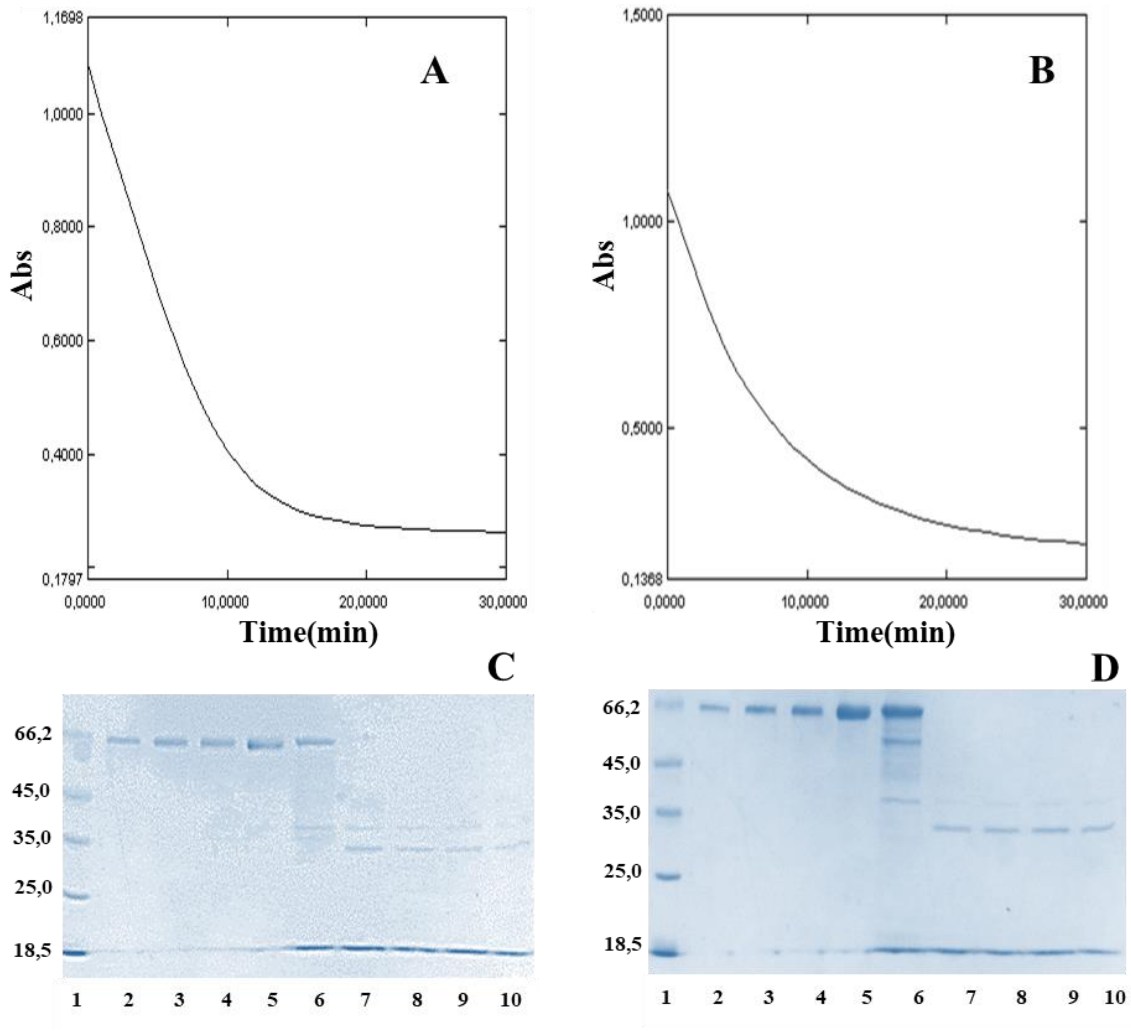

Figure 50. Proteinase K digestion of DH5α (pMMB-77) and BL21 (pET 28a-78) IBs. 1: molecular marker; 2-5 standard protein (0.5-2 μg); 6 control IBs protein; 7-10 digested protein IBs. (A, B) Turbidity of IBs decreased in the presence of PK and (C, D) the gel IB bands disappeared at different incubation times. Samples were taken at 7 min time intervals.

The Coomassie-stained band of the pure IBs (66 kDa) disappeared after fast cleavage and 7 min of incubation, and smaller proteins appeared of about 35.0 kDa, similar to observations reported elsewhere (Morell *et al.*, 2008; Upadhyay *et al.*, 2012; Capitini *et al.*, 2014).

4.2.6 Structural analysis of amyloid structure by microscopy

After the amyloid structure of IBs-77 and IBs-78 was demonstrated by means of CR and ThT, as well as proteolysis when treated by PK, the morphology of the aggregates was studied by microscopy with two approaches, TEM and AFM, before and after the PK treatment.

4.2.6.1 Transmission electron microscopy of digested IBs

IBs are heterogeneous aggregates of misfolded proteins in which polypeptides and DNA can be entrapped. The presence of IBs is due to the nature of the primary structure of a protein expression stage or physicochemical factors (Wang *et al.*, 2010; Lebendiker and Danieli, 2014).

A typical electron-dense ellipsoidal shape without any fibrillary species was observed for purified IBs-77 (Fig.51A). In contrast with previous reports (Wang *et al.*, 2008; Sabaté *et al.*, 2009), the fibrils did not protrude from the IBs-77 before digestion. After being incubated with PK for 30 min, dark electro-dense aggregates, insoluble to PK, could be observed together with amorphous material, with fibrils forming a loose network (Fig. 51B, C, D), although not organized. Similar observations have been reported elsewhere, suggesting the presence of an amyloid scaffold containing the misfolded protein and other polypeptides trapped within (Carrió *et al.*, 2005; Morell *et al.*, 2008; Cano-Garrido *et al.*, 2013; Rinas *et al.*, 2017)

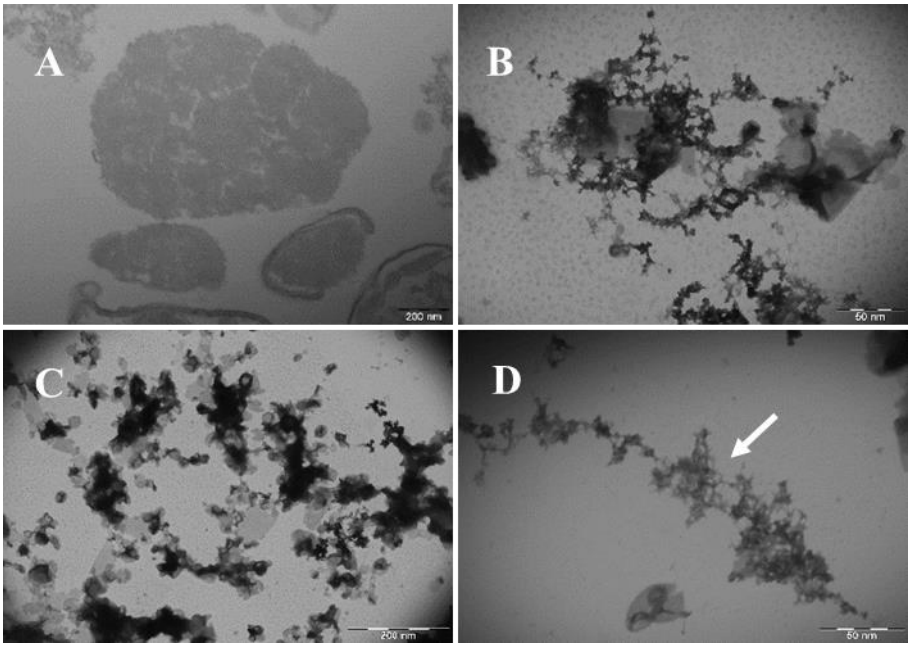

Figure 51. TEM Micrographs of purified IBs-77 aggregates. (A) Purified IBs-77 before digestion; (B, C, D) IBs-77 after digestion, dark and amorphous material that indicated amyloid fibrils. (See white arrow).

The same kind of structure was observed for purified IBs-78 (Fig. 52A), although it was darker and more compact. This suggests that the electrodensity of IBs might be protein- and strain-dependent, as stated by Cano-Garrido et al. IBs-78 showed less solubility than IBs-77 during the purification process, which was less electro-dense and less compact (Cano-Garrido *et al.*, 2013; Cano-Garrido *et al.*, 2016).

After proteinase treatment, de-aggregation occurred (Fig. 52B, C, D). In the protruding fibrils from the IBs particles, two types of materials could be seen: the proteinase-resistant (scaffold) and the fibrillary structure in the pure inclusion body (Morell *et al.*, 2008; Wang, 2009).

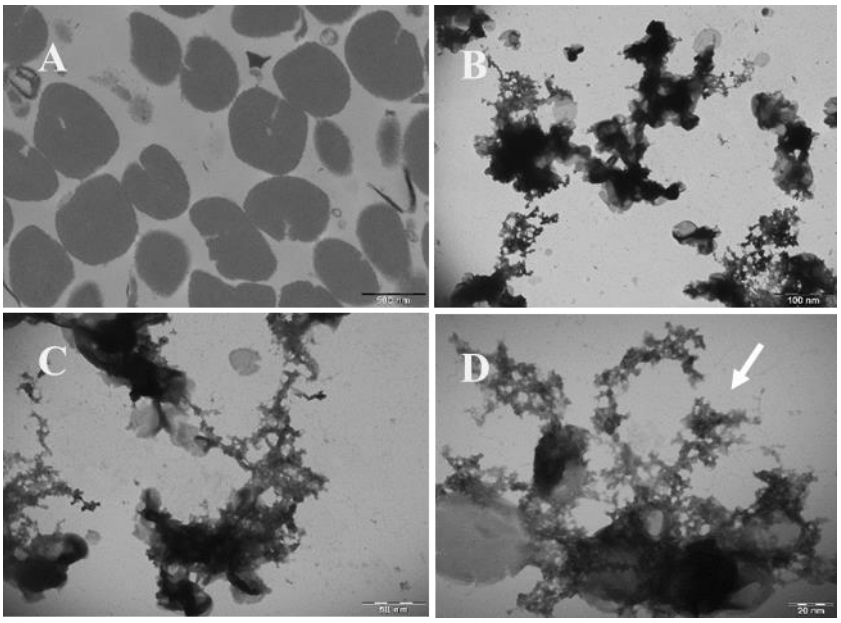

Figure 52. TEM micrographs of purified IBs-78 aggregates. (A) Purified IBs-78 before digestion; (B, C, D) IBs-78 after digestion, dark and amorphous material that indicated amyloid fibrils. (See white arrow).

4.2.6.2 Fresh observation: atomic force microscopy imaging

Atomic force microscopy (AFM) is a powerful single molecule technique that can be used to study the lipid surface nanostructure and measure surface physical properties (Diociaiuti *et al.*, 2002). This technique also provides information about the mechanism of amyloid formation and polymorphism (Ruggeri *et al.*, 2016). Aggregates of numerous amyloidogenic proteins that can be investigated by AFM include α-synuclein, amylin, IgG light chain, lysozyme, and about 40 other proteins. AFM is a rapid and simple method that requires only a small amount of material to obtain high-resolution data in a short time. The use of AFM imaging in protein aggregates has useful applications in nanomedicine and nanotechnology (Gaczynska and Osmulski, 2008). AFM provides direct images of the material and hence avoids distortion in size and roughness. Moreover, the information it can provide of single molecules is useful to determine the size of IBs and even to characterize amyloid structures.

As AFM enables direct observation of protein aggregates in solution we used it to investigate the morphology of the IBs before and after PK digestion. The overview of IBs-77 and IBs-78 samples (Fig. 53) shows that the aggregates of IBs-77 are relatively heterogeneous in size, whereas those of IBs-78 are more variable. Most of the IBs are small, with some prominent corpuscles observed among most of the aggregates. The overview presented in Fig. 53 gives a comparative idea of the differences between the two types of IBs studied.

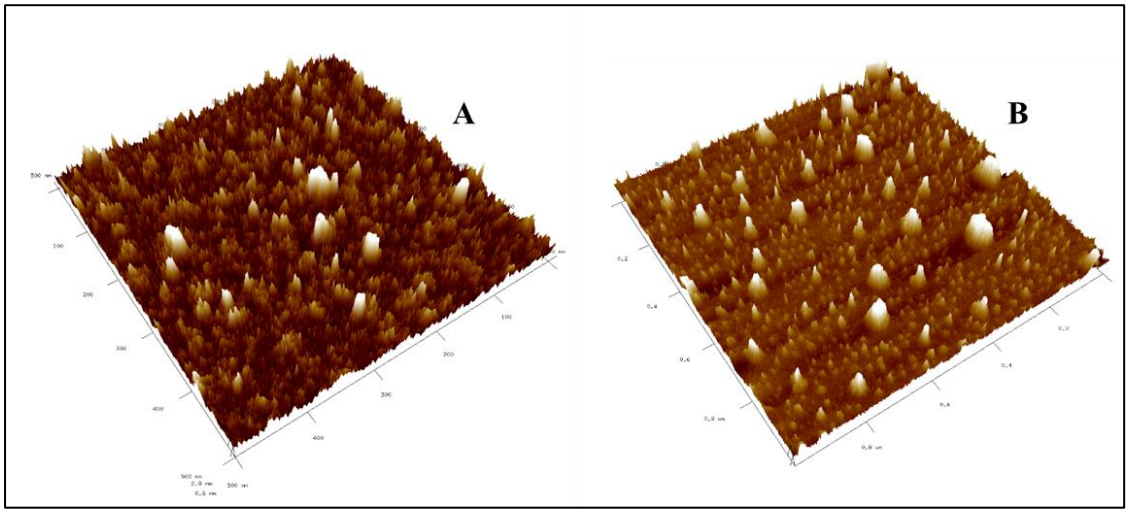

Figure 53. AFM 3-D overview of inclusion bodies produced by (A) DH5α (pMMB-77), IBs-77, scan size of 5000 nm, (B) BL21 (pET 28a-78) IBs-78, scan size of 5000 nm.

A closer view of the aggregates before and after digestion revealed differences after the treatment. The tip of the cantilever recognized differences in nature, in the resistance or texture of the sample. It is possible to recognize regions where the aggregate collapsed after the digestion treatment and even to observe the digested fibrils.

In a more detailes focus, the profile of the IBs-77 aggregate (cross line marked) shows an irregular structure with a height of about 37-42 nm (Fig. 54A). As expected, after digestion (Fig. 54B), released fibrils were visible (white arrow) and after the collapse the decrease in height was calculated as 15-17 nm (Fig. 54B), that is, aggregates diminished by about 61-65 %. The resistant PK fraction may be part of the enzyme or to the scaffold of the aggregate and the PK-resistant protein. It

should be noted that the decrease of height of the IBs-77 is much lower than that reported for green fluorescent protein aggregates (GFP-IBs), which was 200 nm (García-Fruitós *et al.*, 2009) or peptide Aβ42, which was 155 nm (Morell *et al.*, 2008).

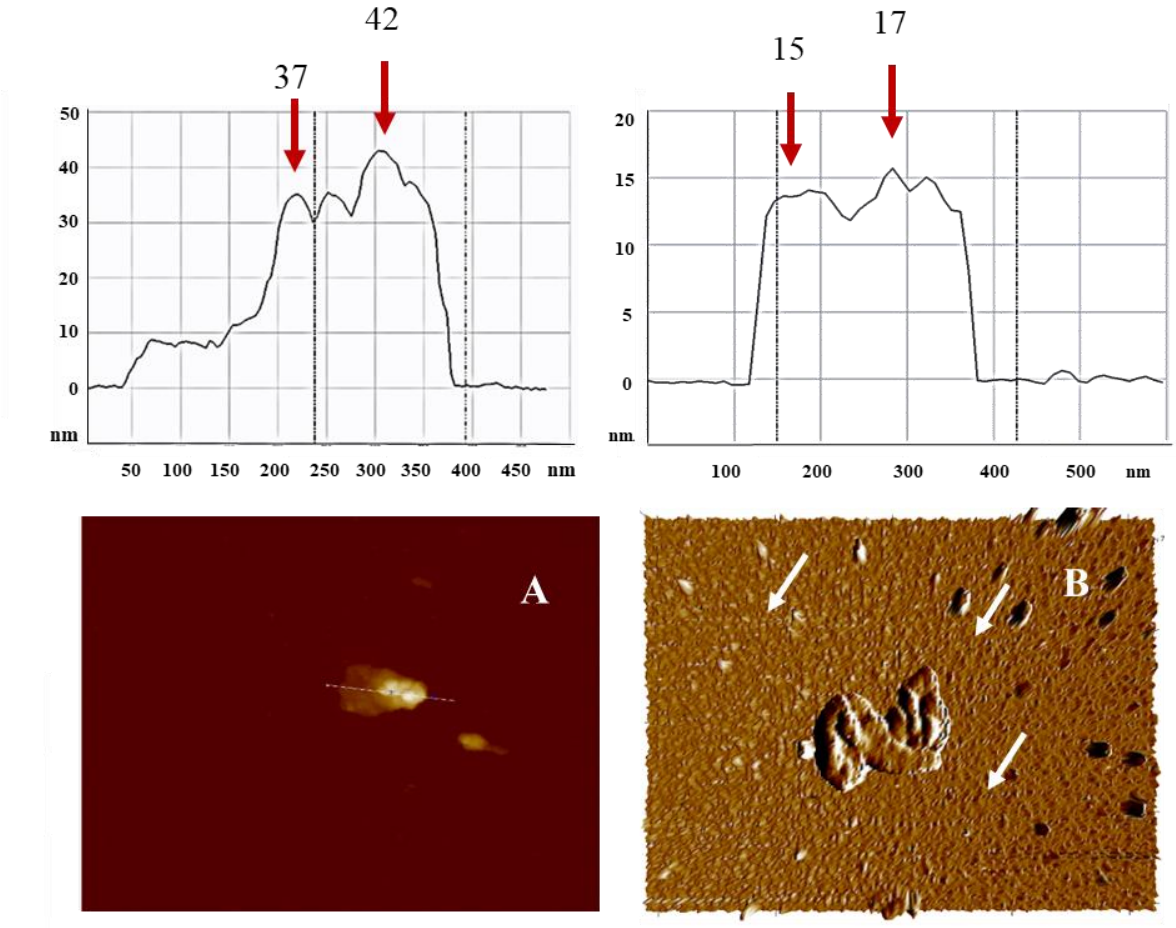

Figure 54. Amplitude AFM images of DH5α (pMMB-77) IBs before and after PK digestion. (A) Individual IBs-77 without PK treatment. (B) IBs-77 after 30 min PK digestion, The diagram represents the profile drawn by the cantilever. The arrowhead indicates the profile defined by the cantilever. Height measurements in nm.

In the case of IBs-78 (Fig. 55), the aggregates were bigger that those of IBs-77, as reflected in the profile plotted by the cantilever across the transversal line (Fig. 55A); the height of the aggregates was 173-183 nm.

The digestion treatment with PK caused the collapse of the aggregates from 30 to 56 nm (Fig. 54B), rendering a more irregular aggregate, as seen in the micrography.

The decrease in height meant the protein was digested, the released fibrils can be observed; the solubilized protein underwent a great collapse, between 69.4% and 83.6%. In Fig. 55B, the roughness of the aggregate is evident, suggesting that the cantilever found less resistance in the digested material (Morell *et al.*, 2008)

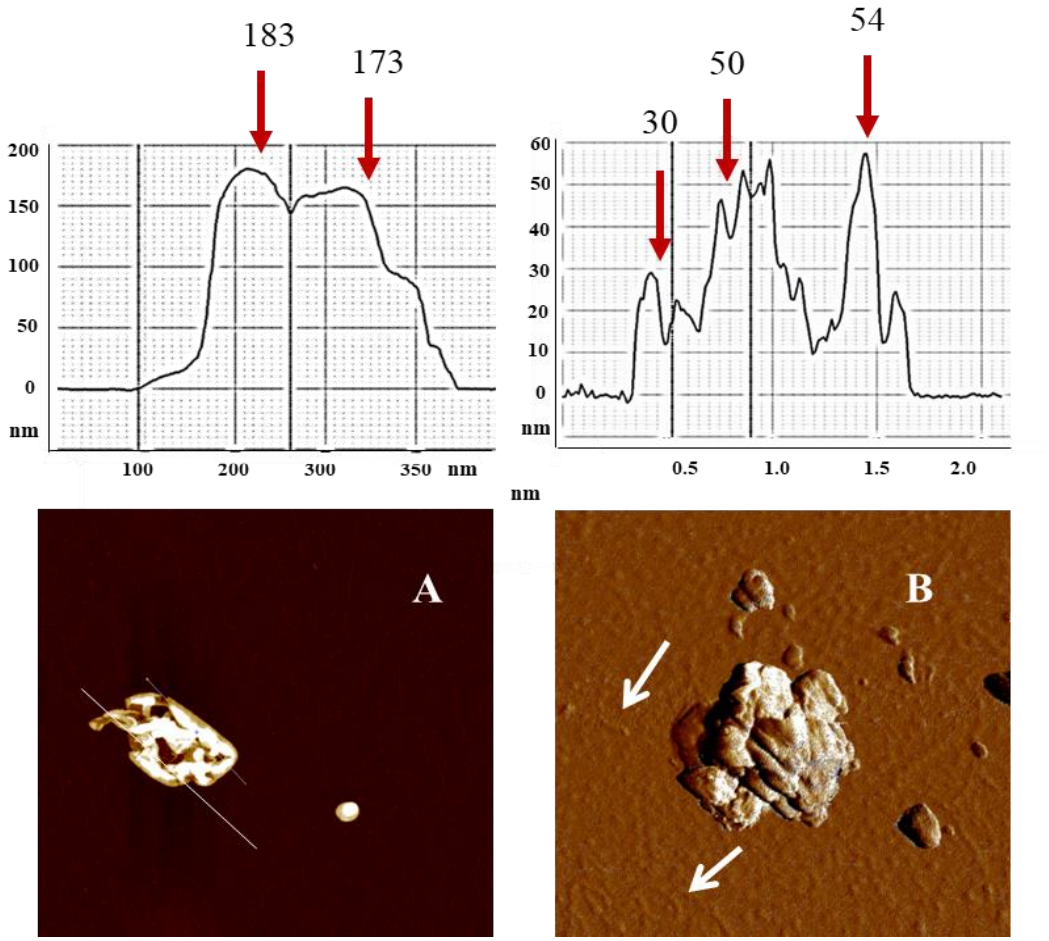

Figure 55. Amplitude AFM images of BL21 (pET 28a-78) IBs before and after PK digestion. (A) Individual IBs-78 without PK treatment, (B) IBs-78 after 30 min PK treatment, about 70% disaggregate. The diagram represents the profile drawn by the cantilever; the arrowhead indicates the profile defined by the cantilever. Height measured in nm. White arrows indicate digested fibrils.

The recombinant enzymes of the oleate diol synthase pathway have been expressed as inclusion bodies with catalytic activity (CatB) and on basis to different methodologies has been demonstrated their amyloid structure. The occurrence of inclusion bodies might be an advantage on the *in vitro* catalysis to the production of hydroxyl fatty acid for different purposes in biotechnological applications.

5. CONCLUSIONS

1. *In vitro* production of 10-H(P)OME, the substrate of 7,10-DS enzyme, was achieved by a new recombinant strain of *P. putida* KT2440 KT2440/pBBR-77, expressing the 10*S*-DOX and using oleic acid as substrate.

2. Both enzymes, 10S-dioxygenase (10*S*-DOX) and 7S,10*S*-diolsynthase (7,10-DS contain one mol of Fe^{+2} bound to the heme group as prostetic group, characteristic property of the FadCCPs subfamily.

3. The optimal temperature was almost shared for both enzymes, 30 ºC for 10*S*-DOX and 35 ºC for 7,10-DS. Nevertheless, the thermal stability of 7,10-DS was slightly higher than of 10*S*-DOX. At 50 ºC only 20% of the activity remained in any case. Both enzymes displayed similar activity in the range of pH 7-10. The presence of divalent cation in the reaction medium decreased the activity of 10*S*-DOX, while in the case of 7,10-DS Mg^{2+}, Cd^{2+}, and Ni^{2+} enhanced the activity

4. Recombinant *E. coli* DH5aα/pMMB-77 and *E. coli* BL21/pET28a-78 under stress conditions can express the corresponding enzymes as inclusion bodies with catalytic activity.

5. The structural study of purified 10*S*-DOX and 7,10-DS inclusion bodies, by FT-IR and dye binding revealed their amyloid structure. Their digestion with Proteinase K, cause the collapse of the nanoparticles, about 61-65% for 10*S*-DOX and 70-84% in the case of 7,10-DS.

6. An experimental screening of the genera *Pseudoalteromonas, Shewanella, Aeromonas, Esinfer, Thauera,* demonstrated that the presence of a putative diol synthase system is not restricted to *P. aeruginosa* as described before.

6. ABBREVIATIONS

10-H(P)OME:	(10S)-hydro(pero-)xy-8(E)-octadecenoic acid
10-HOME:	(10S)-hydroxy-(8E)-octadecenoic acid
10R-HPODE	(10R)-hydro(pero-)xyoctadecadienoic acid
10*S*-DOX	(10S)-dioxygenase
13S-HPODE	(13S)-hydroperoxy-(9Z,11E)-octadecadienoic acid
5,8-DiHODE	(5S,8R)-dihydroxyoctadeca-(9Z,12Z)-dienoic acid
7,10,12-TriHOME	7, 10, 12-trihydroxy-8(E)-octadecenoic acid
7,10-DiHOME:	(7S, 10S)-dihydroxy-(8E)-octadecenoic acid
7,10-DS	Diol synthase
7,8-DiHODE	(7S, 8S)- dihydroxylinoleic acid
7,8-LDS	7,8-Linoleate diol synthase
8,11-DiHODE	(8R,11S)-dihydroxy-(9Z,12Z)-octadecadienoic acids
8R-HPODE	8R-hydro(pero-)xylinoleic
9,10,13-THOD	9,10,13-trihydroxy-11(E)-octadecenoic acid
9,12,13-THOD	9,12,13-trihydroxy-10(E)-octadecenoic acid
9S-HPODE	(9S)-hydro(pero)-xy-(10E,12Z)-octadecadienoic acid
AFM	Atomic force microscopy
BSA	Bovine serum albumin
CatIBs	Catalytically-active inclusion body
CCP	Cytochrome c peroxydases
CR	Congo red
CYP	Cytochrome P450
DMSO	dimethyl sulfoxide
DNA	Deoxyribonucleic acid
DOX	Dioxygenase
DS	Diol synthases
FadCCPs	Fatty acid-di-heme Cytochrome c peroxidases
FTIR	Fourrier Transform Infrared spectroscopy
GCSF	Granulocyte-colony stimulating factor
HFA	Hydroxylated fatty acid
HPLC	High preassure liquid chromatography
IBs	Inclusion bodies
IBs-77	IBs of 10-DOX expressed in *E. coli* DH5α/ pMMB-10*S*-DOX
IBs-78	IBs of 7,10-DS expressed in *E. coli* BL21-7,10-DS
ICP-MS	Inductively coupled plasma mass spectrometer
IPTG	Isopropil-β-D-1-tiogalactopiranósido
LAB	Lactic acid bacterial
LCFA	Long-chain fatty acid
LDS	Linoleate diol synthases
LOX	Lipoxygenases
m/z	Mass-to-charge ratio
MS	Mass spectrometry
O.D.	Optical density

OA	Oleic acid
PGHS	Prostaglandin H synthases
PHA	Polyhydroxyalkanoate
PK	Proteinase K
TEM	Transmission electeron microscopy
Th-T	Thioflavin-T
TIC	Total ion current
TLC	Thin-layer chromatography

7. REFERENCES

Abalos, A., Maximo, F., Manresa, A., and Bastida, J. (2001a) Utilization of response surface methodology to optimize the culture media for the production of rhamnolipids by *Pseudomonas aeruginosa* AT10. *J Chem Technol Biotechnol* **77**: 777–784.

Abalos, A., Pinazo, A., Infante, R., Casals, M., García, F., and Manresa, A. (2001b) Physico chemical and antimicrobial properties of new rhamnolipids produced by *Pseudomonas aeruginosa* AT10 from soybean oil refinery wastes. *Langmuir* **17**: 1367–1371.

Aguilar, A., Wohlgemuth, R., and Twardowski, T. (2018) Perspectives on bioeconomy. *New Biotechnol* **40**: 181–184.

Altschul, F.S., Madden, T.L., Schaffer, A.A., Zhang, J., Zhang, Z., Miller, W., and Lipman, D.J. (1997) Gapped BLAST and PSI-BLAST: a new generation of protein database search programs. *Nucleic Acids Res* **25**: 3389–3402.

Ami, D., Natallelo, A., Gatti-Lafranconi, P., Lotti, M., and Doglia, S.. (2005) Kinetics of inclusion body formation studied in intact cells by FT_IR spectroscopy. *Febs J* **679**: 3433–3436.

Ami, D., Natarello, A., Taylor, G., Tonon, G., and Doglia, S.A. (2006) Structural analysis of protein inclusion bodies by Fourrier transform infrares microscopy. *Biochem Biochim Acta* **1764**: 793–799.

Andeou, A., and Feussner, I. (2009) Lipoxygenases – Structure and reaction mechanism. *Phytochemistry* **70**: 1504–1510.

Andrés, C. De, Mercadé, E., Guinea, J., and Manresa, A. (1994) 7,10-Dihydroxy-8(E)-octadecenoic acid produced by Pseudomonas 42A2: evaluation of different cultural parameters of the fermentation. *World J Microbiol Biotechnol* **10**: 106–109.

Bae, J.-H., Suh, M.J., Lee, N.-Y., Hou, C.T., and Kim, H.-R. (2010) Production of a Value-added Hydroxy Fatty Acid, 7,10-dihydroxy-8(E)-octadecenoic Acid, from High Oleic Safflower Oil by *Pseudomonas aeruginosa* PR3. *Biotechnol Bioprocess Eng* **15**: 953–958.

Baneyx, F. (1999) Recombinant protein expression in *Escherichia coli*. *Curr Opin Biotechnol* **10**: 411–421.

Bassas i Galià, M., Manresa Presas, M.A. (María A., Llorens Llacuna, J., and Universitat de Barcelona. Departament de Microbiologia i Parasitologia Sanitàries. (2007) *Estudi dels polihidroxialcanoats acumulats per Pseudomonas aeruginosa* 42A2 *producció i caracterització*. Universitat de Barcelona.

Bassas, M., Diaz, J., Rodriguez, E., Espuny, M.J., Prieto, M.J., and Manresa, A. (2008a) Microscopic examination in vivo and in vitro of natural and cross-linked polyunsaturated mclPHA. *Appl Microbiol Biotechnol* **78**: 587–596.

Bassas, M., Marqués, A.M., and Manresa, A. (2008b) Study of the crosslinking reaction (natural and UV induced) in polyunsaturated PHA from linseed oil. *Biochem Eng J* **40:** 275–283.

Bassas, M., Rodríguez, E., Llorens, J., and Manresa, A. (2006) Poly(3-hydroxyalkanoate) produced from *Pseudomonas aeruginosa* 42A2 (NCBIM 40045): Effect of fatty acid nature as nutrient. *J Non Cryst Solids* **352**: 2259–2263.

Belcher, J., McLean, K.J., Matthews, S., Woodward, L.S., Fisher, K., Rigby, S.E.J., *et al.* (2014) Structure and Biochemical Properties of the Alkene Producing Cytochrome P450 (CYP152L1) from the *Jeotgalicoccus* sp. 8456 Bacterium. *J Biol Chem* **289**: 6535–6550.

Bender, C.L., Alarcón-Chaidez, F., and Gross, D.C. (1999) *Pseudomonas syringae* phytotoxins: mode of action, regulation, and biosynthesis by peptide and polyketide synthetases. *Microbiol Mol Biol Rev* **63**: 266–92.

Benincasa, M., Abalos, A., Oliveira, I., and Manresa, A. (2004) Chemical structure, surface properties and biological activities of the biosurfactatn produced by *Pseudomonas aeruginosa* LBI. *Antonie Van Leeuwenhoek* **85**: 1–8.

Berg J M, et al. (2002) SGD. Biochemistry (5th edition). ISBN-0716746840.

Bernardez Clark, E. De (2001) Protein refolded for industrial processes. *Biotechnol Eng* **12**: 202–207.

Biancalana, M., and Koide, S. (2010) Molecular mechanism of Thioflavin-T binding to amyloid fibrils. *Biochim Biophys Acta* **1804**: 1405–1412.

Bleé, E. (1995) Oxygenated fatty acids and plant defenses. *INFORM* **6**: 852–861.

Boer, A.L. de, and Schmidt-Dannert, C. (2003) Recent efforts in engineering microbial cells to produce new chemical compounds. *Curr Opin Chem Biol* **7**: 273–278.

Bosch, P., Robert, M., Mercadé, M.E., Parra, J.L., and Guinea, J. (1988) Surface active compounds on microbial cultures. *Tenside Surfactants Deterg* **25**: 208–211.

Braaz, R., Fischer, P., and Jendrossek, D. (2004) Novel type of heme-dependent oxygenase catalyzes oxidative cleavage of rubber (poly-cis-1,4-isoprene). *Appl Environ Microbiol* **70**: 7388–95.

Bradford, M.M. (1976) A apid and simple method for the quantitation of micrograms quantities of protein utilizing the principle of protein-dye binding. *Anal Biochem* **72**: 248–254.

Brash, A.R. (1999) Lipoxygenases. Ocurrence, functions, catalysis, and acquisition of substrate. *J Biol Chem* **274**: 23679–23682.

Brash, R.A., Niraula, N.P., Boeglin, W.E., and Mashhadi, Z. (2014) An ancient relative of cyclooxygenase in cyanobacteria is a linoleate 10S-dioxygenase that works in tandem with a catalase-relate protein with specific 10S hydroperoxide liase activity. *J Biol Chem* **289**: 13101–13111.

Brodowsky, I.D., Hamberg, M., and Oliw, E.H. (1992) A linoleic acid (8R)-dioxygenase and hydroperoxide isomerase of the fungus *Gaeumannomyces graminis*. Biosynthesis of (8R)-hydroxylinoleic acid and (7S,8S)-dihydroxylinoleic

acid from (8R)-hydroperoxylinoleic acid. *J Biol Chem* **267**: 14738–45.

Burton, S.G. (2003) Oxidizing enzymes as biocatalysts. *Trends Biotechnol* **21**: 543–549.

Cano-Garrido, O., Rodríguez-Carmona, E., Díez-Gil, C., Vázquez, E., Elizondo, E., Cubarsi, R., *et al.* (2013) Supramolecular organization of protein-releasing functional amyloids solved in bacterial inclusion bodies. *Acta Biomater* **9**: 6134–6142.

Cano-Garrido, O., Sánchez-Chardi, A., Parés, S., Giró, I., Tatkiewicz, W.I., Ferrer-Miralles, N., *et al.* (2016) Functional protein-based nanomaterial produced in microorganisms recognized as safe: A new platform for biotechnology. *Acta Biomater* **43**: 230–239.

Cao, B., and Loh, K.-C. (2008) Catabolic pathways and cellular responses of *Pseudomonas putida* P8 during growth on benzoate with a proteomics approach. *Biotechnol Bioeng* **101**: 1297–1312.

Capitini, C., Conti, S., Perni, M., Guidi, F., Cascella, R., Poli, A. De, *et al.* (2014) TDP-43 inclusion bodies formed in bacteria are structurally amorphous, non-amyloid and inherently toxic to neuroblastoma cells. *PLoS One* **9**: 1–14.

Carrió, M., González-Montalbán, N., Vera, A., Villaverde, A., and Ventura, S. (2005) Amyloid-like properties of bacterial inclusion bodies. *J Mol Biol* **347**: 1025–1037.

Carrió, M.M., Cubarsi, R., and Villaverde, A. (2000) Fine architecture of bacterial inclusion bodies. *FEBS Lett* **471**: 7–11.

Carrió, M.M., and Villaverde, A. (2001) Protein aggregation as bacterial inclusion bodies is reversible. *FEBS Lett* **489**: 29–33.

Carrió, M.M., and Villaverde, A. (2002) Construction and deconstruction of inclusion bodies. *J Biotechnol* **96**: 3–12.

Choi, H.-Y., Seo, M.-J., Shin, K.-C., and Oh, D.-K. (2015) Production of 10-hydroxy-12,15(Z,Z)-octadecadienoic acid from α-linolenic acid by permeabilized Stenotrophomonas nitritireducens cells. *Biotechnol Lett* **37**: 2271–2277.

Colomer, J.-F., Henrard, L., Lambin, P., and Tendeloo, G. Van (2002) Electron diffraction and microscopy of single-wall carbon nanotube bundles produced by different methods. *Eur Phys J B - Condens Matter* **27**: 111–118.

Davis, E.N., Wallen, L.L., Goodwin, J.C., Rohwedder, W.K., and Rhodes, R.A. (1969) Microbial hydration of cis-9-alkenoic acids. *Lipids* **4**: 356–62.

Desai, J., and Banat, I. (1997) Microbial Production of Surfactants and their commercial Potencial. *Microbiol Mol Biol Rev* **61**: 47–64.

Diociaiuti, M., Bordi, F., Motta, A., Carosi, A., Molinari, A., Arancia, G., and Coluzza, C. (2002) Aggregation of Gramicidin A in Phospholipid Langmuir–Blodgett Monolayers. *Biophys J* **82**: 3198–3206.

Dong, A., Huang, P., and Caughey, W.S. (1990) Protein Secondary Structures in Water from Second-Derivative Amide I Infrared Spectra. *Biochemistry* **29**: 3303–3308.

Drepper, T., Eggert, T., Hummel, W., Leggewie, C., Pohl, M., Rosenau, F., *et al.* (2006) Novel biocatalysts for white biotechnology. *Biotechnol J* **1**: 777–786.

Ellamar J B, Song K S, K.H.R. (2011) One-Step Production of a Biologically Active Novel Furan Fatty Acid from 7,10-Dihydroxy-8(E)-octadecenoic Acid. *J Agric Food Chem* **59**: 8175–8179.

Estupiñán Romero, M. (2015) Comprehensive analysis of *Pseudomonas aeruginosa* oleate-diol synthase activity. *PhD thesis.* University of Barcelona.

Estupiñán, M., Álvarez-García, D., Barril, X., Diaz, P., and Manresa, A. (2015) In Silico/In Vivo Insights into the Functional and Evolutionary Pathway of *Pseudomonas aeruginosa* Oleate-Diol Synthase. Discovery of a New Bacterial Di-Heme Cytochrome C Peroxidase Subfamily. *PLoS One* **10**: e0131462.

Estupiñan, M., Diaz, P., and Manresa, A. (2014) Unveiling the genes responsible for the unique *Pseudomnas aeruginosa* oleate-diol synthase activity. *Biochimica et Biophysica Acta* **1841**: 1360–1371.

F. Brodhun, C. Gobel, E. Hornung, I.F. (2009) Identification of PpoA from *Aspergillus* 586 *nidulans* as a fusion protein of a fatty acid heme dioxygenase/peroxidase and a 587 cytochrome P450,. *J Biol Chem* **284**: 1792–11805.

Frey, P.A., and Hegeman, A.D. (2007) *Enzymatic reaction mechanisms*. Oxford University Press.

Funk, C.D. (2001) Prostagalndins and Leucotrienes: advances in eicosanoid biology. *Science* **294**: 1871–1875.

Gaczynska, M., and Osmulski, P.A. (2008) AFM of biological complexes: what can we learn? *Curr Opin Colloid Interface Sci* **13**: 351–367.

García-Fruitó, E., Vá Zquez, E., Sar Díez-Gil, C., Corchero, J.L., Seras-Franzoso, J., Ratera, I., *et al.* (2011) Bacterial inclusion bodies: making gold from waste. *Trends Biotechnol* **30**: 65–70.

García-Fruitós, E., González-Montalban, N. Morell, M., Vera, A., Ferraz, R.M., Arís, A., Ventura, S., and Villaverde, A. (2005) Aggregation as bacterial inclusion bodies does not imply inactivation of enzymes and fluorescent proteins. *Microb Cell Fact* **4**: 27–32.

García-Fruitós, E., Rodríguez-Carmona, E., Díez-Gil, C., Ferraz, R.M., Vázquez, E., Corchero, J.L., *et al.* (2009) Surface cell growth engineering assisted by a novel bacteria nanomaterial. *Adv Mater* **21**: 4249–4253.

García-Fruitõs, E., Sabate, R., Groot, N.S. De, Villaverde, A., and Ventura, S. (2011) Biological role of bacterial inclusion bodies: A model for amyloid

aggregation. *FEBS J* **278**: 2419–2427.

Gardner, H.W., and Hou, C.T. (1999) All (S) Stereoconfiguration of 7,10-dihydroxy-8(E)-octadecenoic acid from bioconversion od oleic acid by *Pseudomonas aeruginosa*. *JAOCS* **76**: 1151–1156.

Garreta, A., Carpena, X., Busquets, M., Fusté, M.C., Fita, I., and Manresa, A. (2011) Crystallization and resolution of the lipoxygenase of *Pseudomons aeruginosa* 42A2 anf phylogenetic study of the subfamilies of the lipoxygenases. In *Recent Advances in Pharmaceutical Sciences*. Torrero, D.M. (ed.). Transworld Research Network, Kerala, India. pp. 249–273.

Garreta, A., Val-Moraes, S., Garcia-Fernandez, Q., Busquets, M.-, Juan, C.-, Oliver, A., *et al.* (2013) Membrane interaction and cell invasiveness of a secretable lipoxygebnase from *Pseudomonas aeruginosa*. *FASEB* **27**: 4811–4821.

Garscha, U., and Oliw, E.H. (2009) Leucine/Valine Residues Direct Oxygenation of Linoleic Acid by (10 *R*)- and (8 *R*)-Dioxygenases. *J Biol Chem* **284**: 13755–13765.

Garsha, U., and Oliw, E.H. (2007) Steric analysis of 8-hydroxyoctadecanedioic acids and dihydroperoxy-octadecanediois acid by hydroperoxide isomerases. *Anal Biochem* **367**: 238–246.

Gasser, B., Saloheimo, M., Rinas, U., Dragosits, M., Rodríguez-Carmona, E., Baumann, K., *et al.* (2008) Protein folding and conformational stress in microbial cells producing recombinant proteins: a host comparative overview. *Microb Cell Fact* **7**: 11.

Gerven, N. Van, Klein, R.D., Hultgren, S.J., and Remaut, H. (2015) Bacterial amyloid formation: structural insights into curli biogensis. *Trends Microbiol* **23**: 693–706.

Glenner, G., Eanes, E., and DL., P. (1972) The relation of the properties of Congo red-stained amyloid fibrils to the beta-configuration. *J Histochem Cytochem* **20**: 821–826.

Gomila, M., PeÃ±a, A., Mulet, M., Lalucat, J., and GarcÃ-a-ValdÃ©s, E. (2015) Phylogenomics and systematics in *Pseudomonas*. *Front Microbiol* **6**: 214.

Groot, N.S. de, Sabate, R., and Ventura, S. (2009) Amyloids in bacterial inclusion bodies. *Trends Biochem Sci* **34**: 408–416.

Groot, N.S. de, and Ventura, S. (2006) Effect of temperature on protein quality in bacterial inclusion bodies. *FEBS Lett* **580**: 6471–6476.

Guengerich, F.P. (1991) Reactions and significance of cytochrome P450. *J Biol Chem* **266**: 10019–10022.

Guerrero, A., Casals, I., Busquets, M., León, Y., and Manresa, A. (1997) Oxidation of oleic acid to (E)-10-hydroperoxy-8-octadecenoic acid and (E)-10-hydroxy-8-octadecenoic cid by *Pseudomonas* sp. 42A2. 1997. Biochim. Biophys. Acta 1347:75-8. *Biochim Biophys Acta* **134**: 75–78.

Haas, D., and Défago, G. (2005) Biological control of soil-borne pathogens by *Pseudomonads fluorescent*. *Nat Rev Microbiol* **3**: 307–319.

Haba, E., Abalos, A., Jáuregui, O., Espuny, M.J., and Manresa, A. (2003) Use of liquid chromatography-mass spectroscopy for studuing the compositin and properties of rhamnolipids produced by different starins of *Pseudomonas aeruginosa*. *J Surf Det* **6**: 155–161.

Haba, E., Vidal-Mas, J., Bassas, M., Espuny, M.J., Llorens, J., and Manresa, A. (2007) Poly 3-(hydroxyalkanoates) produced from oily substrates by *Pseudomonas aeruginosa* 47T2 (NCBIM 40044): Effect of nutrients and incubation temperature on polymer composition. *Biochem Eng J* **35**: 99–106.

Hamberg, M. (1993) Pathways in the biosyntesis of oxylipins in plants. *J Lipid Mediat* **6**: 375–384.

Hamberg, M., Zhang, L.Y., Brodowsky, I.D., and Oliw, E.H. (1994) Sequential Oxygenation of Linoleic Acid in the Fungus *Gaeumannomyces graminis*: Stereochemistry of Dioxygenase and Hydroperoxide Isomerase Reactions. *Arch Biochem Biophys* **309**: 77–80.

Hansen, H., Garreta, A., Benincasa, M., Fusté, M.C., Busquets, M., and Manresa, A. (2013) Bacterial lipoxygenases, a new subfamily of enzymes? A phylogenetic aporach. *Appl Microbiol Biotechnol* **97**: 4737–4747.

Hörnsten, L., Su, C., Osbourn, A.E., Garosi, P., Hellman, U., Wernstedt, C., and Oliw, E.H. (1999) Cloning of linoleate diol synthase reveals homology with prostaglandin H synthases. *J Biol Chem* **274**: 28219–24.

Hou, C.T., and Bagby, M.O. (1992) 10-Hydroxy-8(Z)-octadecenoic acid, an intermediaty in the bioconversion of oleic acid to 7,10 dihidroxi-8(E)-octadecenoic acid,. *J Ind Microbiol* **9**: 103–107.

Jendrossek, D., and Reinhardt, S. (2003) Sequence analysis of a gene product synthesized by *Xanthomonas* sp. during growth on natural rubber latex. *FEMS Microbiol Lett* **224**: 61–65.

Jeneren, F., Hoffmann, I., and Oliw, E.H. (2010) Linoleate 9R-dioxygenase and allene oxide synthase activities of *Aspergillus terreus*. *Arch Biochem Biophys* **495**: 67–73.

Jeong, Y.-J., Seo, M.-J., Shin, K.-C., and Oh, D.-K. (2015) Production of 8-hydroxy-9,12(Z,Z)-octadecadienoic acid from linoleic acid by recombinant cells expressing H1004A-C1006S variant of *Aspergillus nidulans* diol synthase. *J Mol Catal B Enzym* **115**: 35–42.

Jernerén, F., Garscha, U., Hoffmann, I., Hamberg, M., and Oliw, E.H. (2010) Reaction mechanism of 5,8-linoleate diol synthase, 10R-dioxygenase, and 8,11-hydroperoxide isomerase of *Aspergillus clavatus*. *Biochim Biophys Acta - Mol Cell Biol Lipids* **1801**: 503–507.

Jevševar, S., Gaberc-Porekar, V., Fonda, I., Podobnik, B., Grdadolnik, J., and

Menart, V. (2005) Production of nonclassical inclusion bodies from which correctly folded protein can be extracted. *Biotechnol Prog* **21**: 632–639.

Jin, M., Slininger, P.J., Dien, B.S., Waghmode, S., Moser, B.R., Orjuela, A., *et al.* (2015) Microbial lipid-based lignocellulosic biorefinery: feasibility and challenges. *Trends Biotechnol* **33**: 43–54.

Jones, J.D.G., and Dangl, J.L. (2006) The plant immune system. *Nature* **444**: 323–329.

Joo, Y.C., and Oh, D.K. (2012) Lipoxygenases: Potential starting biocatalysts for the synthesis of signaling compounds. *Biotechnol Adv* **30**: 1524–1532.

Khurana, R., Uversky, V.N., Nielsen, L., and Fink, A.L. (2001) Is Congo Red an Amyloid-specific Dye?. *J Biol Chem Biol Chem* **276**: 22715–22721.

Kim, H., Gardner, H.W., and Hou, C.T. (2000) Production of isomeric 9,10,13 (9,10,13)-trihydroxy-11E(10E)-octadecenoic acid from linoleic acid by *Pseudomonas aeruginosa* PR3. *J Ind Microbiol Biotechnol* **25**: 109–115.

Kim, K.R., and Oh, D.-K.K. (2013) Production of hydroxy fatty acids by microbial fatty acid-hydroxylation enzymes. *Biotechnol Adv* **31**: 1473–85.

Kim, M.J., Seo, M.J., Shin, K.C., and Oh, D.K. (2017a) Production of 8,11-dihydroxy and 8-hydroxy unsaturated fatty acids from unsaturated fatty acids by recombinant *Escherichia coli* expressing 8,11-linoleate diol synthase from *Penicillium chrysogenum*. *Biotechnol Prog* **33**: 390–396.

Kim, M.J., Seo, M.J., Shin, K.C., and Oh, D.K. (2017b) Production of 10S-hydroxy-8(E)-octadecenoic acid from oleic acid by whole recombinant *Escherichia coli* cells expressing 10S-dioxygenase from Nostoc punctiforme PCC 73102 with the aid of a chaperone. *Biotechnol Lett* **39**: 133–139.

Kim, T.M., Kuo, T.M., and Hou, C.T. (2001) Production of a Novel Compound, 7,10,12-Trihydroxy-8(E)-OctadecenoicAcid from Ricinoleic Acid by *Pseudomonas aeruginosa* PR3. *Curr Microbiol* **43**: 198–203.

Knothe, G., Bagby, M.O., Peterson, R.E., and Hou, C.T. (1992) 7,10-Dihydroxy-8(E)-Octadecenoic acid: Stereochemistry and a novel derivative, 7,10-Dihydroxyoctadecanoic acid. *JAOCS* **69**: 367–371.

Krauss, U., Jäger, V.D., Diener, M., Pohl, M., and Jaeger, K.E. (2017) Catalytically-active inclusion bodies—Carrier-free protein immobilizates for application in biotechnology and biomedicine. *J Biotechnol* **258**: 136–147.

Krimm, S., and Bandekar, J. (1986) Vibrational spectroscopy and conformation of peptides, polypeptides, and proteins. *Adv Protein Chem* **38**: 181–364.

Kuo, T.M., Kim, H., and Hou, C.T. (2001) Production of a novel compound 7,10,12-trihydroxy-8(E)-octadecenoic acid from ricinoleicacid by *Pseudomonas aeruginosa* PR3. *Curr Microbiol* **43**: 198–203.

Kuo, T.M., and Nakamura, L.K. (2004) Diversity of Oleic Acid, Ricinoleic Acid

and Linoleic Acid Conversions Among *Pseudomonas aeruginosa* Strains. *Curr Microbiol* **49**: 261–266.

Laemmli, U.K. (1970) Cleavage of structural proteins during the assembly of the head of bacteriophage T4. *Nature* **227**: 660–685.

Lang, I., Göbel, A., Heilmann, I., and Freussner, I. (2008) A lipoxygenase with linoleate diol synthase activity in Nostoc sp PCC 7120. *Biochem J* **410**: 347–357.

Lebendiker, M., and Danieli, T. (2014) Production of prone-to-aggregate proteins. *FEBS Lett* **588**: 236–246.

LeVine, H. (1995) Thioflavine T interaction with amyloid β-sheet structures. *Amyloid* **2**: 1–6

Li, Z., Tran, V.H., Duke, R.K., Ng, M.C.H., Yang, D., and Duke, C.C. (2009) Synthesis and biological activity of hydroxylated derivatives of linoleic acid and conjugated linoleic acids. *Chem Phys Lipids* **158**: 39–45

Liavonchanka, A., and Feussner, I. (2006) Lipoxygenases: Occurrence, functions and catalysis. *J Plant Physiol* **163**: 348–357.

Lindberg, D.J., Wranne, M.S., Gilbert Gatty, M., and Westerlund, F.- (2015) Steady-stat ens time-resolved Thioflavin-T fluorescence can report on morphological differences in amyloid fibrils formed by A(beta)(1-40) and A(beta)(1-42. *Biochem Biophys Res Comm* **458**: 418–423.

Lokko, Y., Heijde, M., Schebesta, K., Scholtès, P., Montagu, M. Van, and Giacca, M. (2018) Biotechnology and the bioeconomy—Towards inclusive and sustainable industrial development. *N Biotechnol* **40**: 5–10

Lyczak, J.B., Cannon, C.L., and Pier, G.B. (2000) Establishment of *Pseudomonas aeruginosa* infection: lessons from a versatile opportunist. *Microbes Infect* **2**: 1051–60.

Lynch, M., and Katju, V. (2004) The altered evolutionary trajectories of gene diuplicates. *Trends Genet* **20**: 544–549.

Martin-Arjol, I. (2014) Polymeric emulsifiers obtained by bactrerial transformation from oily wastes in bioreactor. *PhD thesis*. University of Barcelona.

Martín-Arjol, I., Bassas-Galia, M., Bermudo, E., Garcia, F., Manresa, A., Martín-Arjol, I., *et al.* (2010) Identification of oxylipins with antifungal activity by LC-MS/MS from the supernatant of *Pseudomonas* 42A2. *Chem Phys Lipids* **163**: 341–6.

Martin-Arjol, I., Llorens Llacuna, J., and Manresa, A. (2014) Yield and kinetic constants estimation in the production of hydroxy fatty acids from oleic acid in bioreactor by *Pseudomonas aeruginposa* 42A2. *Appl Microbiol Biotechnol* **98**: 9609–9621.

Martin Arjol I, Busquets M, M.A. (2015) Production of bacterial oxylipins by *Pseudomonas aeruginosa* 42A2. In *Recent Advances in Pharmaceutical Sciences V*.

Diego Muñoz-Torrero, M.P.V. and J.P. (ed.). Research Signpost, pp. 1–17.

Martínez, E., Estupiñán, M., Pastor, F.I.J., Busquets, M., Díaz, P., and Manresa, A. (2013) Functional characterization of ExFadLO, an outer membrane protein required for exporting oxygenated long-chain fatty acids in *Pseudomonas aeruginosa*. *Biochimie* **95**: 290–298.

Martinez, E., Hamberg, M., DBusquets, M., Díaz, P., Manresa, A., and Oliw, E. (2010) Biochemical characterization of hte oxygenation of unsaturated fatty acids by the diogenase and hydroperoxide isomerase of Pseudomonas 42A2. *J Biol Chem*.

Mercadé, M.E., Robert, M., Espuny, M.J., Bosch, P., Manresa, A., Parra, J.L., and Guinea, J. (1988) New surfactant isolated from *Pseudomonas* sp 42A2. *JAOCS* **65**: 1915–1916.

Meyer, J.-M., Geoffroy, V.A., Baysse, C., Cornelis, P., Barelmann, I., Taraz, K., and Budzikiewicz, H. (2002) Siderophore-Mediated Iron Uptake in *Pseudomonas fluorescent*: Characterization of the Pyoverdine-Receptor Binding Site of Three Cross-Reacting Pyoverdines. *Arch Biochem Biophys* **397**: 179–183.

Mogk, A., Schlieker, C., Friedrich, K.L., Schönfeld, H.-J., Vierling, E., and Bukau, B. (2003) Refolding of Substrates Bound to Small Hsps Relies on a Disaggregation Reaction Mediated Most Efficiently by ClpB/DnaK. *J Biol Chem* **278**: 31033–31042.

Morell, M., Bravo, R., Espargaró, A., Sisquella, X., Avilés, F.X., Fernàndez-Busquets, X., and Ventura, S. (2008) Inclusion bodies: Specificity in their aggregation process and amyloid-like structure. *Biochim Biophys Acta - Mol Cell Res* **1783**: 1815–1825.

Mueller, M.J. (2004) Archetype signals in plants: the phytoprostanes. *Curr Opin Plant Bioology* **7**: 441–448.

Naiki, H., Higuchi, K., Matsushima, K., Shimada, A., Chen, W.H., Hosokawa, M., and Takeda, T. (1990) Fluorometric examination of tissue amyloid fibrils in murine senile amyloidosis: use of the fluorescent indicator, thioflavine T. *Lab Invest* **62**: 768–73.

Newcomer, M.E., and Brash, A.R. (2015) The structural basis for specificity in lipoxygenase catalysis. *Protein Sci* **24**: 298–309

Niehaus, W.G., Torkelson, A., Kisic, A., Bednarczyk, D.J., and Schroepfer, G.J. (1970) Stereospecific hydration of the delta-9 double bond of oleic acid. *J Biol Chem* **245**: 3790–7.

Nikel, P.I., Martínez-García, E., and Lorenzo, V. de (2014) Biotechnological domestication of *Pseudomonads* using synthetic biology. *Nat Rev Microbiol* **12**: 368–379.

Nilsson, M.R. (2004) Techniques to study amyloid fibril formation. *Methods* **34**: 151–160.

Nilsson, T., Martinez, E., Manresa, A., and Oliw, E.H. (2010) Liquid chrmomatrography/tandem Mass spectrometric anañysisi of 7,10-dihydroxyoctadecenoic acids, its sotopomers and other 7,10 -dihydroxy fatty acids formed by Pseudomonas aeruginosa 42A2. *Rapid Comm mass spactrometry* **24**: 777–783.

Oliw, E.H. (2002) Plant and fungal lipoxygenases. *Prostaglandins other lipid Mediat* **68**–**69**: 313–323.

Omura, T., and Sato, R. (1962) A new cytochrome in liver microsomes. *J Biol Chem* **237**: 1375–6.

Parra, J.L., Pastor, J., Comelles, F., Manresa, M.A., and Bosch, M.P. (1990) Studies of biosurfactants obtained from olive oil. *Tenside, Surfactants, Deterg* **27**: 302–306.

Parte, A.C. (2014) LPSN—list of prokaryotic names with standing in nomenclature. *Nucleic Acids Res* **42**: D613–D616

Paul S, Hou HT, K.S. (2010) α-Glucosidase inhibitory activities of 10-hydroxy-8(E)-octadecenoic acid: an intermediate of bioconversion of oleic acid to 7,10-dihydroxy-8(E)-octadecenoic acid. *N Biotechnol* **7**: 419–423.

Peláez, M., Orellana, C., Marqués, A., Busquets, M., Guerrero, A., and Manresa, A. (2003) Natural Estolides Produced by *Pseudomonas* sp. 42A2 Grown on Oleic Acid: Production and Characterization. *JAOCS* **80**: 859–866.

Peternel, Š., and Komel, R. (2011) Active protein aggregates produced in *Escherichia coli*. *Int J Mol Sci* **12**: 8275–8287.

Qi, X., Sun, Y., and Xiong, S. (2015) A single freeze-thawing cycle for highly efficient solubilization of inclusion body proteins and its refolding into bioactive form. *Microb Cell Fact* **14**: 24

Ramón, A., Señorale-Pose, M., and Marín, M. (2014) Inclusion bodies: not that bad…. *Front Microbiol* **5**: 56.

Rehm, B.H., and Steinbüchel, A. (1999) Biochemical and genetic analysis of PHA synthases and other proteins required for PHA synthesis. *Int J Biol Macromol* **25**: 3–19.

Ridgway, H.F., Safarik, J., Phipps, D., Carl, P., and Clark, D. (1990) Identification and catabolic activity of well-derived gasoline-degrading bacteria from a contaminated aquifer. *Appl Environ Microbiol* **56**: 3565–75.

Rinas, U., Garcia-Fruitós, E., Corchero, J.L., Vázquez, E., Seras-Franzoso, J., and Villaverde, A. (2017) Bacterial Inclusion Bodies: Discovering Their Better Half. *Trends Biochem Sci* **42**: 726–737.

Rodríguez-Carmona, E., Cano-Garrido, O., Seras-Franzoso, J., Villaverde, A., and García-Fruitós, E. (2010) Isolation of cell-free bacterial inclusion bodies. *Microb Cell Fact* **9**: 71.

Rodriguez, E. (2006) Aplicación de la Metodología de Superficies de Respuesta en

matraces y estrategias de producción en biorreactor para la obtención de biomasa y polihidroxialcanoatos por *Pseudomonas aeruginosa* 42A2. *PhD thesis*. University of Barcelona.

Rodríguez, E., Espuny, M.J., Manresa, A., and Guerrero, A. (2001) Identification of (E)-11-hydroxy-9-octadecenoic acid and (E)-9-hydroxy-10-octadecenoic acid by biotransformation of Oleic acid by *Pseudomonas* sp. 32T3. *JAOCS* **78**.

Ruggeri, F.S., Habchi, J., Cerreta, A., and Dietler, G. (2016) AFM-Based Single Molecule Techniques: Unraveling the Amyloid Pathogenic Species. *Curr Pharm Des* **22**: 3950–70.

Ryan, R.P., Germaine, K., Franks, A., Ryan, D.J., and Dowling, D.N. (2008) Bacterial endophytes: recent developments and applications. *FEMS Microbiol Lett* **278**: 1–9.

Rydberg, P., Sigfridsson, E., and Ryde, U. (2004) On the role of the axial ligand in heme proteins: a theoretical study. *JBIC J Biol Inorg Chem* **9**: 203–223.

Sabaté, R., Espargaró, A., Saupe, S.J., and Ventura, S. (2009) Characterization of the amyloid bacterial inclusion bodies of the HET-s fungal prion Raimon Sabaté1, Alba. *Microb Cell Fact* **8**: 56.

Sambrook, J., Fritsch, E.F., and Maniatis, T. (1989) *Molecular cloning: a laboratory manual.Second edition*. Cold Spring Harbor Laboratory Press, N.Y.

Schroepfer, G.J. (1966) Stereospecific Conversion of Oleic Acid to IO-Hydroxystearic Acid. Biochem 241:5441-5447.

Senger, T., Wichard, T., Kunze, S., Göbel, C., Lerchl, J., Pohnert, G., and Feussner, I. (2005) A Multifunctional Lipoxygenase with Fatty Acid Hydroperoxide Cleaving Activity from the Moss *Physcomitrella patens*. *J Biol Chem* **280**: 7588–7596.

Seo, M.-J., Kang, W.-R., Shin, K.-C., and Oh, D.-K. (2016) Production of 7,8-Dihydroxy Unsaturated Fatty Acids from Plant Oils by Whole Recombinant Cells Expressing 7,8-Linoleate Diol Synthase from *Glomerella cingulata*. *J Agric Food Chem* **64**: 8555–8562.

Seo, M.-J., Shin, K.-C., An, J.-U., Kang, W.-R., Ko, Y.-J., and Oh, D.-K. (2015) Characterization of a recombinant 7,8-linoleate diol synthase from *Glomerella cingulate*. *Appl Microbiol Biotechnol* **100**: 3087–3099.

Seo, M.-J., Shin, K.-C., and Oh, D.-K. (2014) Production of 5,8-dihydroxy-9,12(Z,Z)-octadecadienoic acid from linoleic acid by whole recombinant Escherichia coli cells expressing diol synthase from Aspergillus nidulans. *Appl Microbiol Biotechnol* **98**: 7447–7456.

Shin, K.-C., Seo, M.-J., and Oh, D.-K. (2016) Characterization of a novel 8R,11S-linoleate diol synthase from *Penicillium chrysogenum* by identification of its enzymatic products. *J Lipid Res* **57**: 207–18.

Silby, M.W., Winstanley, C., Godfrey, S.A.C., Levy, S.B., and Jackson, R.W.

(2011) *Pseudomonas* genomes: diverse and adaptable. *FEMS Microbiol Rev* **35**: 652–680.

Singh, A., Upadhyay, V., Upadhyay, A.K., Singh, S.M., and Panda, A.K. (2015) Protein recovery from inclusion bodies of *Escherichia coli* using mild solubilization process. *Microb Cell Fact* **14**: 41.

Sodagari, M., Invally, K., and Ju, L.K. (2018) Maximize rhamnolipid production with low foaming and high yield. *Enzyme Microb Technol* **110**: 79–86.

Stahl, P.D., and Klug, M.J. (1996) Characterization and differentiation of filamentous fungi based on Fatty Acid composition. *Appl Environ Microbiol* **62**: 4136–46.

Su, C., and Oliw, E.H. (1996) Purification and Characterization of Linoleate 8-Dioxigenase from the fungus *Gaeumannomyces graminis* as a Novel Hemoprotein. *J Biol Chem* **271**: 14112–14118.

Tokatlidis, K., Dhurjati, P., Millet, J., Beguin, P., and Aubert, J.. (1991) High activity of inclusion bodies formed in *Escherichia coli* overproducing Clostridium thermocellum endoglucanase D. *FEBS Lett* **282**: 205–208.

Tyedmers, J., Mogk, A., and Bukau, B. (2010) Cellular strategies for controlling protein aggregation. *Nat Rev Mol Cell Biol* **11**: 777–788.

Unzueta, U., Cespedes, M.V., Sala, R., Alamo, P., Sánchez-Chardi, A., Pesarrodona, M., *et al.* (2018) Release of targeted protein nanoparticles from functional bacterial amyloids: A death star-like approach. *J Control Release* **279**: 29–39.

Upadhyay, A.K., Murmu, A., Singh, A., and Panda, A.K. (2012) Kinetics of inclusion body formation and its correlation with the characteristics of protein aggregates in *Escherichia coli*. *PLoS One* **3**: e33951.

Vallejo, L.F., and Rinas, U. (2004) Strategies for the recovery of active proteins through refolding of bacterial inclusion body proteins. *Microb Cell Fact* **3**: 11.

Vazhnova, T., and Lukyanov, D.B. (2013) Fourier Self-Deconvolution of the IR Spectra as a Tool for Investigation of Distinct Functional Groups in Porous Materials: Brønsted Acid Sites in Zeolites. *Anal Chem* **85**: 11291–11296.

Vidal-Mas, J., Busquets, M., and Manresa, A. (2005) Cloning and expression of a lipoxygenase from *Pseudomonas aeruginosa* 42A2. *Antonie Van Leeuwenhoek* **87**: 245–251.

Vidal-Mas, J., Resina-Pelfort, O., Haba, E., Comas, J., Manresa, A., and Vives-Rego, J. (2001) Rapid flow cytometry - Nile red assessment of PHA cellular content and heterogeneity in cultures of *Pseudomonas aeruginosa* 47T2 (NCIB 40044) grown in waste frying oil. *Antonie van Leeuwenhoek*, **80**: 57–63.

Villaverde, A., Corchero, J.L., Seras-Franzoso, J., and García-Fruitós, E. (2015) Functional protein aggregates: just the tip of the iceberg. *Nanomedicine* **10**: 2881–2891.

Wallen, L.L., Benedict, R.G., and Jackson, R.W. (1962) The microbiological production of 10-Hydroxystearic acid from oleic acid. *Arch Biochem Biophys* **99**:249–253.

Wallen, L.L., Davis, E.N., Wu, Y. V, and Rohwedder, W.K. (1971) Stereospecific hydration of unsaturated fatty acids by bacteria. *Lipids* **6**: 745–50.

Wang, L. (2009) Towards revealing the structure of bacterial inclusion bodies. *Prion* **3**: 139–145.

Wang, L., Maji, S.K., Sawaya, M.R., Eisenberg, D., and Riek, R. (2008) Bacterial inclusion bodies contain amyloi-like structure. *PLoS/Biology* **6**: 1791–1801.

Wang, W., Nema, S., and Teagarden, D. (2010) Protein aggregation-Pathways and influencing factors. *Int J Pharm* **390**: 89–99.

Wennman, A., Magnuson, A., Hamberg, M., and Oliw, E.H. (2015) Manganese lipoxygenase of *F. oxysporum* and the structural basis for biosynthesis of distinct 11-hydroperoxy stereoisomers. *J Lipid Res* **56**: 1606–1615.

Wennman, A., and Oliw, E.H. (2013) Secretion of two novel enzymes, manganese 9S-lipoxygenase and epyxy alcohol synthase, by the rice pathogen Magnaporthe salvinii. *J Lipid Res* **54**: 762–774.

Worral, D.M., and Gross, N.H. (1989) The formation of biologically active beta-galactosidase from *Escherichia coli*. *Aust J Biotechnol* **3**: 28–32.

Wu, C., Wang, Z., Lei, H., Zhang, W., and Duan, Y. (2007) Dual Binding Modes of Congo Red to Amyloid Protofibril Surface Observed in Molecular Dynamics Simulations. *J Am Chem Soc* **219**: 1225–1232.

Wu, W., Xing, L., Zhou, B., and Lin, Z. (2011) Active protein aggregates induced by terminally attached self-assembling peptide ELK16 in *Escherichia coli*. *Microb celll factories* **10**: 9.

Zhang, Z., Hou, Z., Yang, C., Ma, C., Tao, F., and Xu, P. (2011) Degradation of n-alkanes and polycyclic aromatic hydrocarbons in petroleum by a newly isolated *Pseudomonas aeruginosa* DQ8. *Bioresour Technol* **102**: 4111–4116.

Zhou, B., Xing, L., Wu, W., Zhang, X.-E., and Lin, Z. (2012) Small surfactant-like peptides can drive soluble proteins into active aggregates. *Microb Cell Fact* **11**: 10.

Zhu, L., Yang, X., Xue, C., Chen, Y., Qu, L., and Lu, W. (2012) Enhanced rhamnolipids production by *Pseudomonas aeruginosa* based on a pH stage-controlled fed-batch fermentation process. *Bioresour Technol* **117**: 208–213.

8. ANNEXES

8.1 ADDITIONAL INFORMATION

NCBI (http://www.ncbi.nlm.nih.gov) was used for multiple sequence alignment (MSA) of all selected species. Multiple amino acid sequence alignment of PA2077 and PA2078 proteins, obtained by ClustalO.

Figure A1. Multiple amino acid sequence alignment of PA2077 and PA2078 proteins, obtained by ClustalO.

Figure A2. TLC chromatography: detection of 10S-H(P)OME produced by *P. putida* (pBBR-77).

Figure A3-A4.5. Graphical summary of protein Blast analysis of PA2077 and PA2078 amino acid for selected species.

Figure A5-A5.3. Functional of similar motifs in PA2077 and PA2078

Figure A6-A6.6. LC-MS/MS analysis of 10-H(P)OME and 7,10-DiHome produced by species.

```
PA2077      1  --MTLSRLSLAILSVLAGAPAFADDSGVDLDQGWNQTQKTAWLEAGQGSRMLPLAWLVAL   58
PA2078      1  MHPTFSRVLLAAALAAAGSPAV--ATEIQLEQGWNAEQRASWYDASLGSRLLPLAWAQAL   58
               *:**: **   . **:**.   : ::*:****  *:::* :*. ***:***** **

PA2077     59  EQRASEEPLMSDALIRQYGYVPHTLGGSSVKVVQGYAVDRSDDSDLTFTKLRWKALQGSR   118
PA2078     59  ERPDSEERLFSEDNARRLGFPLRNWQGGELRLPRGFALDQQDDSQFSDTRLRWKARQSSS   118
               *:  *** *:*:   *: *:  :.  *..::: :*:*:*:.***::: *:***** *.*

PA2077    119  EPWVGPTCSMCHTSHISYQGTQLTVYGGQTMGDLAGFQLEILGALQSTRADTAKFERFAR   178
PA2078    119  EPWVGLNCAGCHSTDISYRGSELTVDAGATLANVQAIFDEVLAALRRTSDDGDKFARFAG   178
               ***** .*: **::.***:*::*** .* *:.:: .:  *:*.**: *  *  ** ***

PA2077    179  KVLGADGLVSGYNDANKARLQAALDATIVRLRDGSHFNLPHDPEFGPGRLDAIGSIFNSV   238
PA2078    179  NVLGSEDSPANR-----ELLKAALVKRA-ALIDTLLSMSATDLQPGPGRLDATGQSLNRA   232
               :***::.  :.        *:***      * *        * : ******* *. :* .

PA2077    239  GYELHADEQIYGAEDAPVSYPFLWNVPQLDRVQWTGFNPNHINVVDIDNRKFDVGALARN   298
PA2078    233  AINSGARHLQANPTDAPTSFPALWHTLQMDKLQSSGFVPN-VKVLDLNGQVFDLGYLAGD   291
               . :  * .   .  ***.*:* **:. *:*::* :** ** ::*:*::.: **:* ** :

PA2077    299  AGEAVGVFADVKVLSPIQSALHIGYPSSINVDNLIRIEDQLGQLKPPAWPNQLFGAPEPT   358
PA2078    292  IGVVQGDYGDVVSH-P--LSGLEGYISSIRVDNLTRVEGLIHKLKAPAWPSQLFGAPDSA   348
               * . * :.**    *   :   ** ***.**** *:*. : :** ****.******: :

PA2077    359  RVAEGRELYRQHCSSCHTPLDRNDLRTPVKTVLTHLQARGEVAPIGTDPWTACNSIAQLK   418
PA2078    349  RLAQGKRLYEENCAACHASIGRDDLQTPIKVRQVRLKAHGDDAPIGTDPWMACNTFTFSS   408
               *:*:*:.**.::*::**: :.*:**:**:*.  .:*:*:*: ******** ***:::  .

PA2077    419  TGY-VRGKPYLSFVGTGQRGFYGKQAYAVDVLQEVVVQALAARGLSVALGAFQTAALGIF   477
PA2078    409  PSGNYFGLFRPSLGTPSGVGIVGRTSKIADMQVPEVFQIM--------LGKKGQLADGIA   460
               .   *    *:   .  *: *: :  .*:    *.* :        **     * **

PA2077    478  DGQLPPLISPVPDSPDADSAEATAADAPGALLLAEN------------VAADSDKARRLE   525
PA2078    461  E-IIHAIVTGQQTLPGSDSLQ---AVPAGQLLLAGAAPADSQAQSLAAGEVPTDKSARKD   516
               :  :  :::     *.:** :   *   * ****                . :**: * :

PA2077    526  QCLAMTSDLMAYKARPLNGIWASPPYLHNGSVATLYDLLLPPDLRPRTFYTGSVEFDPVN   585
PA2078    517  YCLNTEHPFLGYIARPLNGIWATAPYLHNGSVPSLYDLLLPQEQRPATFYTGSHEFDPSR   576
               **     ::.* *********: ******** :******* : ** ****** **** .

PA2077    586  VGYITDAGGANRFLFDSGKPGNANGGHDYGNAQFNEQQRRALVEYMKTL             634
PA2078    577  VGYLTAPGPDNAFLFDTHLEGNSNAGHDFAR-EYDESQRLALLEYLKTL             624
               ***:*  *  * ****:   **:*.***:.. :::*.** **:**:***
```

Figure A1. Multiple amino acid sequence alignment of PA2077 and PA2078 proteins, obtained by ClustalO. The hydrophobic amino acids shown in the figure are highlight by purple box.

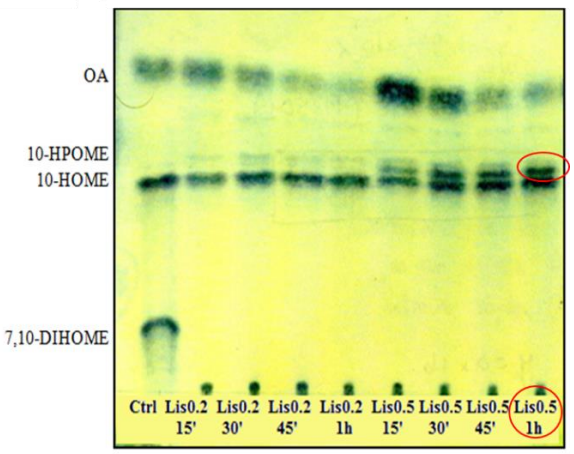

Figure A2. TLC analysis of *P. putida* (pBBR-77) cell extract with 0.2g/L and 0.5g/L incubated at 15 min, 30 min, 45 min and 1 h. The highest amount of 10-HPOME obtain at 1 h with 0.5g/L (red circles).

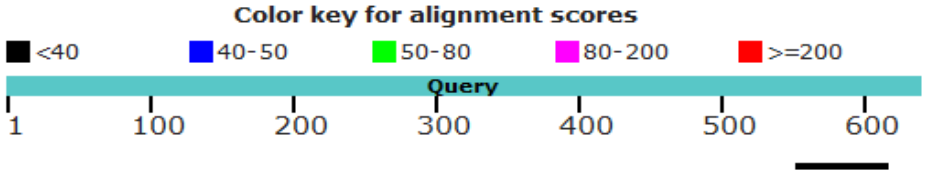

Figure A3. Blast results of *Aeromonas* group (taxid:642) with PA2077 aa. The query bar represents 10% with 36% of identity.

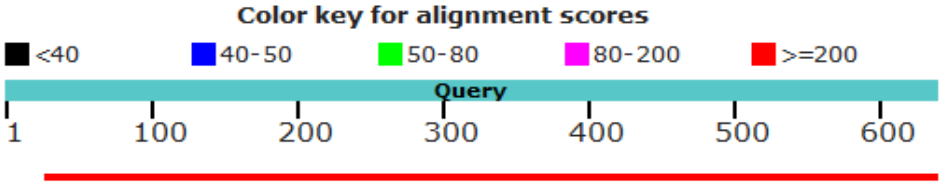

Figure A3.1. Blast results of *Pseudoalteromonas* (taxid:53246) with PA2077 aa. The query bar represents 95% with 34% of identity.

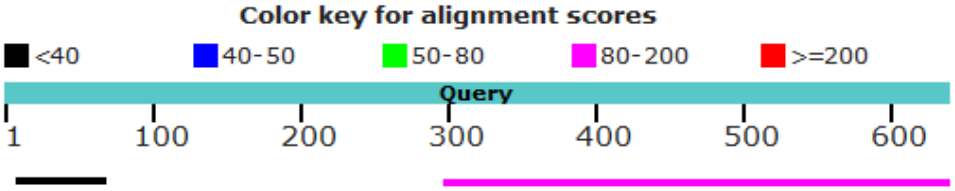

Figure A3.2. Blast results of *Shewanella* with PA2077 aa. The query bar represents 53% with 27% of identity.

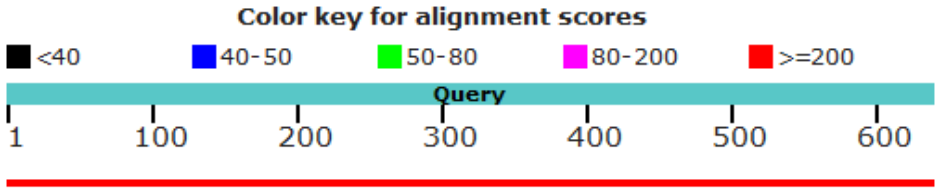

Figure A3.3. Blast results of *Pseudomonas* (taxid: 286) with PA2077 aa. The query bar represents 100% with 99% of identity.

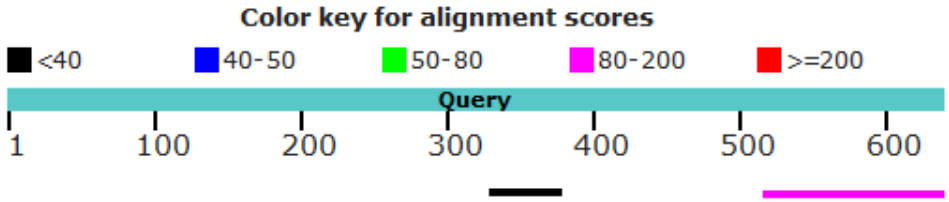

Figure A3.4. Blast results of *Thauera* (taxid:33057) with PA2077 aa. The query bar represents 19% with 39% of identity.

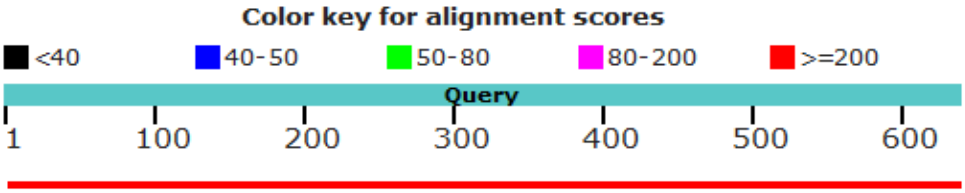

Figure A3.5. Blast results of Sinorhizobium/Ensifer group (taxid:227292) with PA2077 aa. The query bar represents 99% with 36% of identity.

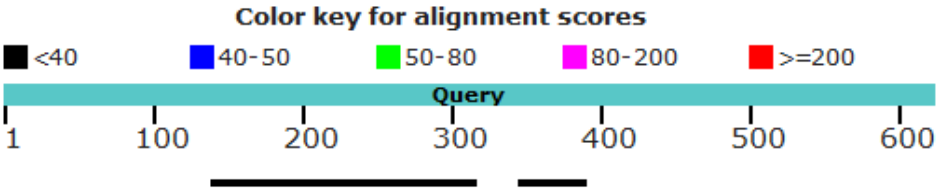

Figure A4. Blast results of *Aeromonas* (taxid: 84642) with PA2078 aa. The query bar represents 28% with 27% of identity.

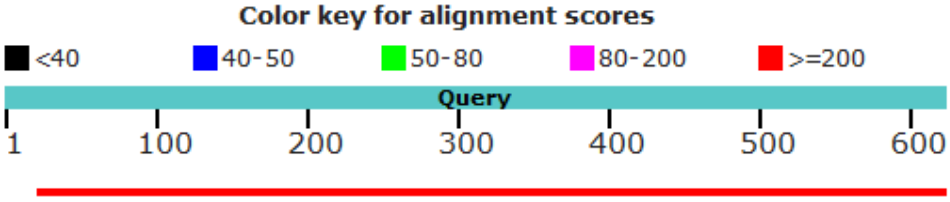

Figure A4.1. Blast results of *Pseudoalteromonas* (TAXID: 53246) with PA2078 aa. The query bar represents 96% with 31% of identity.

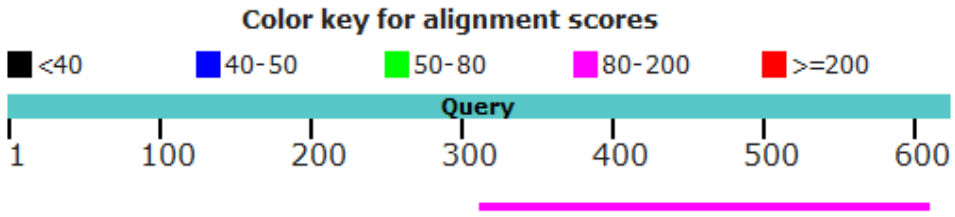

Figure A4.2. Blast results of *Shewanella* (taxid: 22) with PA2078 aa. The query bar represents 47% with 29% of identity.

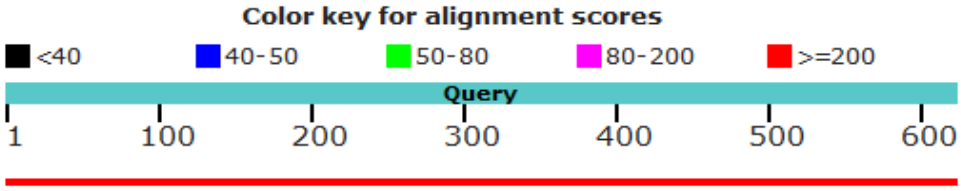

Figure A4.3. Blast results *Pseudomonas* (taxid: 286) with PA2078 aa. The query bar represents 100% with 99% of identity.

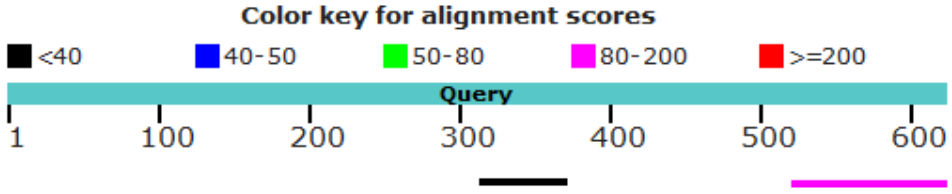

Figure A4.4. Blast results *Thauera* (taxid:33057) with PA2078 aa. The query bar represents 16% with 49% of identity.

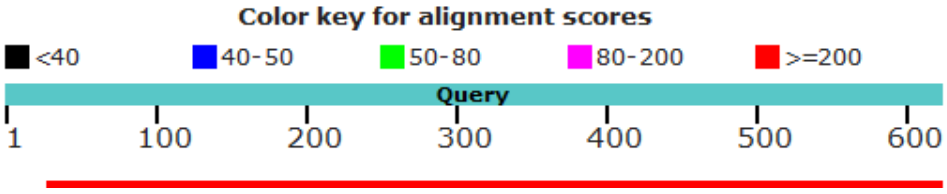

Figure A4.5. Blast results *Sinorhizobium/Ensifer* group (taxid: 227292) with PA2078 aa. The query bar represents 95% with 36% of identity.

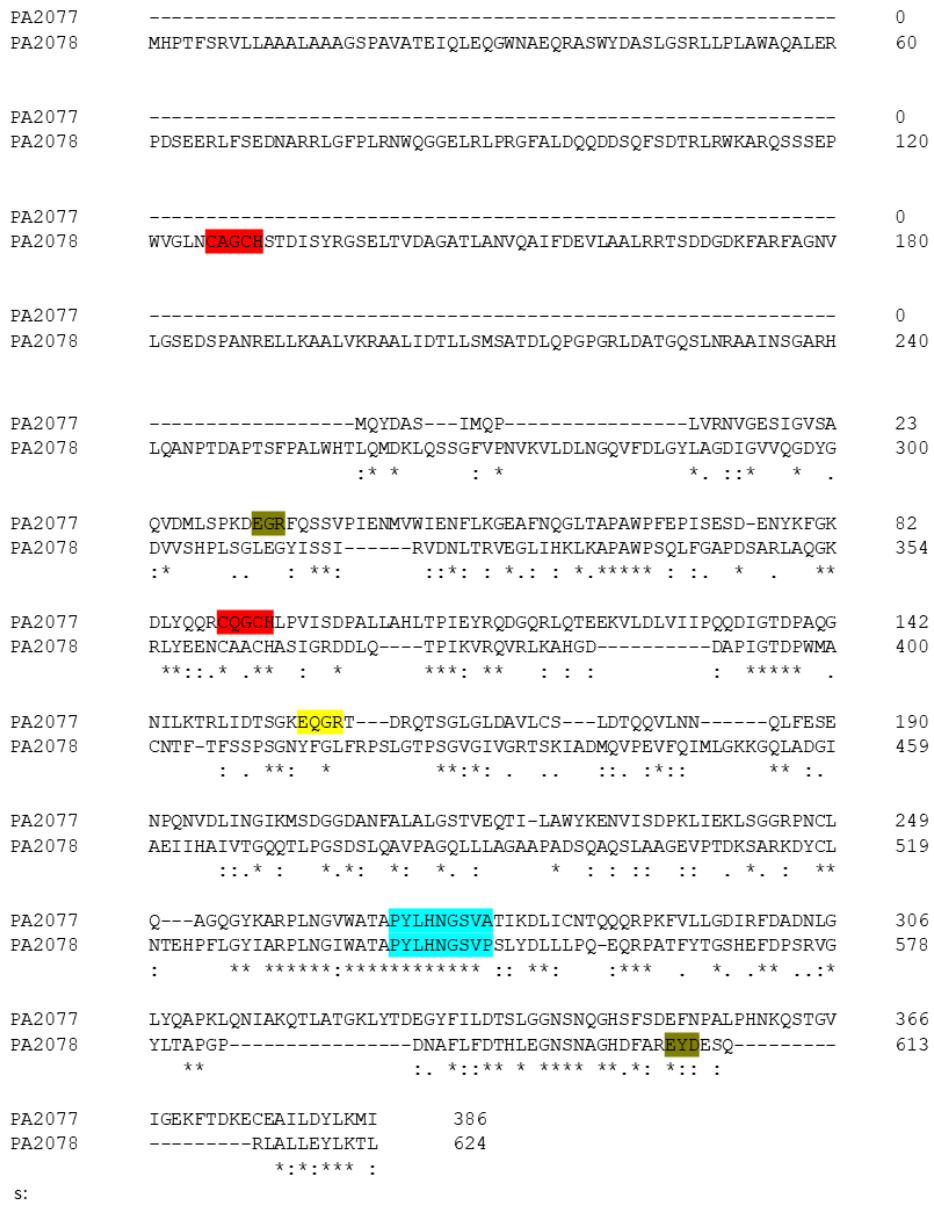

Figure A5. Multiple amino acid sequence alignment of PA2077 and PA2078 in hypothetical protein (*Shewanella denitrificans*) obtained by ClustalO. Conserved heme sequences (CXXCH) are shown in red. The predicted motif for ferrous ion union is depicted in green (EGR or EYD). P450 motifs (EXXR) are in yellow. The signature of oxidases containing the essential histidine like in MauG is shown in blue.

```
PA2077      MSKLHLAFALGAVSLITVVGCSSNQHNAQPDPISITPERGEIPTRTWLDQGWSKQISENF     60
PA2078      MSKLHLAFALGAVSLITVVGCSSNQHNAQPDPISITPERGEIPTRTWLDQGWSKQISENF     60
            ************************************************************

PA2077      WFTNQGSQIIPYNWFVWLEQADSTQLFRHAKHMESLRYLPSKASQKNPGGLPIGFALHSN     120
PA2078      WFTNQGSQIIPYNWFVWLEQADSTQLFRHAKHMESLRYLPSKASQKNPGGLPIGFALHSN     120
            ************************************************************

PA2077      QTTGENWVGMTCAACHTNQIDYKGTKILIDGAPTLANFVLFFDRLVAALNKTLSDDEKFE     180
PA2078      QTTGENWVGMTCAACHTNQIDYKGTKILIDGAPTLANFVLFFDRLVAALNKTLSDDEKFE     180
            ************************************************************

PA2077      RFAKNVLGASYNTVNKNDLKGRLQSIALKTAQRQAVNALPEDYPKDFTSYARLDAFGNIQ     240
PA2078      RFAKNVLGASYNTVNKNDLKGRLQSIALKTAQRQAVNALPEDYPKDFTSYARLDAFGNIQ     240
            ************************************************************

PA2077      NAGTAFALSDLTNKNAPTGPVSYPFLWGTHQSDVVQWNASAPNISIVGPLVRNIGEVVGV     300
PA2078      NAGTAFALSDLTNKNAPTGPVSYPFLWGTHQSDVVQWNASAPNISIVGPLVRNIGEVVGV     300
            ************************************************************

PA2077      FGELDIKEAPFWQRLWGKHTRYSSTVDMIGLGNLESWVKTLKSPQWPTQYFPAIDVEKAA     360
PA2078      FGELDIKEAPFWQRLWGKHTRYSSTVDMIGLGNLESWVKTLKSPQWPTQYFPAIDVEKAA     360
            ************************************************************

PA2077      KGELLYQQQCAGCHEVVPRDKELEDYKANQTLISELGTDPVTAYNASCNMAKTLILEGTK     420
PA2078      KGELLYQQQCAGCHEVVPRDKELEDYKANQTLISELGTDPVTAYNASCNMAKTLILEGTK     420
            ************************************************************

PA2077      ERILIGSKFQEIDNAIDIPVNGVVGLVLKDLPLALKAGNIPERTGADGEKISVLKELENL     480
PA2078      ERILIGSKFQEIDNAIDIPVNGVVGLVLKDLPLALKAGNIPERTGADGEKISVLKELENL     480
            ************************************************************

PA2077      LVQHLKKRGEKANQVETDCVDGKLDNGVYKGRPLNGIWATAPYLHNGSVPSLYELMKKPD     540
PA2078      LVQHLKKRGEKANQVETDCVDGKLDNGVYKGRPLNGIWATAPYLHNGSVPSLYELMKKPD     540
            ************************************************************

PA2077      QRVTEFWVGSREFDPVNVGFDTTTGLNKFKVNTKNGKAMPGNSNKGHSYGTHLSDEQKWQ     600
PA2078      QRVTEFWVGSREFDPVNVGFDTTTGLNKFKVNTKNGKAMPGNSNKGHSYGTHLSDEQKWQ     600
            ************************************************************

PA2077      VIEYMKTL          608
PA2078      VIEYMKTL          608
            ********
```

Figure A5.1. Multiple amino acid sequence alignment of PA2077 and PA2078 in hypothetical protein (*Pseudoalteromonas byunsanensis*) obtained by ClustalO. Conserved heme sequences (CXXCH) are shown in red. P450 motifs (EXXR) are in yellow. The signature of oxidases containing the essential histidine like in MauG is shown in blue.

```
PA2077      MKRKSRFWPILLGFTVLVAAGLYYVVRMFSVDLPDYPKVDKVTWLEQNWSQSQRGWMHHA     60
PA2078      --MRIRRLPLLRSVAILIP----F--LVCGENARADSLPDGVQGLDQGWNDEQRSWWYTA     52
               : *  *:* ..::*:     :   : . :       * *  *:*.*.:.**.* : *

PA2077      DQGTVTFSMPYEWLAALEQPTFTLTAGPPFLSSDYLDRFGFITA-----DSSGLPVGFAH     115
PA2078      SQGSRL--LPLDWIQALETSGS----MEAFLSPAIVARLGYLPNPVSADNPLGLPVGFAV     106
            .**:    :* :*: ***           ***   : *:*::       :  *******

PA2077      GGDLVDPKTAQPWVNP----ATGKPLTTVGLTCAACHTGRFTYKGTAVMVDGGPALTDLG     171
PA2078      DQDKTRSADLMCDTFPAACDALTMRKPWVGLNCSACHTNEIVYQDKRFRVDGAATLADFQ     166
            . * .        . *    *       ***.*:****..:.*:.. . ***. :*:*:

PA2077      KFRKASGLALFFTRYAPFRFDRFATAVLGPQADEKARAVLKKQLDKVLAGGRIEVDLDKK     231
PA2078      AFEEELLASLKATLDDRPKFDRFARKVLKNDISVENRESLESQLREQIAWQQLLA----D     222
             *.:    :*  *     :*****  **  : . : *  *:.** : :*  :: .    .

PA2077      VAEKSIEEGFGRLDALNRIGNQVFSLDL-ERPENYVAQSAPVAFPHIWDTSWFDWVQYNA     290
PA2078      KNSSKVRYGHGRLDAQGHILNKVALVTRQADQPDIIHADAPASYPFIWNTSQQGKIQWNG     282
              ...:. *.***** .:* *:*  :       : :  .**.::*.**:**  . :*:*.

PA2077      SI---M-----------QPMVRNAGEALGVRAFINLTKSE-QPLFASTVKVDTIFEIEQQ     335
PA2078      IASNILKVNLLGKETDIGALVRNTSEVIGVFAHIETDRGKAWRGYDSSVRIVSMLSL---     339
                 :             :***:.*.:** *.*:  :.:    : *:*:: ::::.:

PA2077      LAGKQPTAENGFTGLRPPRWPSNLFGSIDTKLATEGAAVYA-DRCQGCHLPPVGSEGF--     392
PA2078      --------ERQLAELKSPRWPENILPPIDWDKATRGRAHFETFKCADCHKPLAWDDLDSP     391
                    *. :: *: ****.*::  ** . **.* * :   :* .** * . .:

PA2077      -WEQKHWTNENSAGERYLRVPI-INVENIGTDPAQAQ----------SMAERKVKLPSEL     440
PA2078      ALEQMDPI-DDQKTDIFLACNTFLHKSKSGNQKGQKIFAFSGDKITTIEFTRNLLINATV     450
              ** .   ::.  : :*     :: .: *.: .*               *:: : : :

PA2077      GIDTDSFGSALGALVAKTAARWYDN----------QTPPVPAEQREIMNGNRQNGIQAPL     490
PA2078      GAVVGKFDELAGGIFTDVSPTGRPTELAPELAVVEYLPGVTDAVKKDQARQCLEAKHPLL     510
            *  ...*..  *.:.:..:     .            * *    ::    :  :. :  *

PA2077      AYKARPLDGIWATPPFLHNGSVPTIDALLSPAG----------------ERPKTFWLGNR     534
PA2078      AYKARPLNGIWATAPYLHNGSVPSLYDLLLPAKVRNKSTDEPMGEVSGPTRPETFAVGSR     570
            *******:***** *:*******::  ** **                 **:** :*.*

PA2077      EYDPDKLGYLTDELKGGFKF--D-------TAKPGNSNAGHEFSDTPGPGVIGPALKPDE     585
PA2078      EFDPVHVGFVQTVVPGDGSFVFRVRDEASGEPIPGNYNSGHEYGTS--------RLSEQQ     622
            *:** ::*::   : *. .*            *** *:***:. :         *. ::

PA2077      KAALIAYLKTL      596
PA2078      RLELVEYLKTL      633
            :  *: *****
```

Figure A5.2. Multiple amino acid sequence alignment of PA2077 and PA2078 in *Sinorhizobium/Ensifer* group (taxid:227292 hypothetical protein (*Sinorhizobium* sp. GW3)) obtained by ClustalO. Conserved heme sequences (CXXCH) are shown in red. The predicted motif for ferrous ion union is depicted in green (EGR or EYD). P450 motifs (EXXR) are in yellow. The signature of oxidases containing the essential histidine like in MauG is shown in blue.

```
PA2077      MTLKSVLVAASIGAGSLISAAVLANDYTLDQNWSAKDLAVWRDTSQGSRLLPLSWITALE     60
PA2078      MTLKSVLVAASIGAGSLISAAVLANDYTLDQNWSAKDLAVWRDTSQGSRLLPLSWITALE     60
            ************************************************************

PA2077      IKGSKVPFMSDANVQTYGYTPSTLVFAYQSYRLPRGFVVDKESDKALTFSRLRWKDGQSD     120
PA2078      IKGSKVPFMSDANVQTYGYTPSTLVFAYQSYRLPRGFVVDKESDKALTFSRLRWKDGQSD     120
            ************************************************************

PA2077      QEPWVGMNCAACHTANVSFDGYTWEIPGGPTNADFQKFLHAFREALSDTQNDKEKFDRFA     180
PA2078      QEPWVGMNCAACHTANVSFDGYTWEIPGGPTNADFQKFLHAFREALSDTQNDKEKFDRFA     180
            ************************************************************

PA2077      SKVLAGTDTQANRQLLSTALDTLNRFLEEGASLNHTDLVYGPGRVDAVGHILNRVAQLNG     240
PA2078      SKVLAGTDTQANRQLLSTALDTLNRFLEEGASLNHTDLVYGPGRVDAVGHILNRVAQLNG     240
            ************************************************************

PA2077      APQPTPNPSDAPVSYPFLWNTPQHDKVQWNGVAPNLKLGSNGLDIGALARNASEVVGVFG     300
PA2078      APQPTPNPSDAPVSYPFLWNTPQHDKVQWNGVAPNLKLGSNGLDIGALARNASEVVGVFG     300
            ************************************************************

PA2077      DVSFRSDTHFKGFPSSVRIDNLDQLERTLTRLKPPKWPEKLGGIDENKQKRGAELFAQNC     360
PA2078      DVSFRSDTHFKGFPSSVRIDNLDQLERTLTRLKPPKWPEKLGGIDENKQKRGAELFAQNC     360
            ************************************************************

PA2077      SSCHLPLPRDDLKAKIVAKMSTISAETETNRSITTDPWMACNAVQFISDPGKLRGIHLNK     420
PA2078      SSCHLPLPRDDLKAKIVAKMSTISAETETNRSITTDPWMACNAVQFISDPGKLRGIHLNK     420
            ************************************************************

PA2077      IFGEITDQSTLVTQLGVTAREILLNQKHDIVALALKDFMNVEPAPSRVIRKGTFGFLRAF     480
PA2078      IFGEITDQSTLVTQLGVTAREILLNQKHDIVALALKDFMNVEPAPSRVIRKGTFGFLRAF     480
            ************************************************************

PA2077      QSERSRRLQACYALAQDKKKYPTLAYKARPLTGIWATAPYLHNGSVRTLYDLLLPPDKRP     540
PA2078      QSERSRRLQACYALAQDKKKYPTLAYKARPLTGIWATAPYLHNGSVRTLYDLLLPPDKRP     540
            ************************************************************

PA2077      SSFKTGSIMFDPEKVGFVDAFGPGSPFTFDTSLPGNSNAGHDYGASSFLDADRYALIEYM     600
PA2078      SSFKTGSIMFDPEKVGFVDAFGPGSPFTFDTSLPGNSNAGHDYGASSFLDADRYALIEYM     600
            ************************************************************

PA2077      KTL     603
PA2078      KTL     603
            ***
```

Figure A5.3. Multiple amino acid sequence alignment of PA2077 and PA2078 in *Pseudomonas fluorescens* obtained by ClustalO. Conserved heme sequences (CXXCH) are shown in red. P450 motifs (EXXR) are in yellow.

A

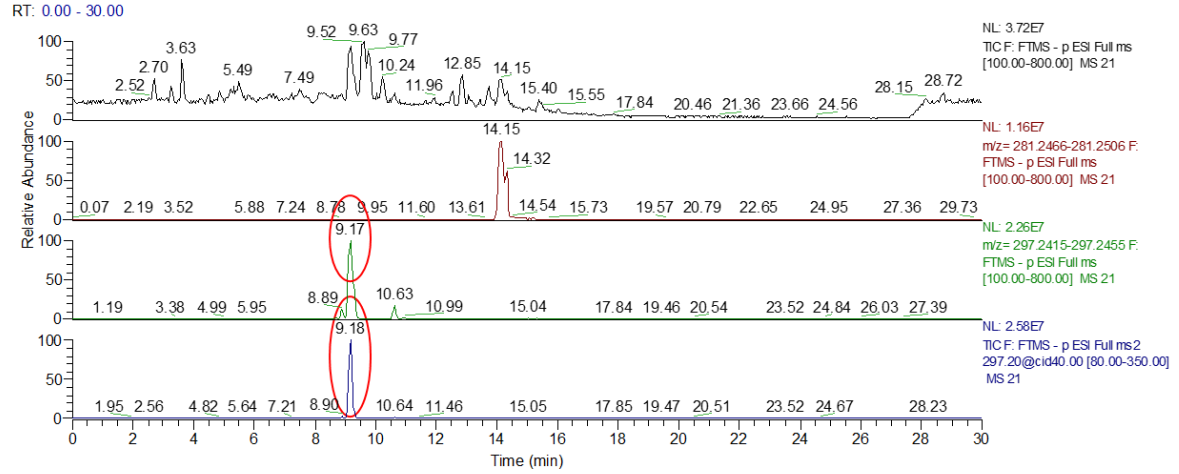

B

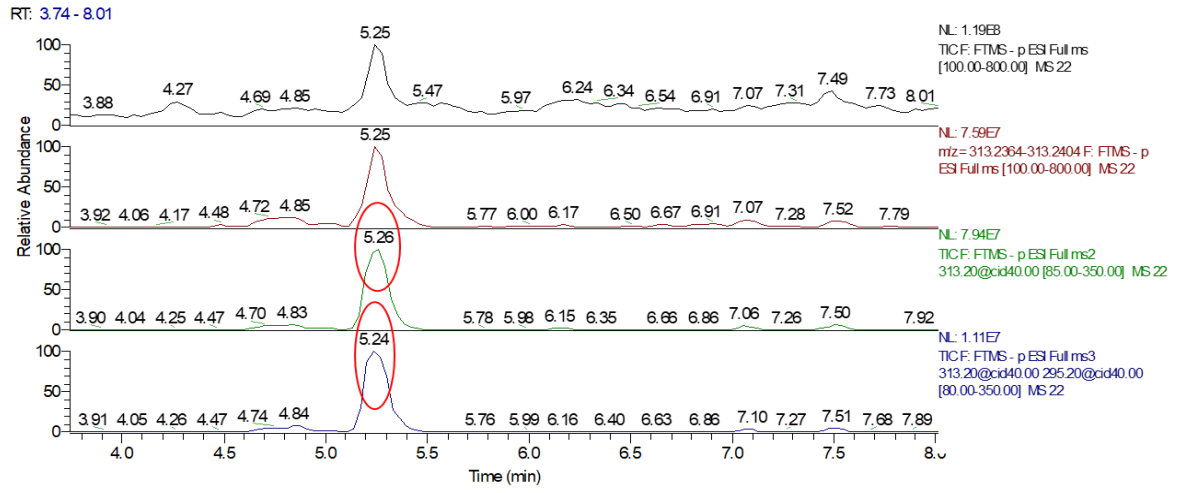

Figure A6. LC-MS/MS analysis of product formed by *P. aeruginosa* during diol synthase activity from OA. A, full scan chromatogram of 10-H(P)OME (peak of 9.17/9.18 min). B, full scan chromatogram of 7,10-DiHOME (peak of 5.26/5.24 min).

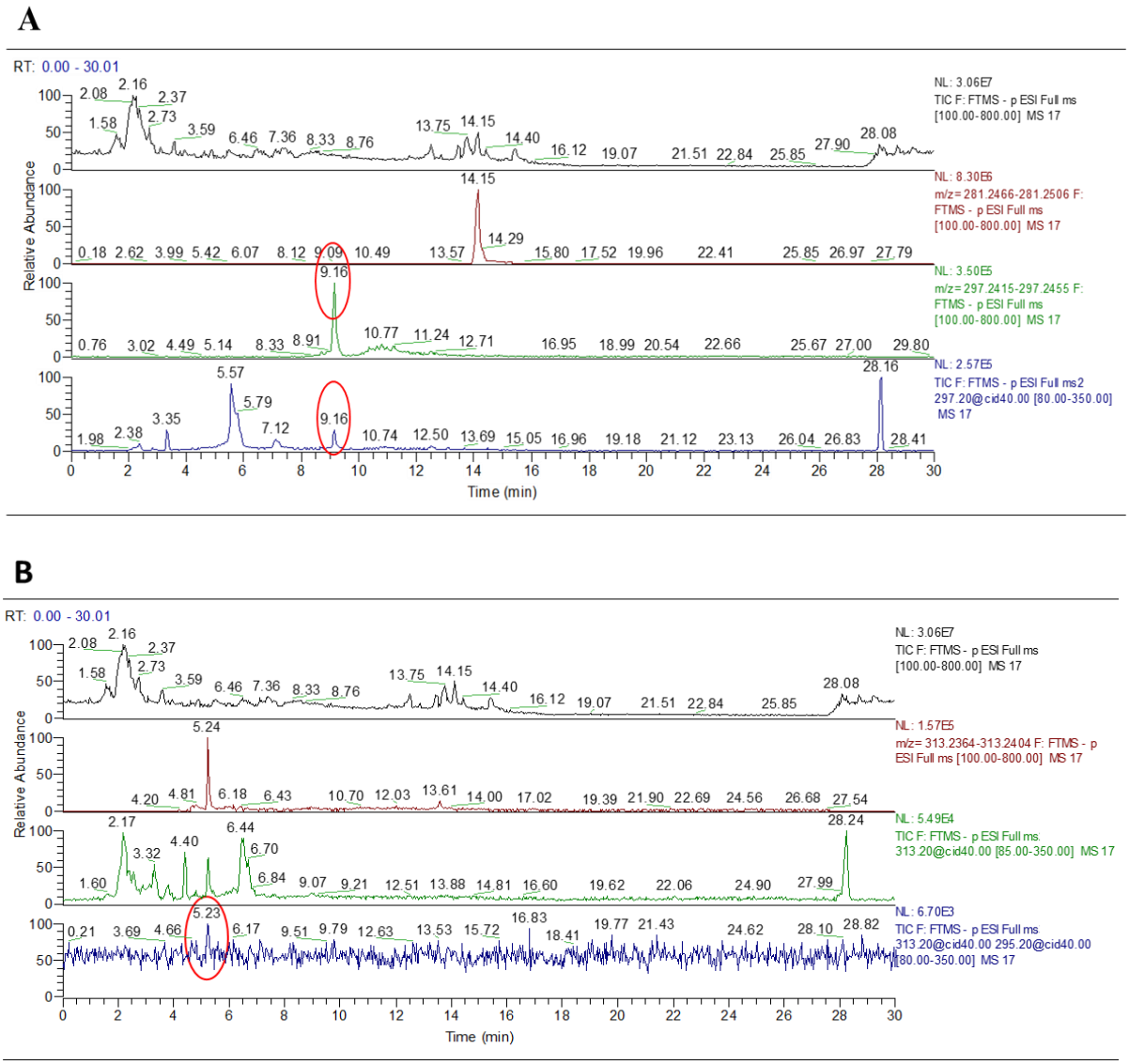

Figure A6.1. LC-MS/MS analysis of product formed by *P. fluorecens* during biotransformation from OA. A, full scan chromatogram of 10-H(P)OME (peak of 9.16 min). B, full scan chromatogram of 7,10-DiHOME (peak of 5.23 min).

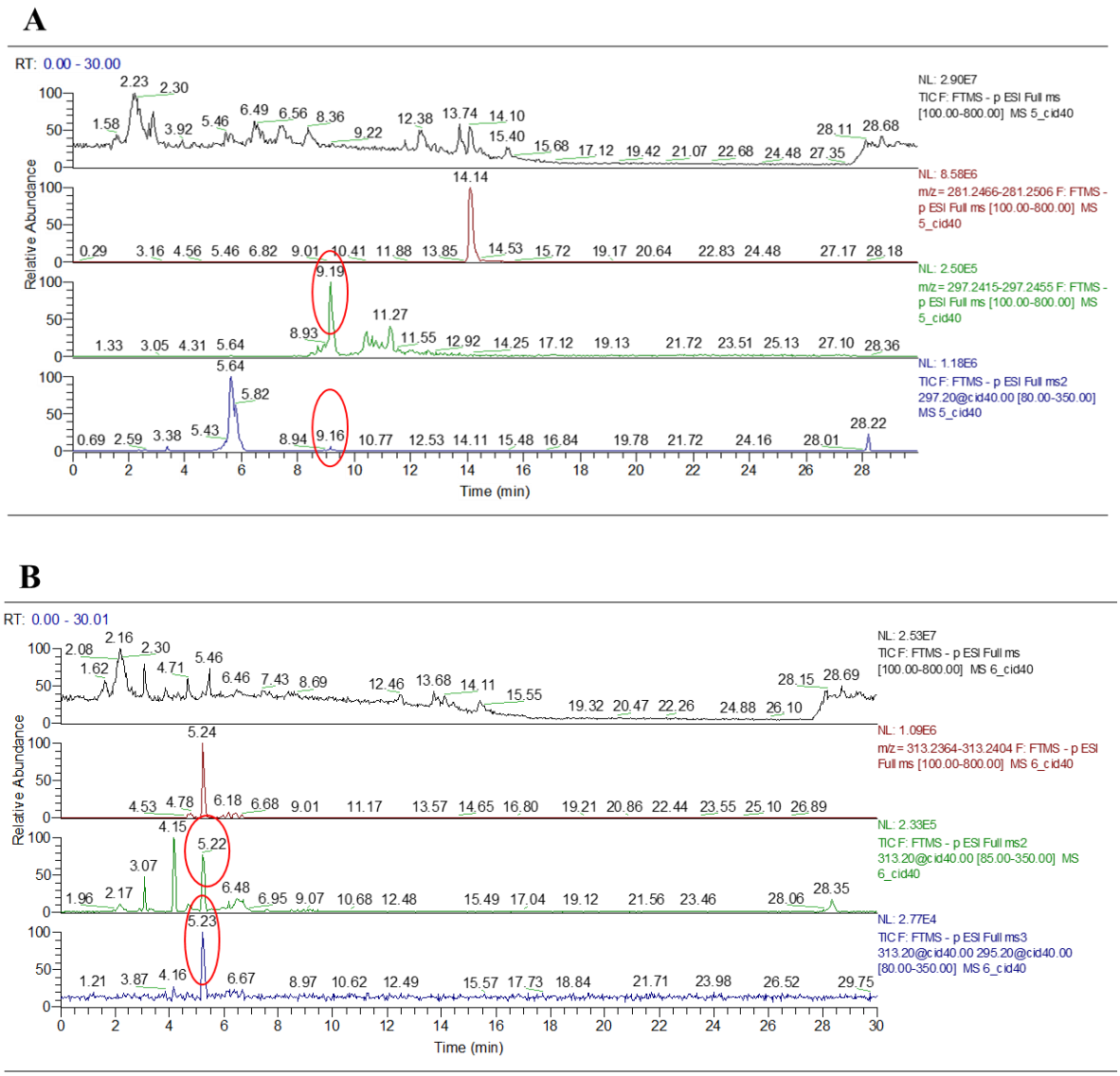

Figure A6.2. LC-MS/MS analysis of product formed by *A. bivalvium* during biotransformation from OA. A, full scan chromatogram of 10-H(P)OME (peak of 9.19/9.16 min). B, full scan chromatogram of 7,10-DiHOME (peak of 5.22/5.23 min).

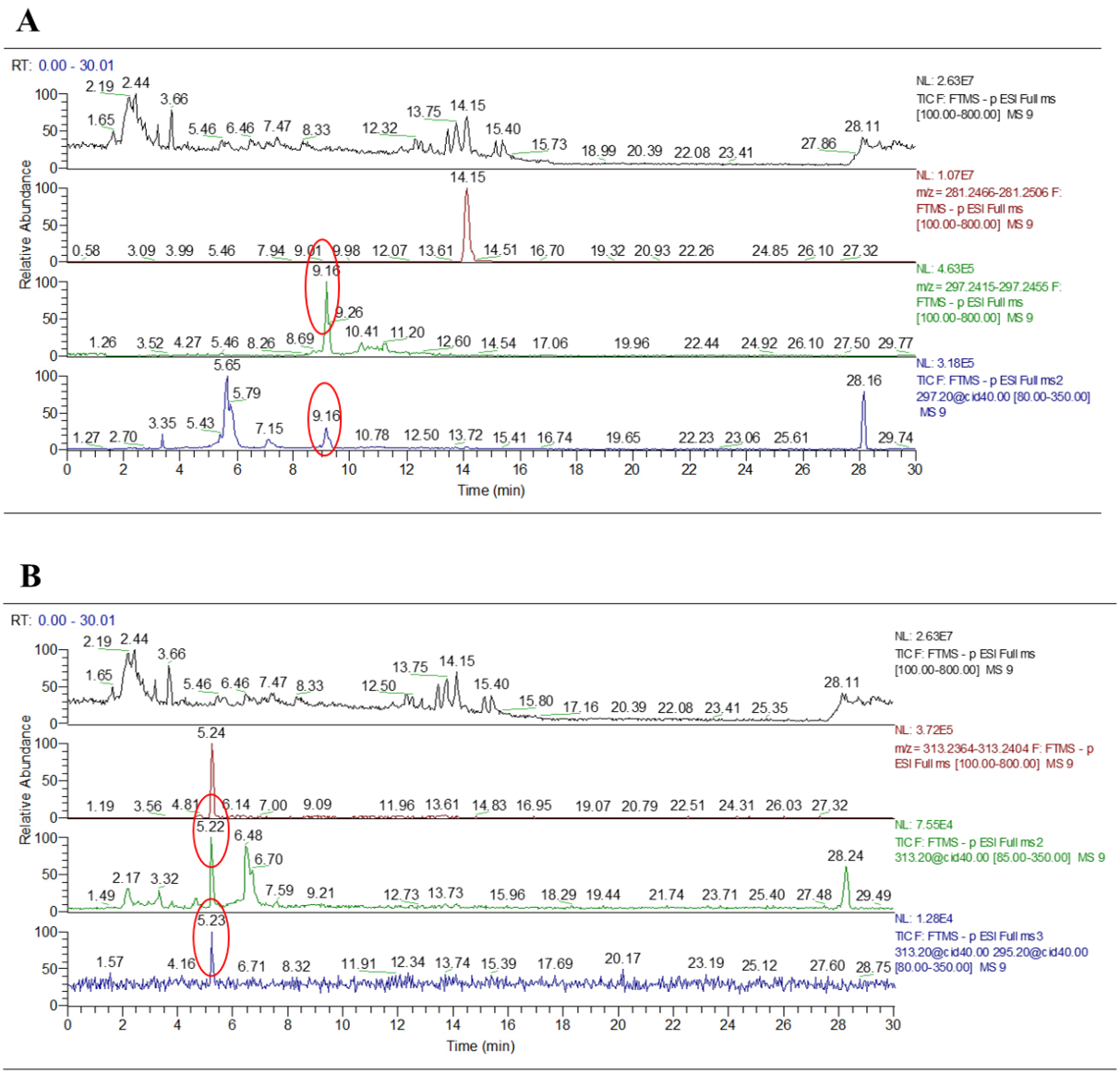

Figure A6.3. LC-MS/MS analysis of product formed by *P. antarctica* during biotransformation from OA. A, full scan chromatogram of 10-H(P)OME (peak of 9.16 min). B, full scan chromatogram of 7,10-DiHOME (peak of 5.22/5.23 min).

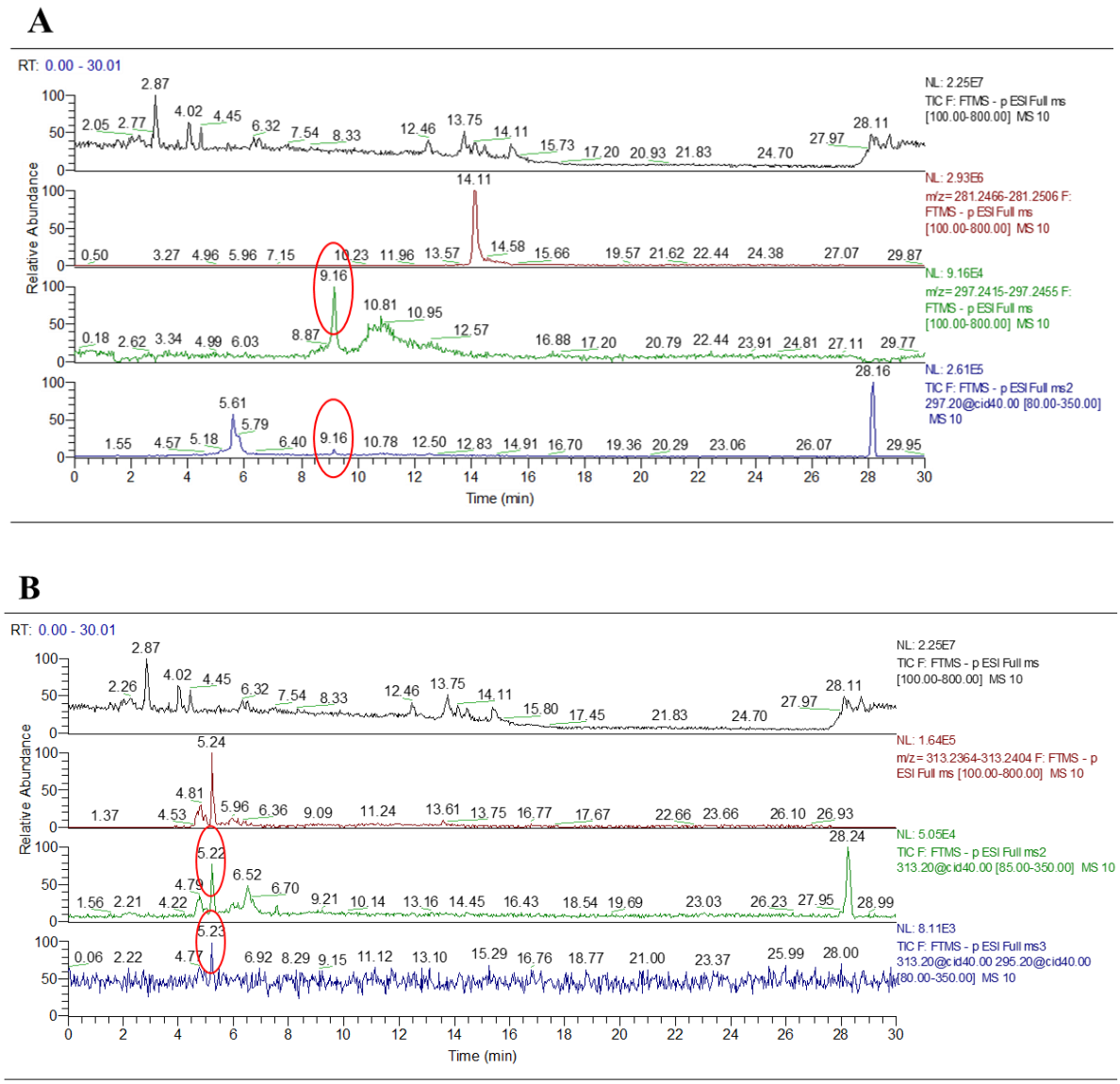

Figure A6.4. LC-MS/MS analysis of product formed by *S. woodyi* during biotransformation from OA. A, full scan chromatogram of 10-H(P)OME (peak of 9.16 min). B, full scan chromatogram of 7,10-DiHOME (peak of 5.22/5.23 min).

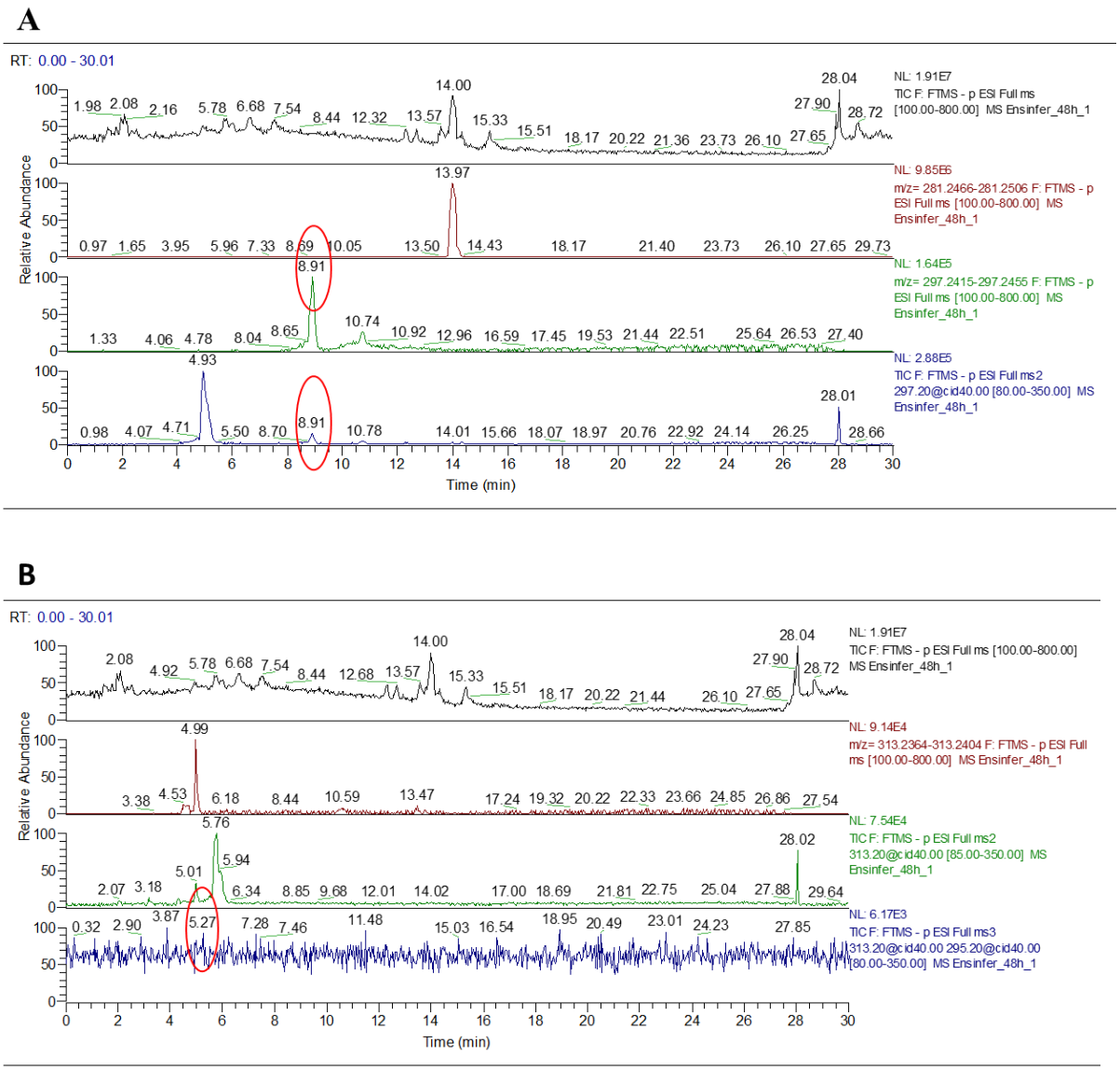

Figure A6.5. LC-MS/MS analysis of product formed by *E. fredii* during biotransformation from OA. A, full scan chromatogram of 10-H(P)OME (peak of 8.91 min). B, full scan chromatogram of 7,10-DiHOME (peak of 5.27 min).

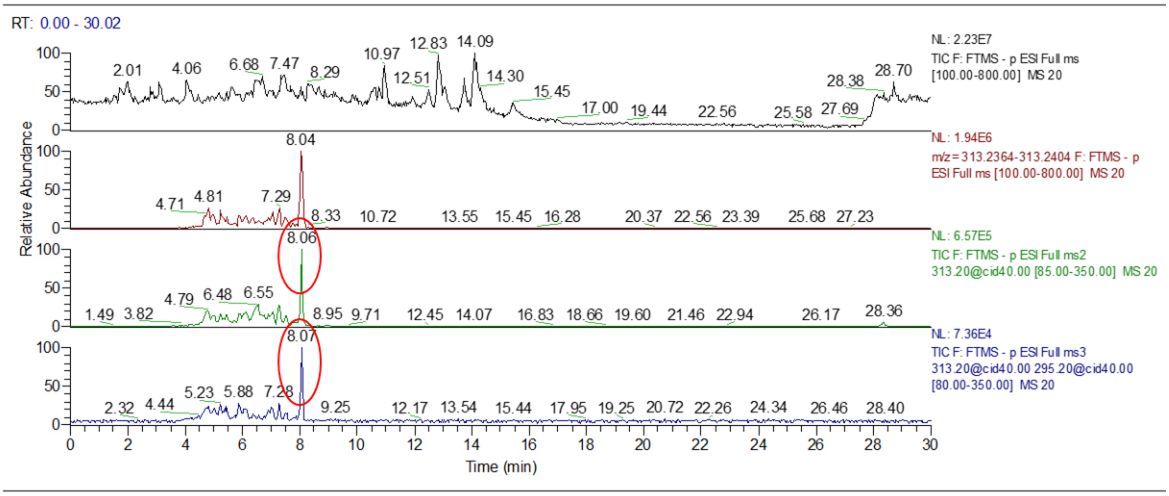

Figure A6.6. LC-MS/MS analysis of product formed by *T. aminoaromatica* during biotransformation from OA. Full scan chromatogram of 10-H(P)OME (peak of 8.06/8.07 min).